การพัฒนาตัวรับรู้ชนิดควอทซ์คริสตรัลไมโครบาลานซ์สำหรับงานตรวจวัดทางชีวภาพซึ่งมีหลายตัวรับรู้ใช้ฐานร่วมกันโดยปราศจากการรบกวน

THE DEVELOPMENT OF INTERFERENCE-FREE MONOLITHIC MULTICHANNEL QUARTZ CRYSTAL MICROBALANCE FOR BIO-SENSING APPLICATIONS

คทา จารุวงศ์รังสี
KATA JARUWONGRUNGSEE

วิทยานิพนธ์นี้เป็นส่วนหนึ่งของการศึกษาตามหลักสูตรปริญญาวิศวกรรมศาสตรดุษฎีบัณฑิต
สาขาวิชาวิศวกรรมไฟฟ้า
คณะวิศวกรรมศาสตร์
สถาบันเทคโนโลยีพระจอมเกล้าเจ้าคุณทหารลาดกระบัง
พ.ศ.2558
KMITL-2015-EN-D-018-210

THE DEVELOPMENT OF INTERFERENCE-FREE MONOLITHIC MULTICHANNEL QUARTZ CRYSTAL MICROBALANCE FOR BIO-SENSING APPLICATIONS

KATA JARUWONGRUNGSEE

A THESIS SUBMITTED IN PARTIAL FULFILLMENT
OF THE REQUIREMENT FOR THE DEGREE OF
DOCTOR OF ENGINEERING IN ELECTRICAL ENGINEERING
FACULTY OF ENGINEERING
KING MONGKUT'S INSTITUTE OF TECHNOLOGY LADKRABANG
2015

KMITL-2015-EN-D-018-210

คณะวิศวกรรมศาสตร์
สถาบันเทคโนโลยีพระจอมเกล้าเจ้าคุณทหารลาดกระบัง
ใบรับรองวิทยานิพนธ์

หัวข้อวิทยานิพนธ์ การพัฒนาตัวรับรู้ชนิดควอทซ์คริสตรัลไมโครบาลานซ์สำหรับงานตรวจวัดทางชีวภาพซึ่งมีหลายตัวรับรู้ใช้ฐานร่วมกันโดยปราศจากการรบกวน

Thesis Title The Development of Interference-Free Monolithic Multichannel Quartz Crystal Microbalance for Bio-Sensing Applications

นักศึกษา นายคทา จารุวงศ์รังสี

รหัสประจำตัว 51060015

ปริญญา วิศวกรรมศาสตรดุษฎีบัณฑิต

สาขาวิชา วิศวกรรมไฟฟ้า

อาจารย์ที่ปรึกษาวิทยานิพนธ์ รศ.ดร.ชูชาติ ปิณฑวิรุจน์

อาจารย์ที่ปรึกษาวิทยานิพนธ์ (ร่วม) รศ.ดร.มนัส สังวรศิลป์

อาจารย์ที่ปรึกษาวิทยานิพนธ์ (ร่วม) ดร.อดิสร เตือนตรานนท์

หมายเลขวิทยานิพนธ์ KMITL-2015-EN-D - 018 - 210

คณะกรรมการสอบวิทยานิพนธ์	ลายมือชื่อ
ผศ.ดร.กิติพล ชิตสกุล	
รศ.ดร.สุรพันธุ์ เอื้อไพบูลย์	
ผศ.ดร.อาทร สรรพานิช	
ผศ.ดร.สุพันธุ์ ตั้งจิตกุศลมั่น	
รศ.ดร.ชูชาติ ปิณฑวิรุจน์	

วัน / เดือน/ ปี ที่สอบ วันจันทร์ที่ 23 พฤศจิกายน พ.ศ. 2558 เวลา 10.00 - 12.00 น.

สถานที่สอบ ณ อาคาร A ชั้น 3 ห้องประชุม 5

คณะวิศวกรรมศาสตร์ รับรองแล้ว

(รองศาสตราจารย์ ดร. คมสัน มาลีสี)

คณบดี คณะวิศวกรรมศาสตร์

วันที่ 23 พฤศจิกายน พ.ศ. 2558

หัวข้อวิทยานิพนธ์	การพัฒนาตัวรับรู้ชนิดควอทซ์คริสตรัลไมโครบาลานซ์ สำหรับงานตรวจวัดทางชีวภาพซึ่งมีหลายตัวรับรู้ ใช้ฐานร่วมกันโดยปราศจากการรบกวน
นักศึกษา	นาย คทา จารุวงศ์รังสี
รหัสประจำตัว	51060015
ปริญญา	วิศวกรรมศาสตรดุษฎีบัณฑิต
สาขาวิชา	วิศวกรรมไฟฟ้า
พ.ศ.	2558
อาจารย์ที่ปรึกษาวิทยานิพนธ์	รศ.ดร.ชูชาติ ปิณฑวิรุจน์
อาจารย์ที่ปรึกษาวิทยานิพนธ์ (ร่วม)	รศ.ดร.มนัส สังวรศิลป์
อาจารย์ที่ปรึกษาวิทยานิพนธ์ (ร่วม)	ดร.อดิสร เตือนตรานนท์

บทคัดย่อ

วิทยานิพนธ์ฉบับนี้ นำเสนอการพัฒนาตัวรับรู้ชนิดควอทซ์คริสตรัลไมโครบาลานซ์สำหรับงานตรวจวัดทางชีวภาพซึ่งมีหลายตัวรับรู้ใช้ฐานร่วมกันโดยปราศจากการรบกวน โดยได้นำเสนอวิธีการใหม่ในการป้องกันการรบกวนจากแรงเฉือนตามขวางที่เกิดขึ้นจากตัวรับรู้ข้างเคียง โดยใช้การสร้างโครงสร้างเสมือนแบบสันเขาด้วยวัสดุโพลีเมอร์ อีกทั้งแก้ปัญหาการรบกวนทางไฟฟ้าระหว่างขั้วไฟฟ้าของตัวรับรู้แต่ละตัวที่อยู่ภายใต้สารละลายเดียวกันจากการเชื่อมต่อทางไฟฟ้าผ่านทางสารละลาย ด้วยการออกแบบช่องทางการไหลแบบแบบขยายออก ซึ่งผลของการพัฒนาตัวรับรู้ดังกล่าว ส่งผลให้ตัวรับรู้แต่ละตัวสามารถทำงานภายใต้สารตัวอย่างเดียวกันอย่างเป็นอิสระ ตัวรับรู้ที่ได้พัฒนาขึ้นนี้นั้น ได้ถูกทำการทดสอบการรับรู้สารทางชีวภาพสองชนิดในเวลาเดียวกัน ได้แก่ อิมมูนโนกอบบูลิน จี หรือ IgG และ ฮิวแมนซีรั่มอัลบูมิน หรือ HSA โดยการตรึงสารทางชีวภาพที่เข้าคู่อย่างจำเพาะเจาะจงกับสารทั้งสอง ได้แก่ แอนติ้อิมมูนโนกอบบูลิน จี หรือ anti-IgG และแอนติ้ฮิวแมนซีรั่มอัลบูมิน หรือ anti-HSA ลงไปบนขั้วของตัวรับรู้ ต่างตัวกัน จากการทดลองพบว่าตัวรับรู้ให้การตอบสนองตรงต่อสารเป้าหมายได้อย่างเป็นอิสระ และให้ผลการวัดได้อย่างเป็นเวลาจริง จึงกล่าวได้ว่าตัวรับรู้ที่พัฒนาขึ้นนี้นั้นสามารถวัดสารทางชีวภาพ เชิงปริมาณ ได้หลายชนิดในเวลาเดียวกันอย่างเป็นเวลาจริง โดยปราศจากปัญหาการรบก่วนระหว่างกันโดยสมบูรณ์

Thesis	THE DEVELOPMENT OF INTERFERENCE-FREE MONOLITHIC MULTICHANNEL QUARTZ CRYSTAL MICROBALANCE FOR BIO-SENSING APPLICATIONS
Student	Mr. Kata Jaruwongrungsee
Student ID.	51060015
Degree	Doctor of Engineering
Program	Electrical Engineering
Year	2015
Thesis Advisor	Assoc.Prof.Dr.Chuchart Pintavirooj
Thesis Co-Advisor	Assoc.Prof.Dr.Manas Sangworasil
Thesis Co-Advisor	Dr.Adisorn Tuantranont

ABSTRACT

In this study, a new interference-free multichannel monolithic quartz crystal microbalance (MQCM) platform was produced for bio-sensing applications. Firstly, interference due to thickness-shear vibration mode coupling between channels in MQCM array is effectively suppressed by interposing a polydimethylsiloxane wall between adjacent QCM electrodes on a quartz substrate to form inverted-mesa-like structure. In addition, the electrical coupling due to the electrical impedance of solution is diminished by extending the flow path between them with an extended-design flow channel. The electrical testing results show that individual QCM signal is unaffected by those of adjacent channels under liquid loading, signifying the achievement of interference-free MQCM. The MQCM is applied for multi-analyte biosensing of IgG and HSA. The anti-IgG and anti-HSA are separately immobilized on two adjacent QCM electrodes, which are subsequently blocked with BSA to avoid unspecific binding. The MQCM biosensors are tested with single- and double-analyte solutions under continuous flow of buffer. The IgG and HSA QCM sensors only show frequency shift responses to their corresponding analytes and there are very small cross frequency shifts due to remnant unspecific binding. Moreover, MQCM sensors show approximately linear frequency shift response with analyte concentration. Therefore, the developed MQCM platform is promising for real-time interference-free label-free detection and quantification of multiple bio-analytes.

กิตติกรรมประกาศ

วิทยานิพนธ์ฉบับนี้สำเร็จลุล่วงตามวัตถุประสงค์ด้วยความกรุณาจากอาจารย์ที่ปรึกษาทั้งสามท่าน ได้แก่ รศ.ดร. ชูชาติ ปิณฑวิรุจน์, รศ.ดร. มนัส สังวรศิลป์ และ ดร. อดิสร เตือนตรานนท์ ซึ่งคอยชี้แนะ ให้คำปรึกษา และมอบประสบการณ์อันเป็นประโยชน์ยิ่ง ตลอดระยะเวลาที่ข้าพเจ้าได้ศึกษา ข้าพเจ้าขอกราบขอบพระคุณอาจารย์ที่ปรึกษาทั้งสามท่านไว้ในโอกาสนี้

ขอกราบขอบพระคุณ ดร. อนุรัตน์ วิศิษฏ์สรอรรถ ผู้ซึ่งให้ความรู้ คำแนะนำด้านวิชาการ ตลอดจนการสนับสนุนในด้านต่างๆ จนสามารถสร้างชิ้นงานซึ่งนำเสนอในวิทยานิพนธ์ฉบับนี้ได้เป็นผลสำเร็จ

ขอกราบขอบพระคุณ ดร. พรพิมล ศรีทองคำ บนสรวงสวรรค์ ที่ได้กรุณามอบความรู้และประสบการณ์ด้านการวัดสารทางชีวภาพด้วยเทคนิคคิวซีเอ็มแก่ข้าพเจ้าอย่างมาก

ขอกราบขอบพระคุณ ผศ.ดร. จำรัส พร้อมมาศ ผู้ซึ่งเป็นท่านแรกที่กรุณาแนะนำข้าพเจ้าให้ได้เข้าใจในหลักของการวัดสารทางชีวภาพด้วยเทคนิคคิวซีเอ็ม

ขอขอบคุณ อ. เพชร นันทิวัฒนา สำหรับการสนับสนุนและให้คำปรึกษาในด้านต่างๆ ด้วยดีเสมอมา

ขอขอบคุณ สมาชิก ห้องปฏิบัติการวิจัยนาโนอิเล็กทรอนิกส์และเครื่องกลจุลภาค (MEMS LAB) และศูนย์นวัตกรรมการพิมพ์อิเล็กทรอนิกส์และอิเล็กทรอนิกส์อินทรีย์ (TOPIC) ในศูนย์เทคโนโลยีอิเล็กทรอนิกส์และคอมพิวเตอร์แห่งชาติ (NECTEC) ทุกท่าน โดยเฉพาะ น.ส. อุไรวรรณ ไหววิจิตร ที่ได้ให้การสนับสนุนในงานวิจัยชิ้นนี้ตลอดมา

ขอขอบคุณ กำลังใจที่สำคัญยิ่งในการทำวิทยานิพนธ์ฉบับนี้ให้ลุล่วง จาก น.ส. อุษา สังขนาค และ ด.ช. ธีร์ธนินทร์ จารุวงศ์รังสี ภรรยา และบุตร ของข้าพเจ้า

สุดท้ายนี้ ข้าพเจ้าขอกราบขอบพระคุณ บิดา-มารดา ของข้าพเจ้า (นาย วุฒิชัย จารุวงศ์รังสี และนาง ยุภาวรรณ จารุวงศ์รังสี) ที่ได้ให้กำเนิด อบรมเลี้ยงดู และสนับสนุนข้าพเจ้าทุกด้านตลอดจนถึงวันนี้

คทา จารุวงศ์รังสี

สารบัญ

Chapter 1
INTRODUCTION

1.1 STATEMENT AND SIGNIFICANCE OF THE PROBLEMS

Quartz crystal microbalance (QCM) is a method that has been widely used in physical, chemical and biological sensing applications. For sensing applications, it will be coated with a chemically or biologically sensitive film to sense very small amount of adsorbed target substances in gas or liquid medium. The target substance will bind or react with the sensing film resulting in mass and/or viscosity-density change, which can be generally detected by resonance frequency shift.

The key advantages of QCM for chemical and biosensing include quantitative, label-free and real-time detection capability with very high sensitivity and fast response. However, QCM's characteristics can be considerably affected by environment conditions such as temperature and pressure, making it unpractical for many sensing applications whose environmental conditions can be largely varied. A dual QCM scheme has been developed to minimize such environmental effects. The environmental effects can be completely eliminated if the characteristics of two QCMs are identical. Since QCMs made on different substrates can hardly be identical due to crystal manufacturing variation, dual-QCM resonators on a single quartz substrate, which is the simplest version of monolithic multichannel QCM (MQCM), have been designed to effectively cancel the environmental effect.

MQCM system containing more than two QCM channels on a single substrate has then been proposed for multi-analyte detection. The development of MQCM leads to miniaturization of QCM devices because the size and spacing between QCMs are necessarily small as the array size increases. MQCM offers some additional benefits including less sample/reagent consumption and wider functionality such as multi-dynamic range detection. However, conventional planar MQCM suffers from strong acoustic interference problem because acoustic wave induced by one QCM can propagate through the substrate and then interfere with the wave generated by other QCMs. Several sophisticated schemes have been devised to minimize the acoustic coupling. Modification of quartz substrate structure has been the most widely used approach for this purpose. Various modified quartz structures including mesa, inverted-mesa, convex and more complicated shapes have been widely studied to minimize acoustic interference in MQCM. Among these, inverted-mesa shape is the most commonly used due to highly effective inference cancellation and

relatively high sensitivity compared with other structures. Despite its promising performances, MQCM with inverted-mesa or other structures that require quartz substrate modification involve expensive and complicated fabrication processes. Thus, alternative simple method for realizing effective MQCM is still needed.

1.2 GOAL AND OBJECTIVE

As the matter of fact that, the main problem of using MQCM based sensor in real-world applications is the interference between adjacent channels. Particularly, when operating this device in liquid-phase, the interference occur both mechanical and electrical. Even there are many interference blocking technique have been presented, but none of them are truly solve the interference problem in liquid phase. Hence, the most important objective of this study is to invent the new MQCM platform that truly breakthrough the problem.

1.3 HYPOTHESIS TO BE TESTED

Previously, several techniques that use to eliminate the mechanical interference of the MQCM have been presented. Most of the techniques are based on modifications of the quartz substrate, to entrap the energy inside the vibrating area. Even through it is one of the most effective way to block the interference, but in the other hand, they are suffering in high-cost and complicated fabrication process. Therefore, instead of modification, our hypothesis is to fabricate the artificial structure to working in the same way. With this scheme, the mechanical interference problem should be solve effectively without conscious of high-technology fabrication technique. In addition, there is also the other problem, the electrical interference when operating in liquid-phase. This impact occurs from the electrical coupling through conductive liquid sample which linked to multiple electrodes. The assumption to solve this problem is to separate the testing area of those electrodes with lab-on-a-chip fabrication technology.

In this work, we proposed an inverted-mesa-like structure formed by interposing a polydimethyl-siloxane (PDMS) wall between adjacent QCM electrodes on a single quartz substrate to achieve the interference-free MQCM that is coupled with real-time flow system for multi-analyte bio-sensing applications. Additionally, the electrical coupling between adjacent channels due to impedance of solution is suppressed by extending the flow path between them with a serial extended-design flow channel. Moreover, the serial extended-flow design can prevent turbulent flow of analyte within the system that may cause

unpredictable sensing response. The MQCM is applied for real-time multi-analyte biosensing of immunoglobulin G (IgG) and human serum albumin (HSA).

1.4 PROCESS OF THE STUDY

The process of this study can be divided into four phase as follow. Firstly, the study of using individual QCM as a chemical sensor. Next, the study of using individual QCM as a biological sensor. Then, the study of MQCM fabrication and its problems. Lastly, the new MQCM with no interference problem is studied and demonstrated as a multichannel biological sensor.

Chapter 2
QCM AND MQCM

In the world of weight or mass measurement, the term of sensitivity is the major key to be deliberated. The higher sensitivity, the higher detail of mass can be detected. Even there are numerous kind of weight measurement technique have been announced up till now, but among them there are just a few technique that capable of weighing in molecular scale. Accordingly, the detecting of chemical or biological molecule can also be performed by those molecular weighing technique. The quartz crystal microbalance (QCM), an ultra-high sensitivity mass sensing device, is one of the most promising method capable of weighing mass of molecules. Since this is the main method used in this study, the related principle will be presented in this chapter. In addition, the principle of monolithic multichannel quartz crystal microbalance (MQCM) which is a group of QCMs that was fabricated on a substrate monolithically also be provided here.

2.1 QUARTZ CRYSTAL AND QUARTZ CRYSTAL MICROBALANCE

2.1.1 Piezoelectricity and Quartz crystal

Piezoelectricity, the most important property of a quartz crystal, makes it able be used as a resonator. The word Piezo, derived from the Greek word "Piezin", meaning to "to press". So, the piezoelectricity was defined as "electric polarization produced by mechanical strain in crystals belonging to certain classes, the polarization being proportional to the strain and changing sign with it" by Cady [1]. Electric polarization can be produced inside any piezoelectric material when it was deformed (bending, shear, torsion, tension, and compression). It provides a source of electromotive force (voltage) as illustrated in Figure 2.1(a). On the contrary, the converse effect can be occurred as well, the mechanical movement can be produced when a voltage applied across the piezoelectric material, as shown in Figure 2.1(b). Figure 2.1(c) shows the piezoelectric effect of the quartz crystal that is fabricated to operate in thickness-shear mode (TSM).

The quartz crystal is formed from silicon and oxygen ($Si0_2$). Characteristics of the crystal depend on the unit cells of crystal growing. Each cell is identical and consists of atoms arranged in a repetitive geometric pattern. The geometric of quartz crystals was illustrated by Figure 2.2 Most of the physical properties of a crystal are direction dependent

(anisotropic), therefore, changes during the growth of the crystal which affects anisotropy result in crystal imperfections. Optic axis, the major axis of quartz growth, is not anisotropic to light, therefore light passes readily. For the quartz resonator cutting, the optic axis is labeled as Z-axis in an orthogonal X, Y and Z coordinate system. Figure 2.3(a) and Figure 2.3(b) show the photograph of a naturally growth quartz crystal cluster and synthetically growth quartz crystal by the hydrothermal method respectively.

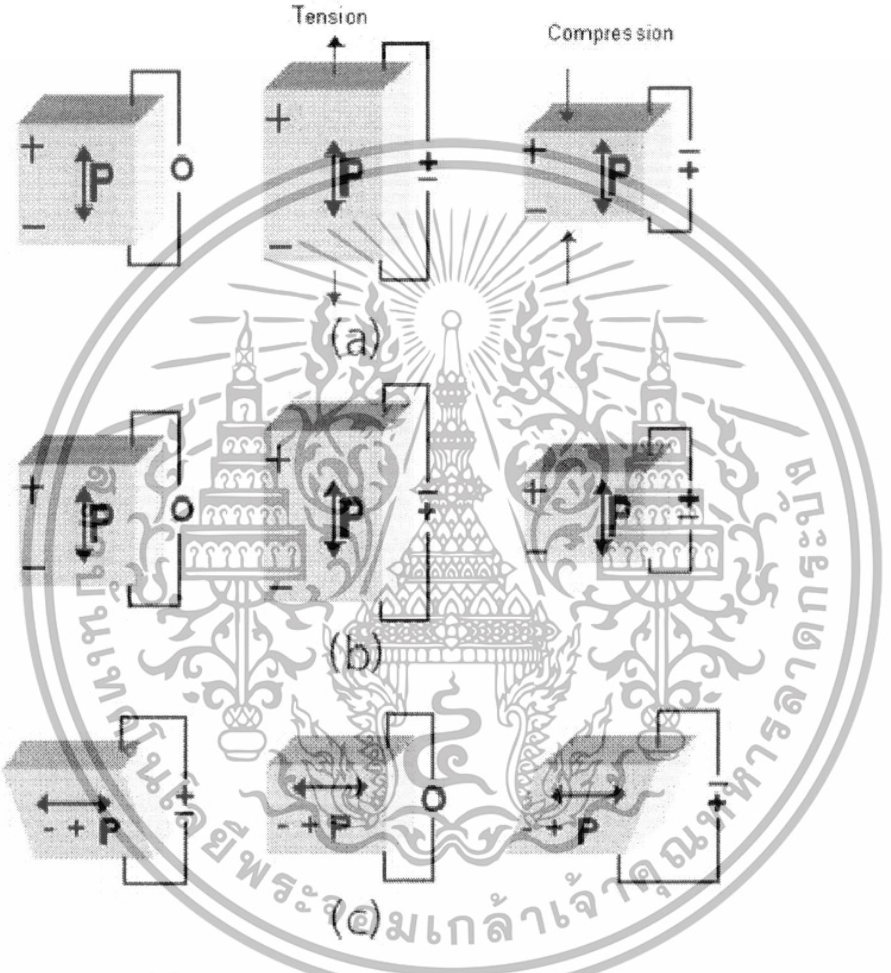

Figure 2.1 Schematics of (a) direct piezoelectric effect, (b) converse piezoelectric effect, and (c) thickness-shear motion piezoelectric effect [2].

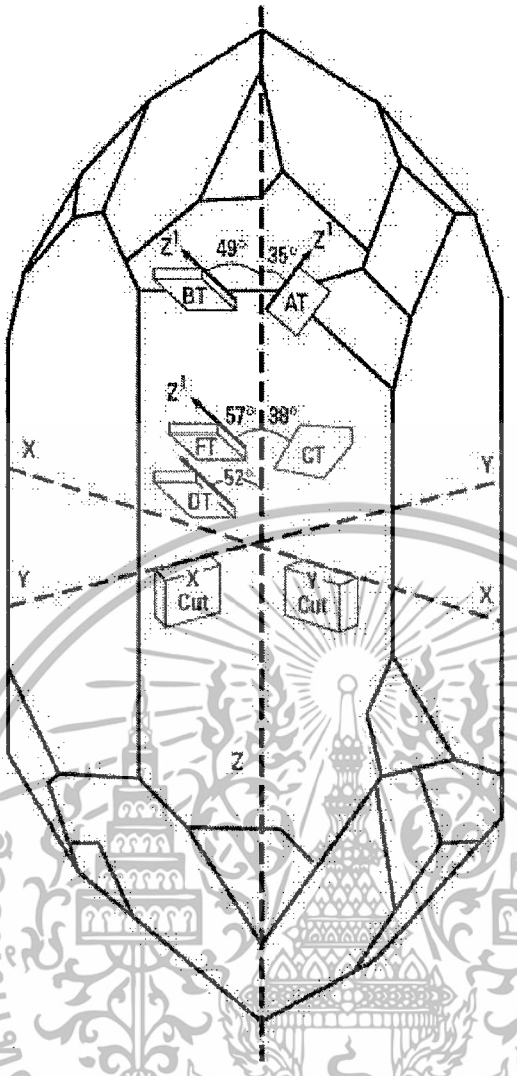

Figure 2.2 Typical crystal cuts from a doubly terminated quartz crystal [3].

Cutting the crystal at various angles, provide the variation in physical and electrical parameters of the resonator. For example, an X plate crystal, the major face normal to the X axis, voltage generated when compressed is fairly large and frequency decreases when temperature increases. For Y cut plate, voltage can be generated just by shear stress but exhibits a positive temperature coefficient. Numerous other cuts can be made simply by changing the angle and the axis of reference.

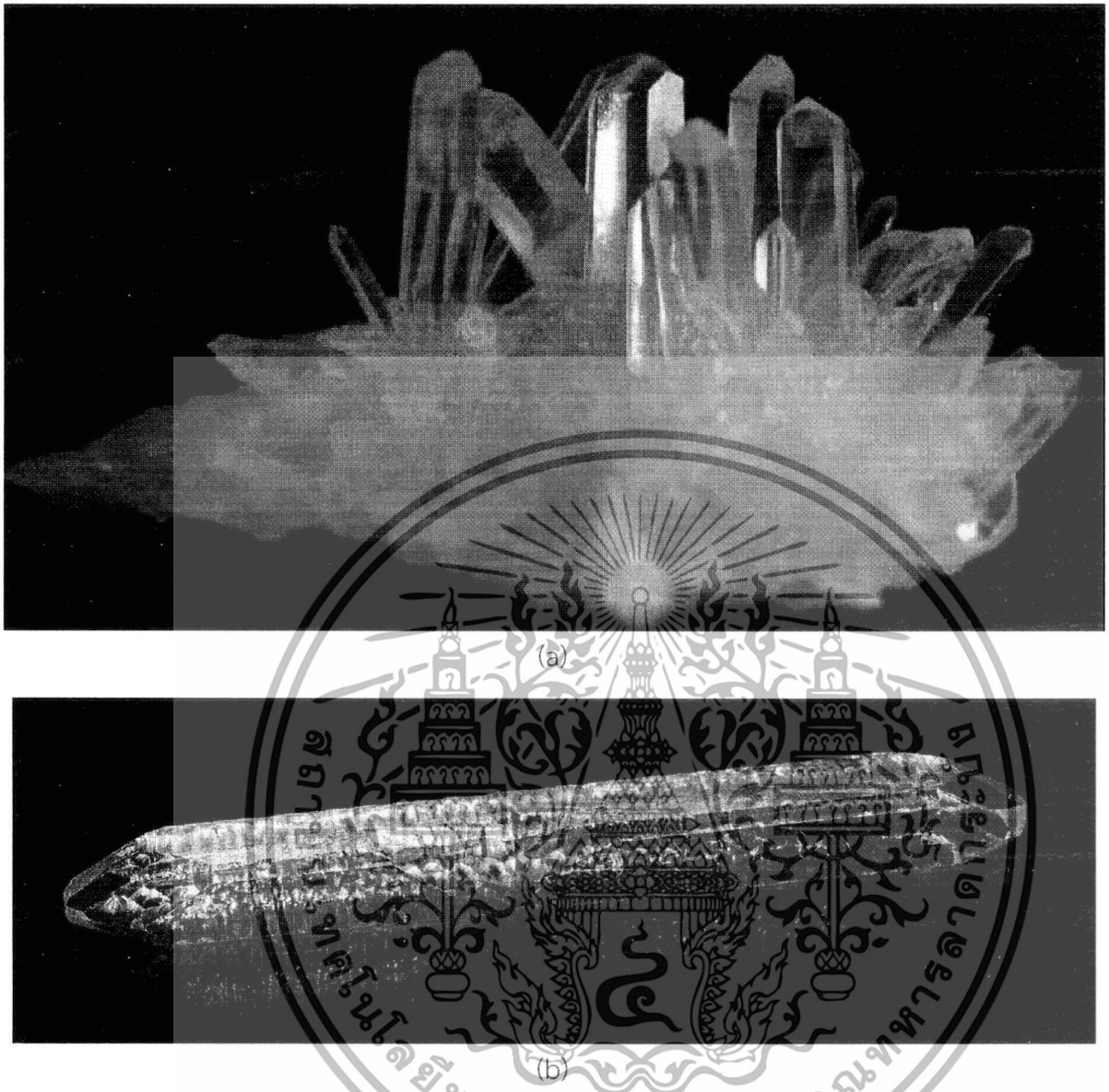

Figure 2.3 Photographs of (a) a natural quartz crystal cluster [4] and (b) a synthetic quartz crystal [5].

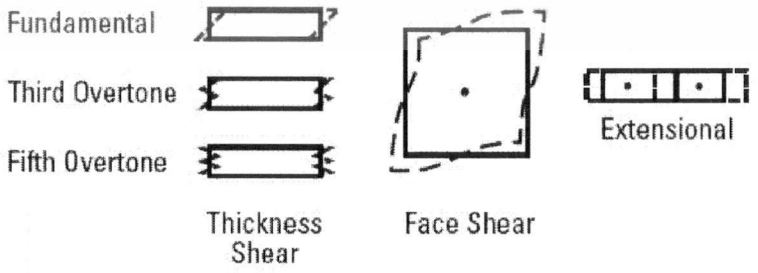

Figure 2.4 Vibration modes of various crystal cuts and the thickness shear overtone [3].

Stress of quartz is produced when it is subjected to a voltage. When the voltage is alternate at the proper rate, the crystal will steadily vibrate and produce an AC signal. The mode of vibration depends upon the crystal cut, such as extensional-mode for X-cut, thickness shear mode (TSM) for AT-cut. The various vibration modes were illustrated in Figure 2.4. The vibration set-up in the quartz crystal may produce both harmonic and non-harmonic signals and overtones. The harmonic overtones are desirable since they allow the production of higher frequency crystal resonators using essentially the same cut. Non-harmonic overtones, on the other hand, are undesirable as they may lead to the generation of unwanted signals at frequencies spaced close to the one desired. When unwanted signals occur, they could also change with environmental influences. The various vibrations may then cancel, causing the crystal to stop resonating. This phenomenon is termed an activity dip since the crystal activity stops and starts due to a changing environment. Crystals having unwanted signals could also shift from one resonate point to another producing a frequency jump which would be an undesirable effect.

2.1.2 Quartz crystal microbalance

Quartz crystal microbalance (QCM), an ultra-sensitive mass sensor, is one of the most powerful methods for chemical and biological sensing. QCM has a wide range of applications in many fields [6-11] such as thin-film measurement, chemical analysis, gas sensor, humidity sensor, and biosensor. Figure 2.5 show the diagram illustrated of using QCM as a sensing device and the photograph of commercially available QCM. Typically, QCM based sensor utilize a thin AT-cut quartz plate with two electrodes patterned on both sides and coated with various sensing materials to enhance the sensitivity to target analyte. When electrically excited, quartz crystal oscillates mechanically due to piezoelectric effect and the oscillation is maximized at a fundamental resonance frequency in a thickness-shear mode (TSM) with faces undergoing in-plane displacement. Butterworth-van Dyke model [12], the equivalent circuit of QCM, was described in Figure 2.6. The model has been useful in predicting the frequency shifts and losses of an AT-cut quartz crystal in QCM applications.

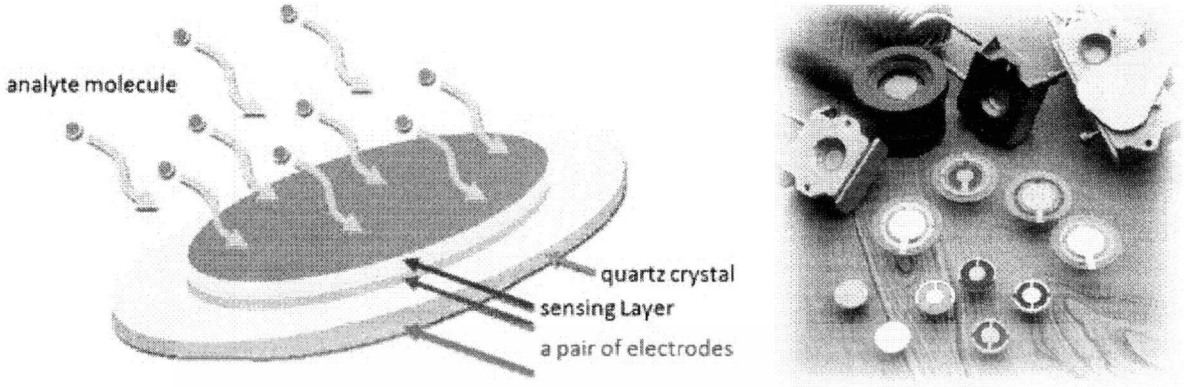

(a) (b)

Figure 2.5 The picture illustrated of, (a) basic diagram of QCM, and (b) photograph of commercially available QCM [13].

Figure 2.6. Butterworth-van Dyke model of Quartz Crystal Resonator.

The BVD electrical model consists of two arms. The motional arm has three series components modified by the mass and viscous loading of the crystal: (1) R_m (resistor) corresponds to the dissipation of the oscillation energy from mounting structures and from the medium in contact with the crystal (i.e. losses induced by a viscous solution), (2) C_m (capacitor) corresponds to the stored energy in the oscillation and is related to the elasticity of the quartz and the surrounding medium, and (3) L_m (inductor) corresponds to the inertial component of the oscillation, which is related to the mass displaced during the vibration.

Owing to piezoelectric effects, the resonant properties of crystal can be influenced by external physical loading, which may be classified into two main types, gravimetric and

viscoelastic loading. In the first case, gravimetric force due to mass rigidly deposited on the crystal surface is balanced by a force originating from the shear gradient inside the crystal, leading to the resonance frequency shift (Δf_g), which is governed by Sauerbrey's equation [14, 15]:

$$\Delta f_g = -\frac{2f_O^2}{\sqrt{\rho_q \mu_q}} \frac{\Delta M}{A} \tag{2.1}$$

$$f_0 = \frac{v}{2t_q} = \frac{\sqrt{\frac{\mu_q}{\rho_q}}}{2t_q} \tag{2.2}$$

where f_0 is the fundamental resonance frequency, ΔM is the mass deposited on QCM surface, A is the active electrode area, v is the acoustic wave velocity, ρ_q is the density of crystal (2.648 g/cm^3 for quartz), μ_q is the shear modulus of the cut face (2.947×10^{11} g/cm×s^2 for AT-cut quartz) and t_q is the crystal thickness. With this loading effect, QCM has been routinely used for thickness monitoring in physical vapor deposition processes.

For the viscoelastic loading, resonance frequency is changed due to acoustic-fluid damping interaction when QCM operates in viscoelastic medium such as liquid [16]. Unlike gravimetric loading, there are large changes of dissipation factor and resonant resistance due to energy losses of shear wave that travels through non-rigidly adsorbed layers [17-20]. The viscoelastic resonance frequency shift (Δf_v), dissipation factor change (ΔD) and resonant resistance change (ΔR) are given by:

$$\Delta f_v = -f_O^{3/2} \sqrt{\frac{\eta_L \rho_L}{\pi \mu_q \rho_q}} \tag{2.3}$$

$$\Delta D = 2f_O^{1/2} \sqrt{\frac{\eta_L \rho_L}{\pi \mu_q \rho_q}} \tag{2.4}$$

$$\Delta R = \left(2\pi \eta_L \rho_L f_o\right)^{1/2} A / k^2 \tag{2.5}$$

where η_L, ρ_L and k are viscosity, density and electromechanical coupling factor of the liquid medium, respectively. Both dissipation factor and resonant resistance can be directly measured experimentally. The combined measurements of frequency shift and changes in the dissipation factor and resonant resistance have been termed, *QCM-D* and *QCM-R*, respectively [21]. With the combined mass and viscosity-density effects, QCM can be applied for bio/chemical sensing by coating with a chemically or biologically sensitive film to sense very small amount of adsorbed gases such as volatile organic compounds (VOCs) [22, 23] and environmental pollutants [24-26] and liquid phase biochemicals. QCM/QCM-D evolves a solution measurement capability in analytical chemistry and electrochemistry applications due to wide detection range capability and very broad measurement applicability. Moreover, *electrochemical quartz crystal microbalance (EQCM)* variant, in which QCM is employed as a working electrochemical electrode, allows advanced electrochemical studies. Great amount of work relating to QCM/QCM-D/EQCM has been summarized in a number of review articles, which go over the utilization of QCM in analytical electrochemistry [27-29], QCM application areas in biosensors [30-36], drug discovery [11, 37] and complex biopolymeric/biomimetic/ biomolecular systems [6, 9].

2.2 MONOLITHIC MULTICHANNEL QUARTZ CRYSTAL MICROBALANCE

The main advantages of QCM in sensing fields include high sensitivity, high stability, fast response and low cost. In addition, it provides label-free detection capability for bio-sensing applications. However, QCM faces a major technical disadvantage of substantial characteristic dependence on environmental parameters particularly temperature. The problem can be partially alleviated by using AT-cut QCM surface (35.25° with respect to z-axis) because it has relatively low temperature coefficient compared to other well-characterized quartz crystal cuts [38]. Nevertheless, its performance is still not satisfactory for many sensing applications with largely varied environmental conditions. The environmental effects can be more effectively minimized by a dual QCM scheme [39-42], in which reference and sensing QCMs are employed. Both QCMs should have almost identical characteristic and present in the same environmental condition but reference QCM is prevented from sensing target species by the absence of sensing layer.

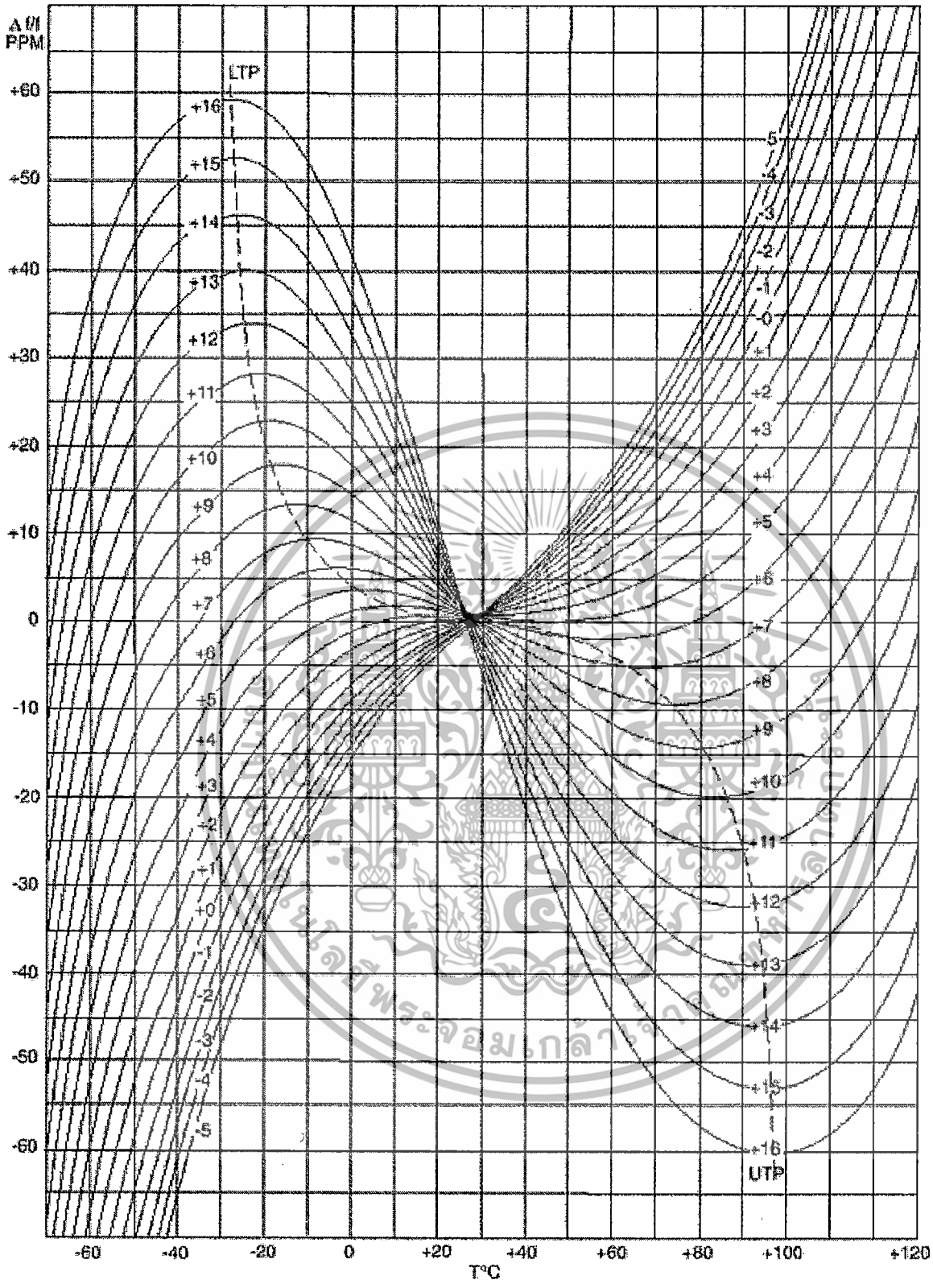

Figure 2.7 Temperature vs. frequency plots of AT cuts quart crystal with a few variation of angle rotation, LTP represents the Lower Temperature Turnover.

In general, this scheme may be implemented in two ways. The first mean is to use a simple combination of two independent QCMs [39-42]. This method is found not to be very successful because QCMs made on different substrates can hardly be identical due to variation of crystal production. Figure 2.7 shows the temperature vs. frequency plots of AT cuts quart crystal with a few variation of angle rotation, it can be seen that even just a few second error of cutting angle will change the characteristic of the quartz over all temperature range. The QCM mismatch problem can be effectively eliminated by employing dual-QCM resonators on a single quartz substrate since two QCMs can be made highly identical [42]. However, the approach gives rise serious interference problems because acoustic wave induced by one QCM can interfere with the wave generated from the nearby QCM [43]. In addition, mass or stress loading on one QCM will induce spurious frequency shift on the other. The problems become particularly serious for two closely spaced identical QCMs [44].

Multiple QCM array system has been developed following the dual QCM scheme for advanced physical, chemical and biological sensing with environmental compensation [45]. In this system, one QCM is used as a reference and other QCMs are coated with different sensing layers. Multiple QCM array systems implemented by a simple combination of several independent QCMs are considered not suitable for general applications not only due to QCM mismatch problem but also bulkiness. Multiple microbalances on a single quartz substrate, commonly referred to as monolithic multichannel quartz crystal microbalance (MQCM) [46], are thus considered highly promising. Moreover, the development of MQCMs leads to miniaturization of QCM devices because the size and spacing between QCMs are necessarily small as the array size increases. QCM miniaturization leads to additional benefits including lower cost, less sample/reagent consumption, faster sensing response and shorter diagnostic time [47]. Furthermore, QCMs in an array can be designed to have varying sensitivity, selectivity and dynamic range. Therefore, MQCM will be a versatile sensor platform with high performance and wide functionality. However, MQCM technology faces challenging strong acoustic interference problems that cannot easily be solved. It not only affects MQCM performance but also constrains the miniaturization.

2.2.1 Conventional MQCM

A conventional MQCM utilizes a few hundrends micron thick AT-cut quartz crystal plate with an array of electrode pairs deposited on both sides. The size of electrode pairs and the spacing between them depend on the number and density of QCM in the array. For a MQCM system, acoustic wave induced by one QCM will propagate laterally through

the substrate over a specific distance and if another QCM is located within vicinity of the acoustic field, acoustic interference occurs [48]. For a small MQCM array, spacing between adjacent QCMs would be sufficiently large, interference is thus negligible and conventional MQCM structure can function properly. For a large MQCM array, distance between adjacent QCMs must be small due to space limitation and hence strong acoustic interference is inevitable. The interference generally causes fundamental resonance frequency change to all acoustically coupled QCMs and spurious frequency shift due to mass or stress loading on neighboring QCMs. The problem becomes particularly serious when all QCMs are identical and operate at the same resonance frequency [44].

Acoustic interference in MQCM is highly complicated due to convolution of the simultaneous vibration motions from several resonators on one quartz plate. Further, it depends on several parameters of MQCM device including spacing between adjacent electrodes, geometry, dimensions and thickness of each electrode, mechanical and piezoelectric properties of quartz substrate and mechanical properties of electrode material. Consequently, analysis of MQCM and its interference characteristics are mainly experimental. Typically, interference between two adjacent QCMs is examined experimentally by impedance measurement of the two QCMs under exchanged external load and an electrical equivalent circuit is used to model and describe the response [43]. Electrical equivalent circuits including Butterworth–Van-Dyke (BVD) model [49] and transmission line representation [50] have been effectively used for QCM measurement analysis. Interference is introduced in a BVD circuit model by a complex coupling resistance between two BVD branches. In an equivalent circuit model, MQCM configuration is simplified into one-dimensional structure and the vibration profile is assumed to be uniform throughout the electrode surface. The results evaluated from the model are mainly valid in the region near the resonance frequency, which is calculated by applying Kirchhoff's law. Electrical circuit modeling can provide good estimation and prediction for experimental observation. However, it cannot provide physical understanding and correlation between interference behaviors and physical parameters because it neglects some mechanical important features including modes coupling and energy trapping of electrode layer [48].

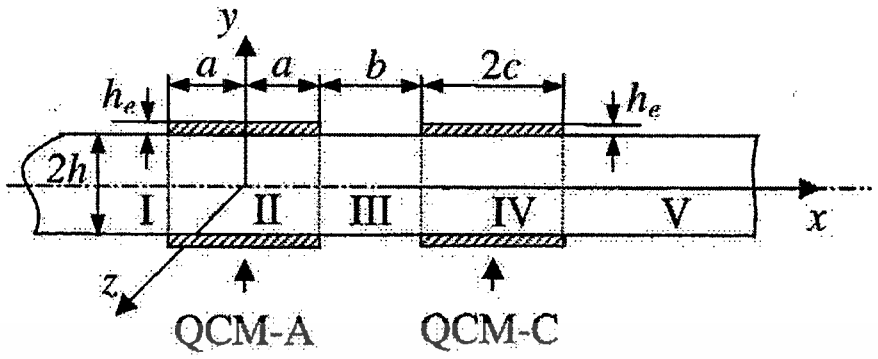

Figure 2.8 MQCM structure with two QCM strips at regions II and IV. Regions I, III, and V are base quartz.

Theoretical modeling can provide insight understanding of interference mechanisms as well as relationship between interference behaviors and physical parameters. In general, theoretical analyses are performed on simplified models of complex real world problems so that analytical or semi-analytical solutions can be obtained. Recently, the theoretical analysis on interference of MQCM has been conducted using a simplified MQCM model with two generalized QCMs on a monolithic quartz crystal plate as illustrated in Figure 2.8. The simple model of two generalized QCMs is chosen to represent two nearest-neighbor QCMs in a monolithic MQCM array. Two quartz crystal microbalances, QCM-A and QCM-C, are formed on an infinitely wide quartz plate with a thickness of 2h and electrode widths of 2a and 2c, respectively. The thickness of the electrode and separation between two QCMs are h_e and b, respectively. The analysis is based on one-dimensional modified Mindlin's theory with piezoelectric effect, which comprises a set of partial differential equations [51]. The effects of electrode sizes, spacing between two QCMs and QCM position on interference characteristics are extracted from the theoretical solutions.

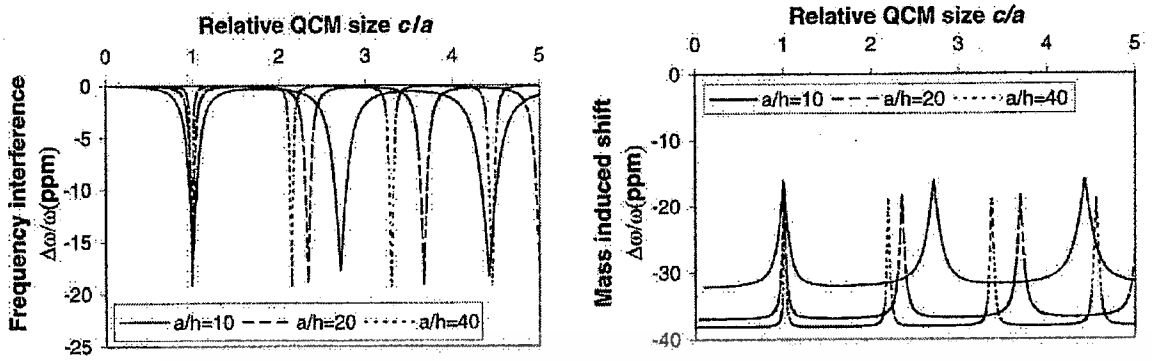

Figure 2.9 (a) FI and (b) MSI as a function of (c/a) value at different (a/h) values.

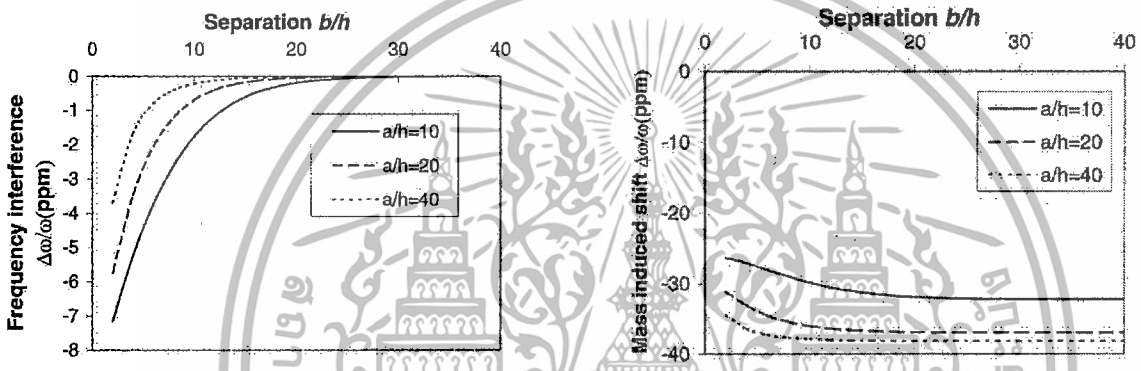

Figure 2.10 (a) The influence of separation between QCMs (b/h) on FI and MSI, (b) at a fixed relative size between QCMs (c/a) of 0.5.

The interference has been quantitatively characterized in terms of frequency interference (FI) and mass induce shift (MIS). FI is defined as the normalized frequency change $(\Delta\omega/\omega)_f$ of one QCM due to a mass loading on another QCM while MIS $(\Delta\omega/\omega)_m$ is the normalized change in resonance frequency due to the adsorption of mass on its own electrode. MIS can be significantly modified due the presence of neighboring devices in MQCM. FI and MIS are mathematically the same but they arise from different physical mechanisms. From the theoretical analysis, two parameters including relative width between two QCMs (c/a) and separation relative to QCM thickness (b/h) at a fixed QCM width relative to QCM thickness (a/h) are the most important factors that affect the FI and MSI. Theoretically calculated FI and MSI as a function of c/a value at different a/h values are illustrated in Figure 2.9 (a) and (b) respectively. Similarly, FI and MSI as a function of b/a value at different a/h values are shown in Figure 2.10 (a) and (b) respectively.

In Figure 2.9 (a), FI of QCM-A is computed when a fixed mass is placed on QCM-C with different QCM-A widths (a/h) of 10, 20, and 40 and a constant separation (b/h) of 20. It can be seen that FI has several peaks at different c/a values. The largest FI for all a/h values occurs near c/a =1 where the two electrodes have the same width. This corresponds to the strongest fundamental acoustic coupling of QCMs operating at the same resonance frequency. At higher values of c/a, FI peaks for various QCM widths (a/h) appear at different c/a values. These peaks is attributed to anharmonic overtones excited from QCM-C and coupled into QCM-A. The overtone coupling peaks (c/a > 1) periodically occurs at c/a periods of ~1.7, 1.34 and 1.14 for a/h = 10, 20, and 40, respectively. Thus, strong interference occurs over a broader range of c/a for smaller electrodes. On the other hand, anharmonic interference amplitudes of smaller electrodes as seen in Figure 2.9 (a) are slightly lower than larger ones. Consideration of MIS offers an alternative perspective of interference. Figure 2.9 (b) shows MIS with identical parameters as those in Figure 2.9 (a) but the mass is placed on QCM-A instead. It can be seen that MIS decreases by a factor of ~0.5 for fundamental and anharmonic interference peaks. Thus, the mass sensitivity of QCM-A is considerably reduced due to acoustic interference from QCM-C. In addition, MIS is found to slowly increase as electrode width (a/h) increases.

The influence of separation between QCMs (b/h) on FI and MSI are demonstrated in Figure 2.10 (a) and (b) at a fixed relative size between QCMs (c/a) of 0.5. It is seen that FI is high for small separations and then decreases rapidly with increasing separation as expected. In addition, FI for smaller electrodes is considerably higher than larger one and thus smaller electrodes require larger relative spacing. In contrary, MIS decreases slightly for small separations (b/h < 5) and it is not strongly dependant on the separation for c/a = 0.5. More recently, similar theoretical analysis on a more general MQCM model with an arbitrary number of QCMs on a monolithic quartz crystal plate is reported [52]. However, the analysis is limited to a special condition that all QCMs have the same electrode width and interelectrode spacing and only the influences of the width and spacing on interference are evaluated. Some conclusions can be drawn from the theoretical analyses. Firstly, the microbalance channels of the devices may be designed to have different electrode sizes to avoid strong frequency interference. Secondly, a large electrode size is helpful for acoustic energy trapping. However, the size of electrode may be restricted by the number of channels mounted on quartz plate, and the large size of electrode may also bring higher order modes and introduce higher order frequency interference. Lastly, the separations

need to be large to avoid strong frequency interference when all the channels have the same size and same resonance frequency.

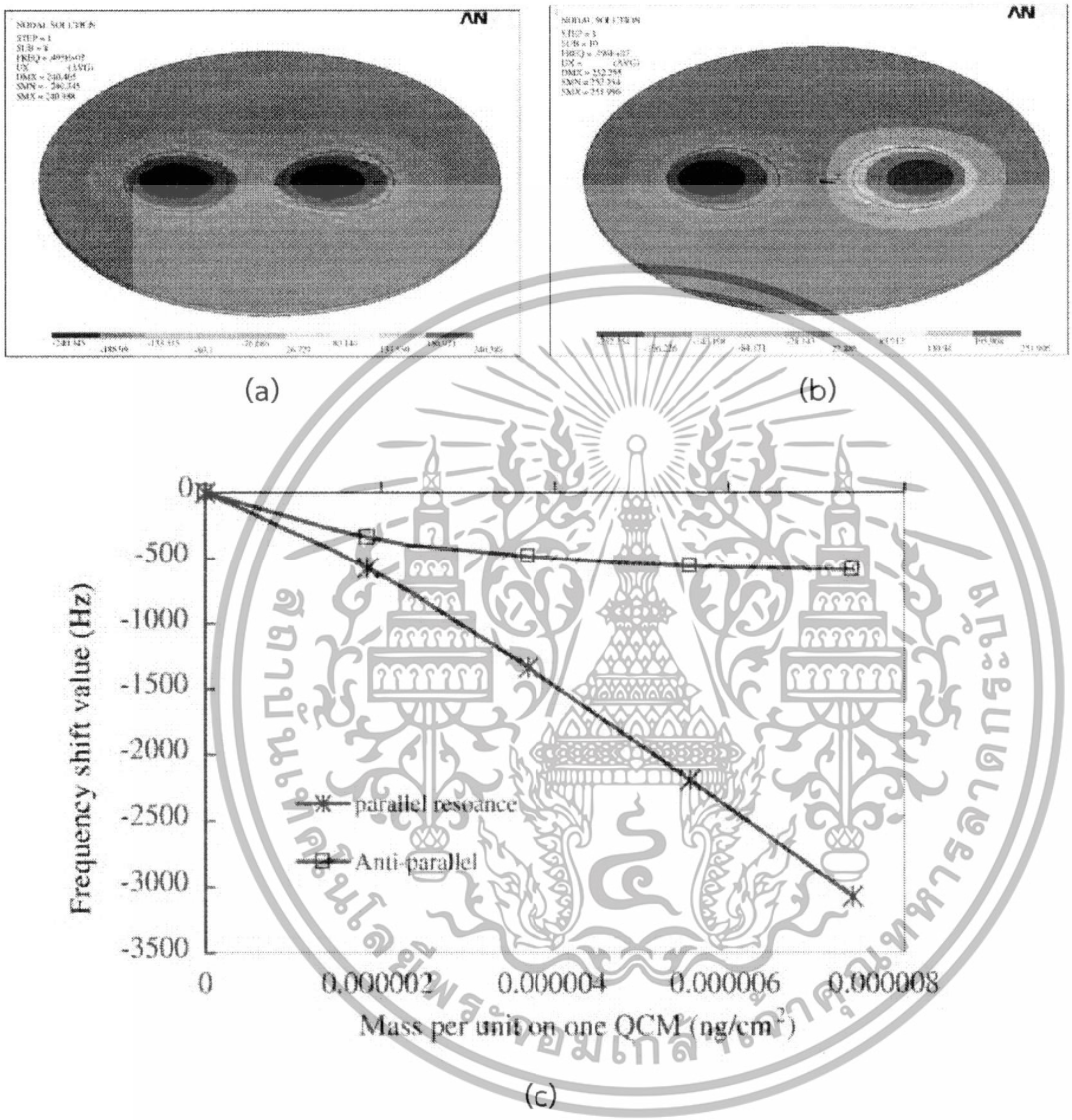

Figure 2.11. The vibration shapes of (a) the TSM parallel resonance and (b) anti-parallel resonance of QCM pair (c) mass deposited on one QCM surface, both parallel and anti-parallel resonance frequencies.

The theoretical calculation can provide insightful understanding of interference effects for MQCM and can be used to guide MQCM design. However, it cannot provide accurate prediction for real world 3D MQCM structures as 3D geometries such as edge effects of electrode layers and crystallographic orientation of electrode relative to quartz substrate cannot be directly included in the analysis. 3D simulation is thus required for more accurate design and analysis of MQCM devices. Recently, 3D simulation of a MQCM model with two symmetric QCMs on a monolithic quartz crystal plate has been reported [48]. The simulation is conducted using finite element analysis (FEA) method with the commercial software package, ANSYS. The ANSYS package provided electro-mechanical coupled field element, which includes piezoelectric effect. The full piezoelectric tensor formulation included in the package can account for anisotropic behaviors of piezoelectric crystals. 3D FEA simulation can thus provide considerably more quantitative information than 1D theoretical modeling. In addition to frequency interference, self-mass sensitivity and mutual-mass sensitivity, vibration mode shape and crystallographic orientation of an electrode pair can be obtained from 3D simulation results.

For example, 3D simulation reveals the phenomenon of resonance splitting into parallel and anti-parallel mode for a QCM pair when two identical QCMs operate at almost the same resonance frequency. The vibration shapes of the TSM parallel resonance and anti-parallel resonance of QCM pair are illustrated as shown in Figure 2.11 (a) and (b), respectively. The diameter, thickness of both gold electrodes and spacing between them are 6mm, 100 nm and 3 mm, respectively. The parallel resonance (with f_1 = 4954960.1 Hz) results in the shear displacement overlapping of two QCMs, while antiparallel resonance (with f_2 = 49571192.6 Hz) cause the two QCMs to have opposite displacements. The displacement overlap in parallel resonance mode induces the acoustic coupling between two channels significantly. With mass deposited on one QCM surface, both parallel and anti-parallel resonance frequencies decrease. Figure 2.11 (c) shows the frequency shift as function of mass absorption on one QCM channel for QCM pair with 100 nm thickness electrode. It can be seen that the parallel resonance frequency shift is linearly proportional to the mass absorbed while the anti-parallel resonance one decreases non-linearly and the sensitivity of the frequency shift for anti-parallel resonance decreases as the mass absorption per unit area increases. This results from the fact that the mass absorbed on one QCM results in asymmetrical detuning the two resonators and hence the splitting between the parallel and anti-parallel resonance frequencies increased.

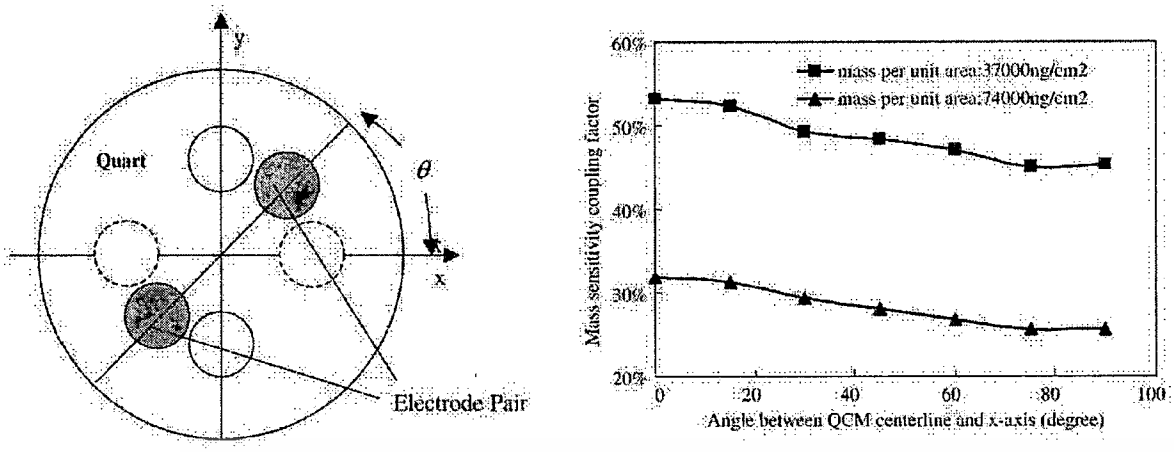

Figure 12. Frequency coupling factor of the QCM pair as a function of the angle θ.

Moreover, 3D simulation can provide the effect of anisotropic piezoelectric property of AT-cut quartz plate in X–Y plane on interference. The coupling between a QCM pair is not the same for different angle θ to the x-direction as schematically shown in Figure 2.12 (a) because acoustic waves propagate with different velocities in different directions within the crystal plate. In this analysis, the interference is evaluated in term of mass–frequency influence coupling factor, which is defined by:

$$\alpha_i = \frac{\psi_{i-j}}{\psi_{i-i}} \tag{2.5}$$

$$\psi_{i-j} = \frac{\Delta f_i}{\Delta m_j} \tag{2.6}$$

where Δm_j is the mass per unit area added on the surface of QCM-j, Δf_i the frequency shift of QCM-i, i and j are the label of individual QCM. Figure 2.12 (b) shows the frequency coupling factor of the QCM pair as a function of the angle, θ. It can be seen that the coupling strength is lowest when QCM pair located in y-direction (θ = 90°) and the dependency on θ has two fold symmetry around x and y axes. In addition, it is found that the frequency split between parallel and anti-parallel of QCM pair decreases as θ increases

from 0° to 90°. The results indicate that the thickness shearing deformation transferred in x-direction of quartz crystal is more than that in y-direction. Therefore, QCM pair will be matched when their locations in x-y plane are at the same angle or 180° apart. This consideration should be taken into account in MQCM design.

Interference among QCMs in conventional MQCM may be alternatively avoided by mean of successive oscillation or multiplexing. In this case, only one or a few QCMs can resonate at a time so that interference can completely be eliminated. This scheme is limited to applications, which do not require real-time or high speed measurement.

In addition to acoustic interference, other problems of conventional MQCM include spurious vibration, limited sensitivity and limited size of QCM electrodes. Spurious vibration occurs due to coupling between thickness shear (TS) and other modes including thickness flexural (TF), face shear (FS), thickness twist (TT) and higher order modes. The coupling between TS and TF occurs due to crystal edge effect and it is strong because both modes have a similar displacement field [53]. The coupling between TS and FS or TS and TT is relatively weak. In addition, the shear rotation about the z-axis is more than an order of magnitude less than the shear rotation about the x-axis or deflection in the y-direction [54].

Other important problems of MQCM are the limitation of sensitivity and electrode size. The mass sensitivity and diameter of MQCM electrode are both limited by the thickness of the crystal. The sensitivity is proportional to the square of resonance frequency, which is inversely proportional to quartz thickness. The thickness of quartz crystal is limited to around 100 μm because thinner quartz plates are too fragile and cannot be practically processed. The thickness constraint also limits diameter of electrode because small-diameter electrode QCM does not resonate or resonates with a very low Q factor if the diameter of the electrode to thickness of the crystal ratio is below 5 [55]. This limits miniaturization of conventional MQCM devices.

2.2.2 MQCM based on modified quartz substrate structure

Several methods have been developed to eliminate or minimize interference and other problems of conventional MQCM. Modification of quartz substrate structure is found to be the most effective approach to solve the problems. In this section, various MQCM schemes based on modification of quartz substrate structure will be described.

2.2.2.1 MQCMs with mesa shape designs

The most basic concept for minimizing the coupling of acoustic energy between adjacent QCMs is to increase the difference in the resonance frequency between the

electrodes and inter-electrode portions of the quartz plate. A direct way to increase the resonance frequency difference is to vary the quartz thickness between the electrode and inter-electrode regions. This can practically be done by means of standard micromachining process. The structure with varying quartz thickness in steps are commonly termed, *Mesa*, which can be subdivided into plano-mesa [56, 57], plano-inverted-mesa [58, 59], bi-mesa [56, 57, 60] and bi-inverted-mesa [61]. For plano-mesa structure, square cavity with reduced quartz thickness is formed in the inter-electrode regions while the other side is still planar. On the other hand, square trenches are created in the electrode regions for plano-inverted-mesa structure. For bi-mesa and bi-inverted-mesa structures, square cavities are made symmetrically on both sides.

The interference and acoustic energy trapping behaviors of the quartz mesa structure of different designs have been experimentally demonstrated [57, 62]. It has been shown that the acoustic energy of the thickness shear mode of mesa-shaped MQCMs is considerably better confined within electrode regions than that of conventional MQCM and the separation between two adjacent resonators can thus be reduced using mesa-type MQCM. With inverted-type-mesa designs, QCM resonators can operate at higher resonance frequency than those of non-inverted designs because the quartz plate thickness in the electrode area is decreased [59, 61, 63, 64]. This scheme can thus solve the limitation of mass sensitivity of conventional MQCMs. Comparing between bi-mesa and plano-mesa schemes, QCMs with bi-mesa designs exhibit better resonance characteristics with lower spurious vibration mode and higher Q-factor than plano-mesa configuration because of the symmetric structure [56]. However, plano-mesa scheme are more practical than bi-mesa structure because fabrication process is considerably simpler and its top planar surface is more suitable for most applications than step-profile surface [45]. Therefore, plano-inverted-mesa structure has been most commonly used in MQCM devices.

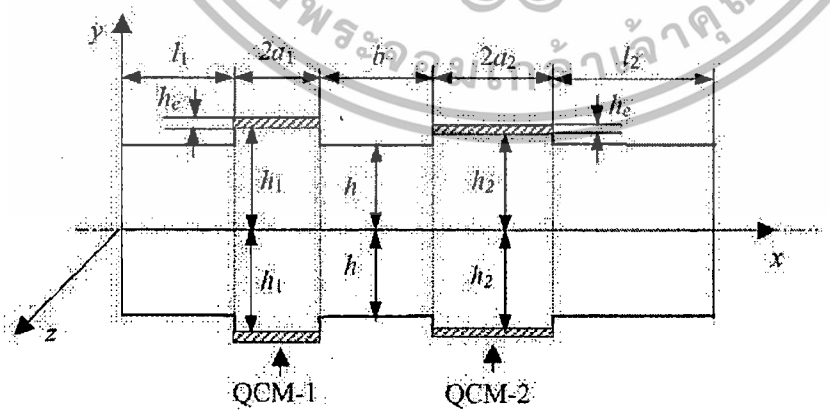

Figure 2.13. Two generalized mesa-shaped QCMs on a monolithic quartz crystal plate.

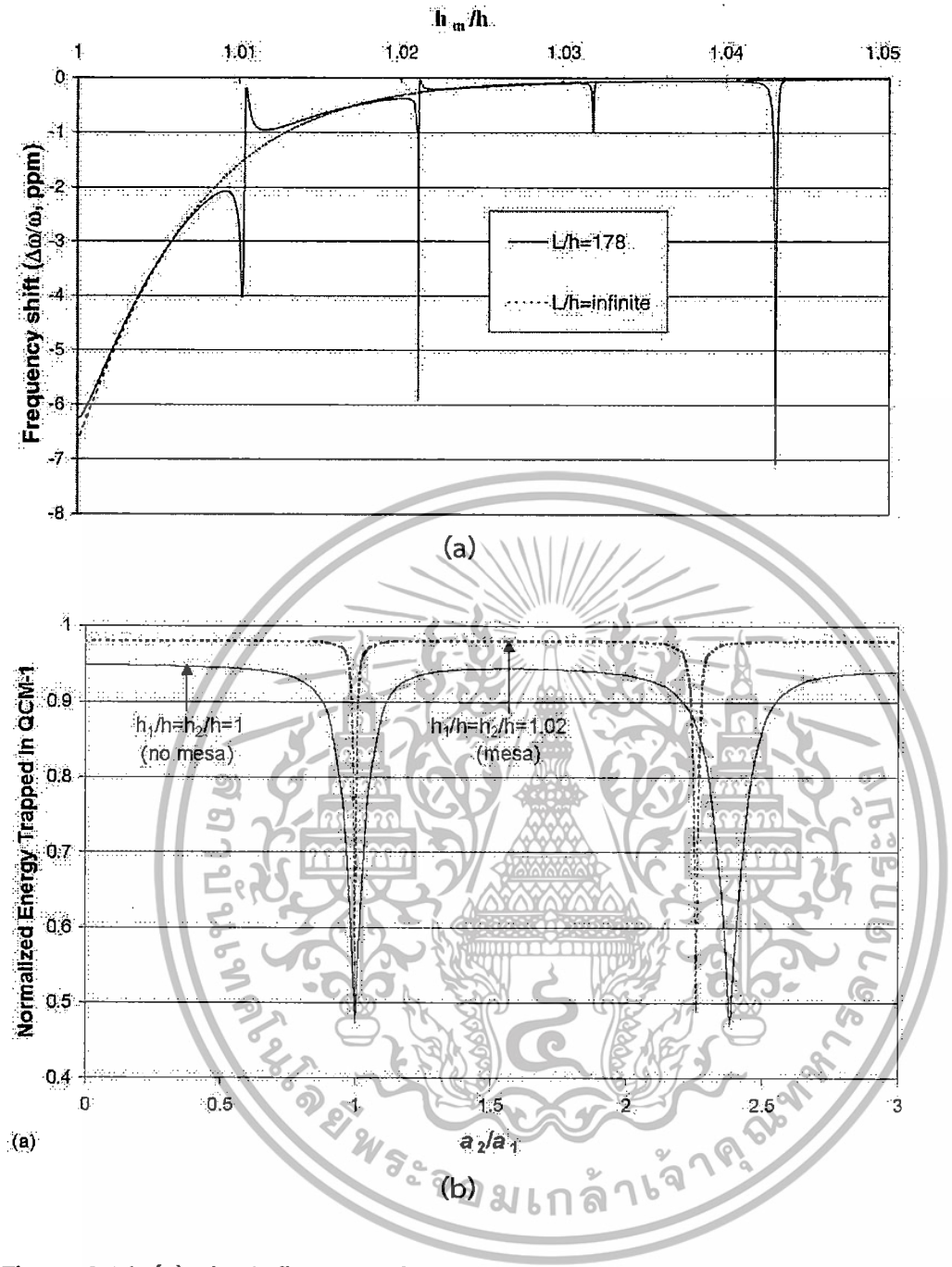

Figure 2.14. (a) The influence of mesa height on frequency interference, **(b) The effect of the relative electrode width (a_2/a_1) on energy trapped in QCM-1.**

Recently, bi-mesa MQCM has been theoretically analyzed [65, 66] based on one-dimensional modified Mindlin's theory, which has also been used for analysis of conventional MQCMs. Two generalized mesa-shaped QCMs on a monolithic quartz crystal plate as illustrated in Figure 2.13 is used as a model to represent two adjacent QCMs in

MQCM structures. Two quartz crystal microbalances, QCM-1 and QCM-2, are formed on the surfaces of two mesas with quartz thickness of $2h_1$ and $2h_2$, mesa widths of $2a_1$ and $2a_2$, and distances to edges of l_1 and l_2, respectively. The thickness of the electrode, quartz thickness outside electrode regions, separation between mesas and the total quartz length are h_e, 2h, b and L, respectively. In this analysis, the Mindlin's equations for the coupled vibrations of TS and TF mode are used and piezoelectric effect is neglected. The kinetic and potential energies per cycle in the different portions of the mesa structure are computed. The kinetic energy consists of deflective and rotational kinetic energies while the potential energy contains rotational and extensional potential energies.

The interference behaviors of mesa shaped MQCM are evaluated in terms of frequency interference (FI) described in the previous section and normalized energy-trapped of QCM-1, which is defined as the ratio of energy trapped within QCM-1 section to the total energy in the quartz plate. The effects of mesa height, electrode sizes, spacing between two QCMs and QCM position on interference behaviors are acquired from the theoretical calculation. The influence of mesa height on frequency interference is shown in Figure 2.14 (a). The ratio of electrode width in this example is $a_2/a_1 = 0.95$, which is in a strong fundamental coupling region. The other fixed dimensions include $a_1/h = 20$, $b/h = 20$ and $l_1/h = l_2/h = 40$ ($L/h = 178$). The heights of the two mesas, h_1 and h_2, are both equal to h_m. It can be seen that FI decreases monotonically with increasing mesa height for the infinite plate case. When the plate has a finite length, FI graph still follows the same curve but periodical spikes occur. These peaks correspond the coupling of TF and TS modes due to the existence of boundaries. It can be notice that a small relative mesa height ($h_m/h > 1.03$) can effectively reduce frequency interference between two adjacent QCMs. Thus, only small etching depth is needed to form mesa structure with low interference and this can considerably simplify mesa-MQCM fabrication process. However, strong coupling regions due to the presence of a boundary still exist for mesa structure with specific relative heights and thus these must be avoided in the mesa-MQCM design.

In this analysis, the energy trapped in QCM structure has been considered with different MQCM parameters. The energy trapped in QCM-1 is determined when only QCM-1 is under excitation. For mesa-MQCM with above parameters, energy trapped in QCM-1 is found to increase as relative mesa height increases and negative peaks, where the trapped energy decreases markedly, also appear at the same relative mesa height as those of FI as shown in Figure 2.14 (a). At these peaks, nearly half of the energy is found to escape to other parts of the plate in the form of a flexural wave [66]. The effect of the relative electrode width (a_2/a_1) on energy trapped in QCM-1 for mesa and no mesa structures is

demonstrated in Figure 2.14 (b). It is seen only small relative mesa height of 1.02 can considerably increase energy trapped in QCM-1 except the regions near the peaks of fundamental ($a_2/a_1=1$) and anharmonic coupling ($a_2/a_1>1$). At the peaks of coupling regions, the maximum loss from QCM-1 can be half of the total acoustic energy and Most of the escaping energy is trapped in QCM-2. The main benefits of the mesa structure are to narrow the range of strong coupling region and reduce interference outside these regions. These give considerable flexibility for the design of MQCM devices.

2.2.2.2 MQCMs with convex shape designs

Mesa design can offer considerable improved MQCM performance in terms of interference reduction and sensitivity enhancement. However, the straight edge mesa structure cannot effectively correct mode coupling problems between the fundamental TS and spurious modes [62]. As illustrated in the previous section, the coupling between TS and TF modes remain quite substantial in mesa-shaped MQCM. The coupling is undesirable because energy is taken from the usable frequency vibration and results in damping and lower Q-factor. High Q-factor is important for ultra-sensitive detection in liquid mode. Several structures including dual-step mesa [62], multi-step mesa [67] and spherical convex [55, 68-70] structures have been developed to reduce mode coupling problems so that the energy of the oscillation is better trapped at the center and very little dissipation occurs at edges. Among these, the spherical convex-shape structure can theoretically separate vibrating modes most effectively. Spherical convex-shaped MQCMs, which include plano-convex [68] and bi-convex [55, 69] designs as illustrated in Figure 2.15 (a), have been reported.

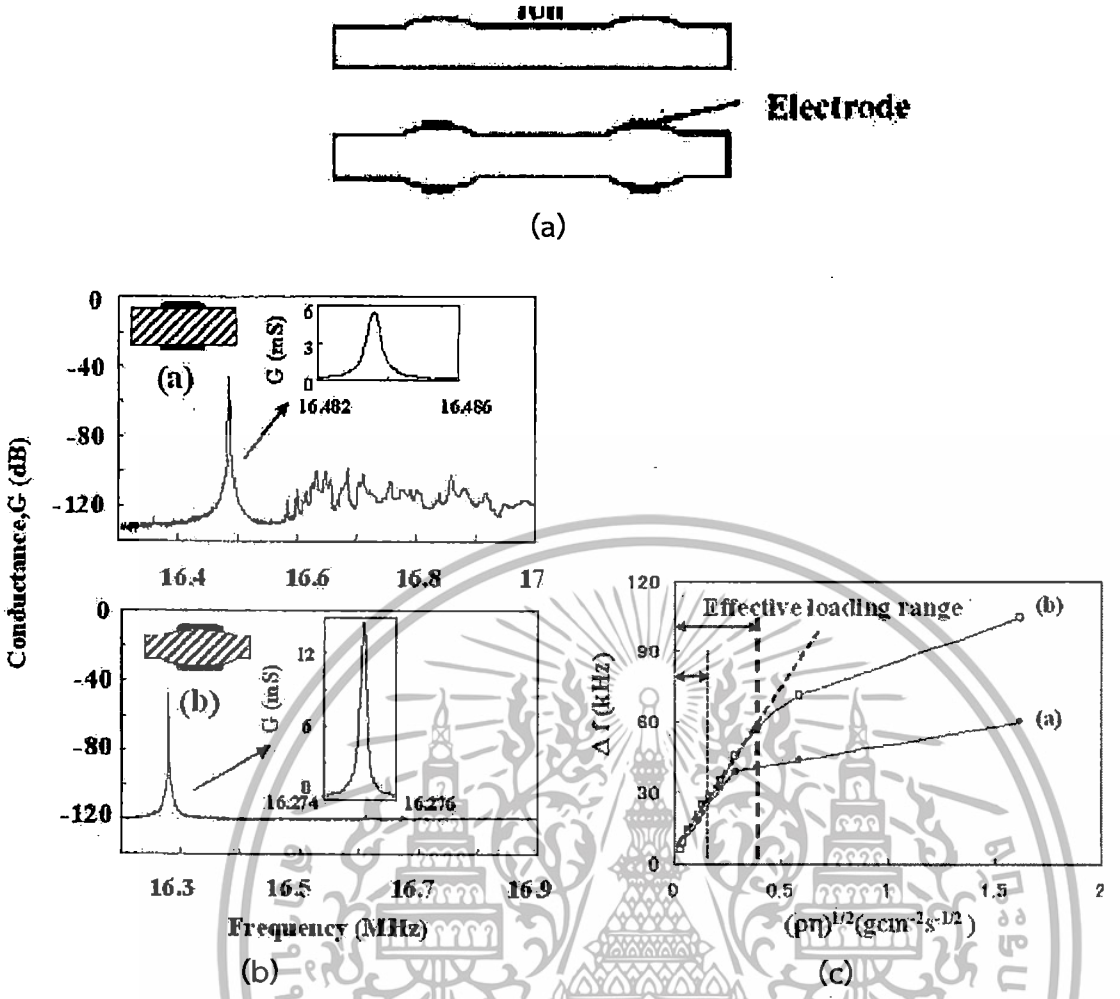

Figure 2.15. The resonant spectra in air of the spherical bi-convex and reference planar QCM structures.

Some sophisticated processes have been developed to realize convex-shaped 3D QCM structures. Firstly, planoconvex quartz-crystal unit is fabricated based on a laborious mechanical polishing method [68]. Recently, the miniaturized beveled bi-convex QCM has been developed by photoresist thermal melting [69] and photoresist reflow with solvent vapor process [55]. The later process is particularly promising because diameter, curvature and height of spherical convex shape can be well controlled with moderate cost and reproducibility. In this process, spherical shaped photoresist on quartz substrate is formed after photolithographic patterning and reflow in a suitable organic solvent. Reactive ion etching in SF_6/Xe gas mixture [69] is then used to transfer spherical structure into quartz-crystal substrate. Spherical bi-convex MQCM structures with diameter ranging from 100 μm to 2 mm and height from 1 to 7 μm have been realized and the resonant characteristics have been studied.

The resonant spectra in air of the spherical bi-convex and reference planar QCM structures are shown in Figure 2.15 (b). It is evident that the spherical bi-convex QCM exhibits very sharp resonant peak with negligible spurious vibrating modes while the planar QCM resonates with numerous spurious vibration. The spherical convex-shape can effectively decouple the vibrating modes in QCM. An optimum Q-factor of ~80000, which is twice higher than that of the 100 μm-thick planar QCM, is obtained from the spherical convex shape with diameter and height of 2 mm and 1.7 μm, respectively. The spherical bi-convex and planar QCM are also studied in viscoelastic liquid using glycerol/water mixtures contacted on one side of QCM. The frequency shift versus square root of density-viscosity product, $(\rho\eta)^{1/2}$, is shown in Figure 2.15 (c). The effective loading range in Figure 2.15(c) is defined as the range in which the resonance frequency shift is linearly proportional to $(\rho\eta)^{1/2}$. It is seen that the effective loading range of the spherical bi-convex QCM is considerably larger than that of the planar QCM. In addition, the maximum viscosity in this region for the spherical biconvex QCM (η = 128 mPas) is found to be approximately *5* times larger than that for the planar QCM (q=24.1 mPas).

2.2.2.3 MQCMs with x-axis inversion

X-axis inversion [71-73] is a useful method that can increase the difference in the resonance frequency between the electrode and inter-electrode portions of the quartz plate. An advantage of this technique is that it does not require physical removal of quartz material from the plate. It is the phenomenon that x crystallographic axis of quartz crystal is locally rotated by 180° under a specific thermal treatment as illustrated in Figure 2.16 (a). In the treatment process, an AT-cut plate is coated with a thin Cr or NiCr film on a desired pattern and then is heated at 520-560°C in a vacuum. X-axis inversion would occur only in the area under the metal film because of the mechanical stress induced by the thermal expansion difference between the quartz plate and the film. In the inversion area, the y axis is also inverted and the cut angle changes from $+\theta$ to $-\theta$ AT-cut. Alternatively, x-axis inversion can be formed by applying heating current to the metal film. In this case, heat is more concentrated on the patterned metal film and x-inversion can occur at a relatively low temperature of 480-500°C with DC current density of 13.3-16.7 mA/mm^2. This method is advantageous due to relatively low process temperature but it requires additional electrical connection, which can be cumbersome for complex patterns.

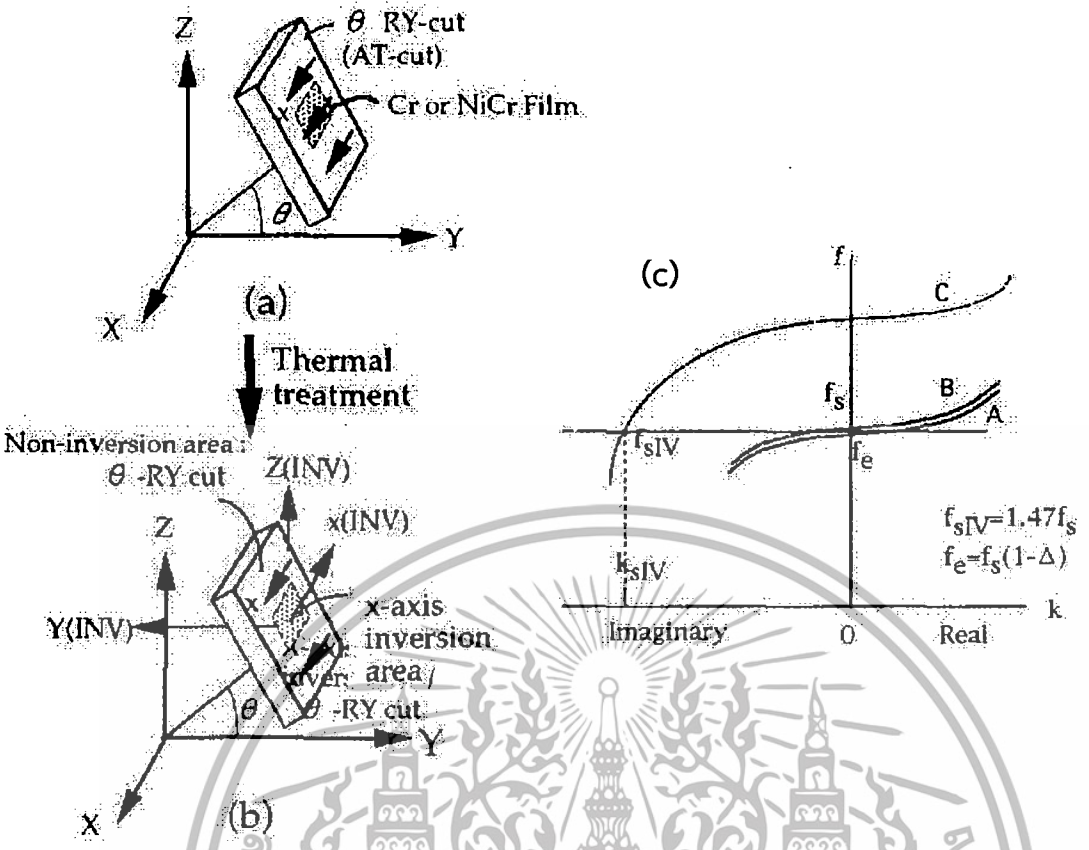

Figure 2.16. X-axis inverted area exhibits different dispersion characteristics of the elastic wave propagation from non-inverted one.

X-axis inverted area exhibits different dispersion characteristics of the elastic wave propagation from non-inverted one as illustrated in Figure 2.16 (b). Graph A, B and C in the figure are the dispersion curves for non-inverted AT-cut quartz areas with and without electrode and x-axis inverted area with no electrode, respectively. The graphs indicate that the cut-off frequency of the x-axis inverted area is higher than that of the non-inverted area by a factor of 1.47. As a result, plate wave excited at the electrode area is highly attenuated as it propagates into the x-axis inverted area. The attenuation of the wave in the x-axis inversion area is proportional to the ratio of W and H, where W is the width of the x-axis inversion area and H is the plate thickness. From theoretical calculation, attenuation is estimated to be more than 70 dB for W/H = 3. Thus, adjacent resonators can be effectively mechanically isolated by an interposed x-axis inverted region and x-axis inversion can be applied for acoustic decoupling in MQCM device.

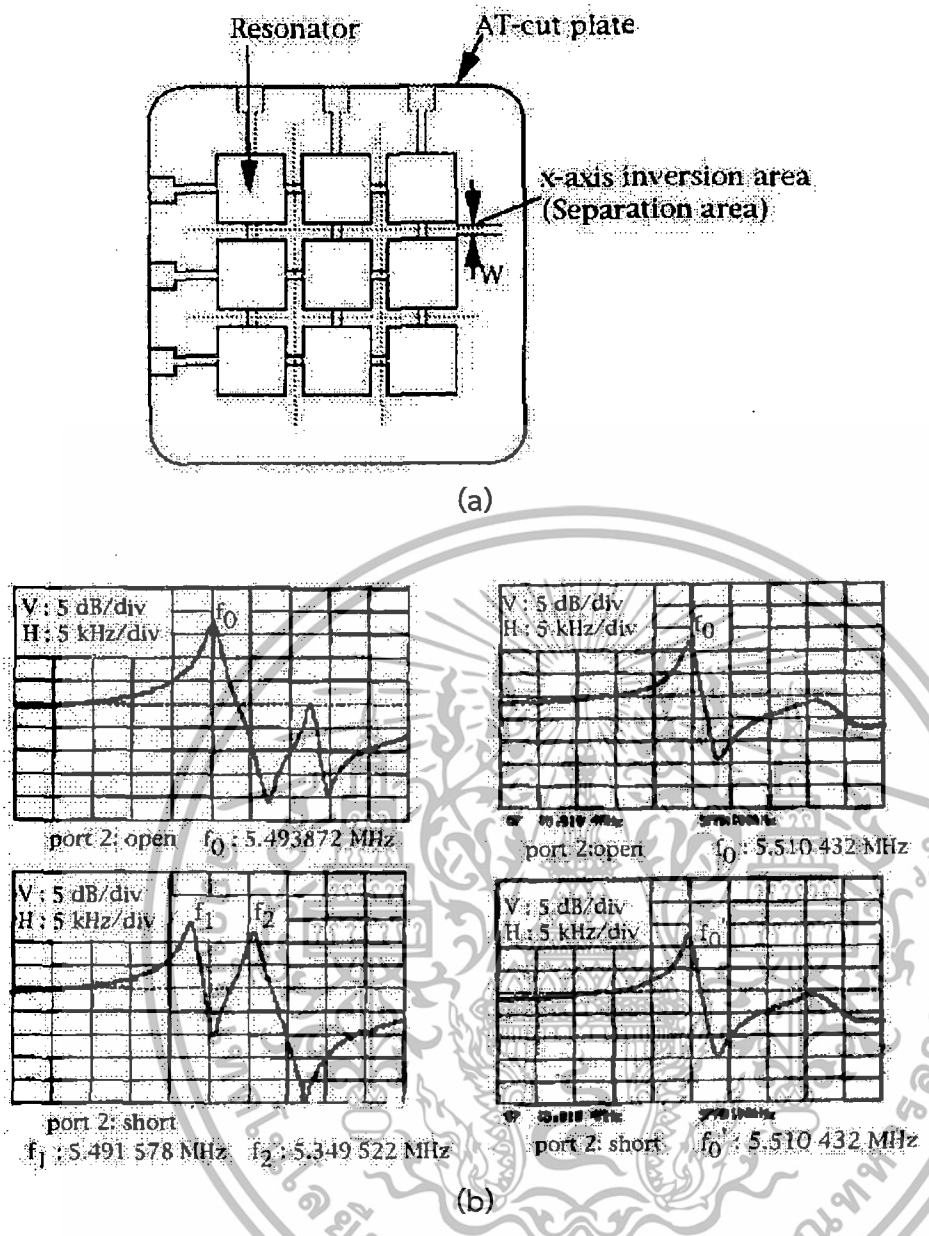

Figure 17. (a) MQCM structure with x-axis inversion
(b) the impedance- frequency response of the first QCM is measured.

MQCM structure with x-axis inversion has been proposed as illustrated in Figure 2.17 (a) [71]. In the structure, x-axis inversion areas are formed in the space between adjacent QCM electrodes. X-axis inversion areas are first created by Cr film deposition and thermal treatment. Quartz surface is then lightly etched by buffered oxide etching solution and Cr film is etched way, leaving the pattern of x-axis inverted region on substrate. Finally, QCM electrode film is deposited by sputtering or evaporation and pattern of electrode array is aligned to the x-axis inverted pattern by standard photolithography. The acoustic decoupling

between two adjacent QCMs separated by x-axis inversion region has been experimentally demonstrated by mean of two-port network measurement. In the measurement, ac input is applied to the first QCM at port 1 while both electrodes of the second QCM at port 2 are either open or short and impedance- frequency response of the first QCM is measured. Figure 2.17 (b) shows frequency response for conventional MQCM with no x-axis inversion area. The length and width of QCMs electrodes and spacing between them are 4 mm, 3 mm and 1.5 mm, respectively. It can be seen that one resonant peak occurs when port 2 is open while two resonant peaks appear at different frequencies when port 2 is short.

This indicates the mechanical coupling between two resonators under the short circuit condition. Figure 2.17 (c) demonstrates the resonance characteristics of similar MQCM with 0.8 mm wide x-axis inversion region between the QCMs. It is evident that the frequency response of the first QCM is not affected by the termination of the second QCM. This result demonstrates that both resonators are effectively isolated by the x-axis inversion area.

2.2.3 MQCM sensing platforms

An array of QCMs may be differently formed into a variety of MQCM sensing platforms for various types of sensing or measurement applications. In this section, potential MQCM sensing platforms will be explained [45].

2.2.3.1 MQCM as a static multichannel detector

In this platform, identical QCMs in an array are deposited with different sensing layers or receptors and MQCM is set in a simple sample cell as illustrated in Figure 2.18. Additionally, one channel of MQCM should be used as a reference, which has no receptor, to compensate for the influences from the temperature, viscosity, and density of the sample. In these cases, simple measurements with one drop of an electrolyte solution without an electrolytic cell are also possible [45]. Different receptors will accept additional mass from target species by means of binding, adsorption or deposition causing resonance frequencies of underlying QCMs to change accordingly.

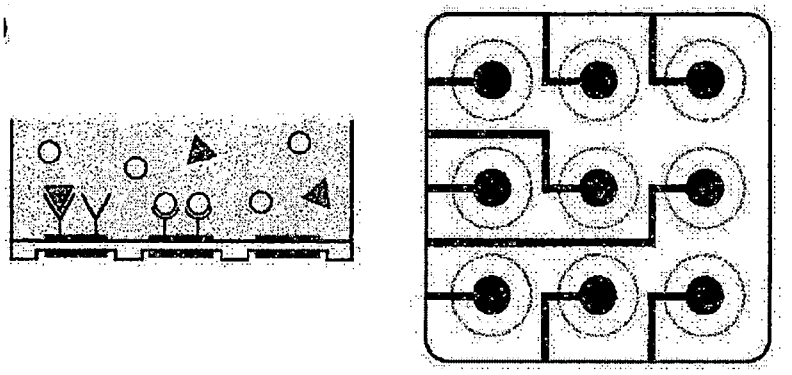

Figure 2.18. MQCM with static cell detection.

The main type of applications for this platform is multicomponent analysis, which is used to identify a multicomponent mixture and/or its ingredients with respective concentrations. There are three main schemes for multicomponent analysis. Firstly, QCMs are bound with different receptors, which are selective to individual component in the target mixture. The resonance frequency shift of QCM coated with each receptor can be used to directly identify the presence of each component and determine its concentration. The scheme can work only when the receptors with very high specificity to target species are available. Existing receptors with such a specific property include complementary DNAs and antigen/antibody [10, 34, 74]. Thus, this technique can only be applied to some specific biosensing while it cannot generally be implemented for chemical and gas sensing.

Secondly, a group of different receptors coated on QCMs has low selectivity towards a set of components in the mixture. When receptors are exposed to target components, they respond differently according their selectivity, producing resonance frequency shifts to related QCMs. The presence and concentration of all target components are then determined from recognized relationships of selectivity parameters of all components. The number of different receptors should be the same as the number of components to obtain unique determination. Examples of receptors in this system are ligands for metal ions [75, 76]. In an application, a QCM system with four different ligands having different affinity toward four metal ions can be used to determine the concentrations of the four metal ions [45].

Lastly, an array of different receptors having wide sensitivities towards various components is used to recognize the whole mixture. In this case, components in the mixture and their individual concentrations cannot be resolved. Most receptors found in nature fall within this category. These include gas-sensitive polymeric and organic materials, electrochemical electrode materials and biochemical enzymes. The QCM array with these receptors gives a pattern of resonance frequency shifts resulting from different receptors'

sensitivities toward various ingredients in the composite, which can be analyzed based on pattern recognition methods. Commonly used pattern recognition methodologies are principal component analysis (PCA) [77-83], linear discriminant analysis (LDA) [78, 84, 85] and neural network [81-83, 86]. The main applications for this scheme are odor sensor or electronic nose and taste sensor or electronic tongue.

2.2.3.2 Series MQCM as a multichannel detector in the flow injection analysis

A series of identical QCMs with different receptors can alternatively be applied to flow injection analysis for real-time detections as illustrated in Figure 2.19. There are some important considerations when MQCMs are operated in a flow injection system. Firstly, the structure of MQCM surface in contact with fluid flow should be planar and smooth so that the solution flow will not be disturbed. Thus, MQCM structures with non-smooth surfaces including bi-mesa, bi-inverted-mesa and bi-convex may not be suitable for flow injection analysis [45].

Secondly, analyte should be uniformly dispersed throughout the flow chamber so that all QCMs see the same sample concentration. The effect of flow chamber geometry and flow parameters on sample dispersion in flow injection system with integrated MQCM device has recently been studied by fluid dynamic simulations and flow injection experiments [87]. Figure 2.19 (b) and (c) show simulated velocity profile of fluid flow at a flow rate of 100 µl/min in MQCM chambers with circular and rectangular designs, respectively. It can be seen that MQCM with circular chamber design suffers from non-uniform sample distribution due to turbulent effect while such problem does not occur to MQCM chamber with rectangular design[88]. The results agree to experimental observation that there is a significant variation in resonance frequency shift responses of identical QCMs located in the circular chamber.

A flow injection system containing inverted-mesa MQCM in 20mm×20mm×0.7mm square chamber has been demonstrated [14]. The influence of flow rate on uniformity of analyte distribution and the resonant characteristics of QCM is also studied. Figure 2.19 (d) shows resonant spectra of a QCM under different flow rates. It is seen that flow rate considerably affects the resonant behaviors of QCM. In addition, spurious oscillation modes induce under low and high flow rate conditions and undesired oscillation is minimized at an optimum flow of 500 µl/s. Thus, flow rate is another important parameter that must be optimized when QCM operates in a flow injection system.

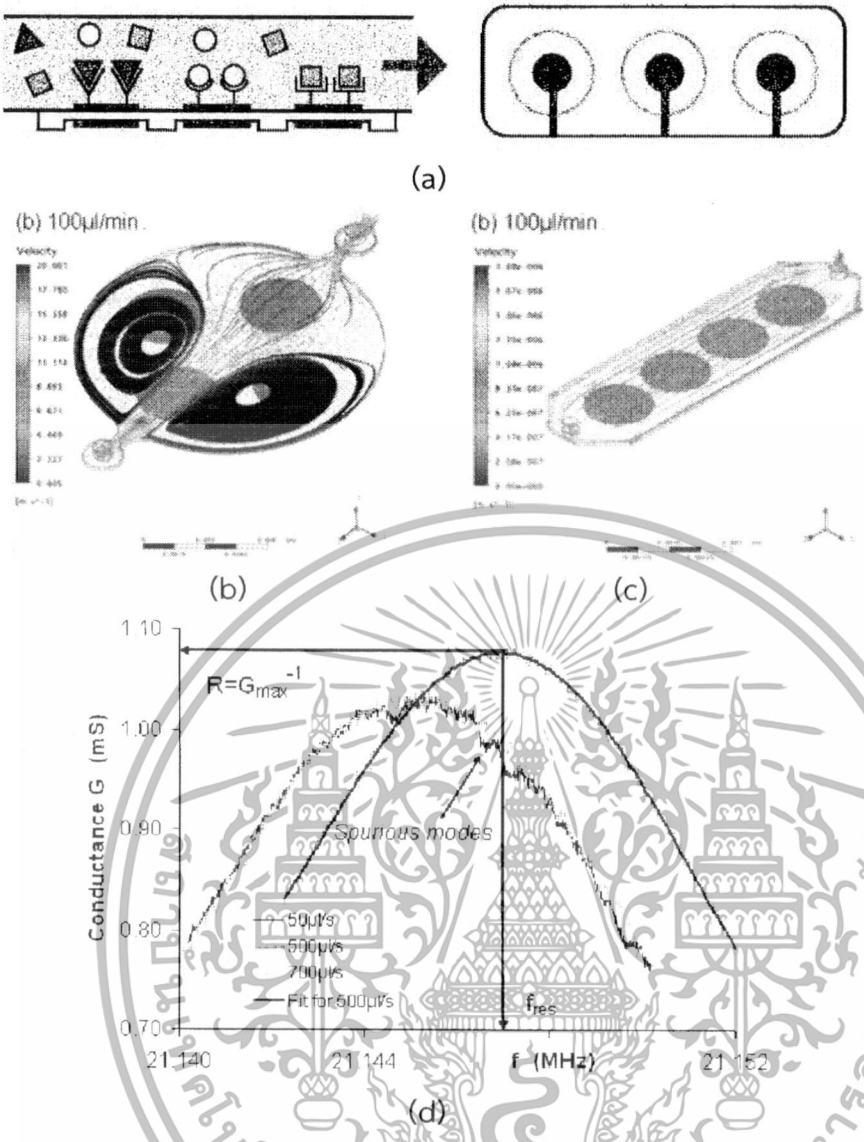

Figure 2.19. A series of identical QCMs with different receptors applied to flow injection analysis for real-time detections.

2.2.3.3 Multifrequency QCM as a multi-sensitivity and multi-dynamic range detector

Various QCMs in MQCM can be designed to operate different resonance frequencies. This platform is termed *multi-frequency QCM (MF-QCM)*. MF-QCM can typically be made in two configurations as shown in Figure 2.20. The first structure of multi-frequency QCM array is based on inverted-mesa structures with different mesa thickness [89] as illustrated in Figure 2.20 (a). This structure can be formed by standard mesa micromachining process with additional pattering and etching steps. By this scheme, resonance frequency, mass sensitivity and dynamic range of QCMs can be varied over a wide range of magnitude.

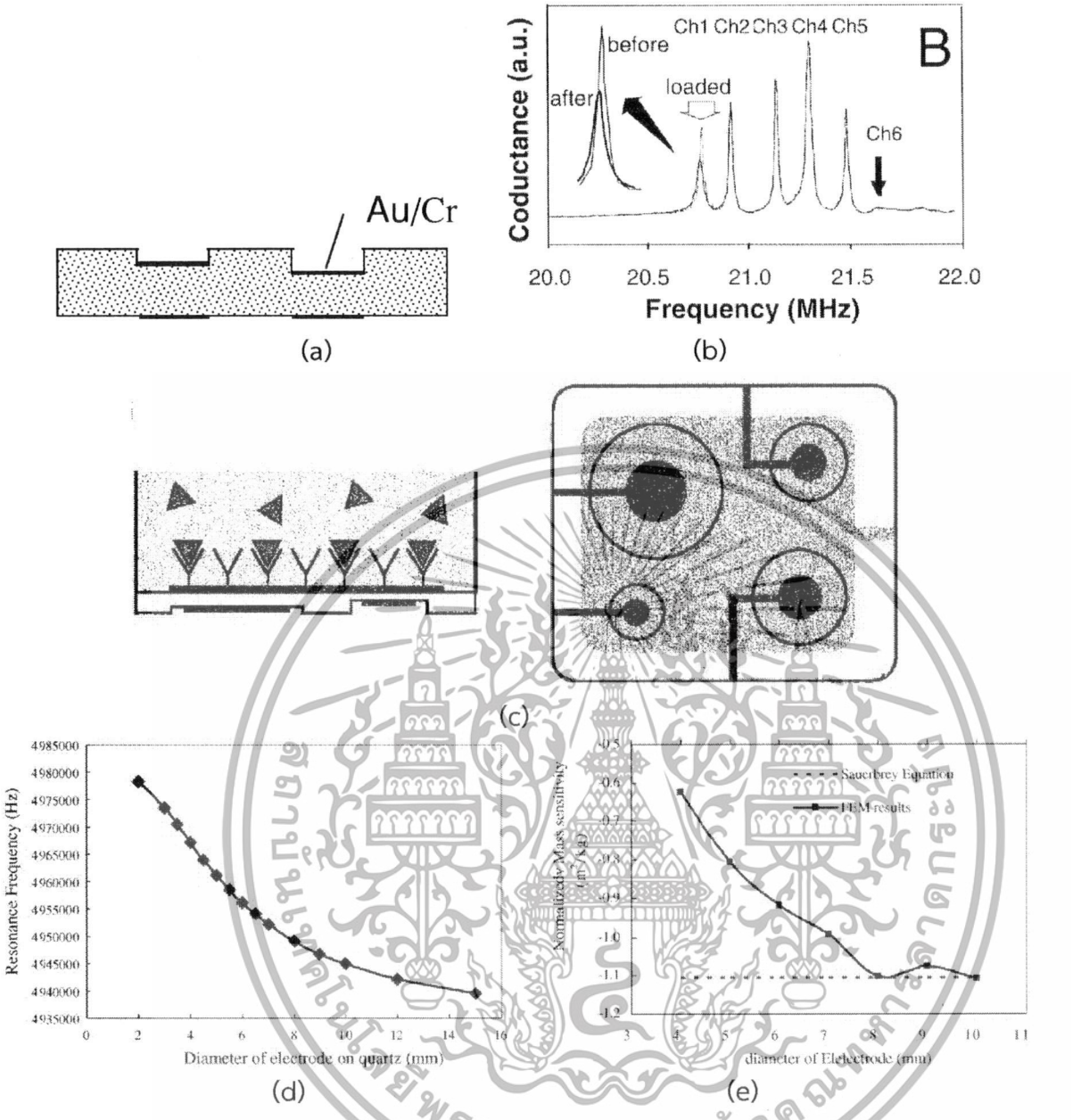

Figure 2.20. Multi-frequency / Multi-dynamic range MQCM.

Figure 2.20 (b) shows typical resonant characteristics of a 6-channel MF-QCM. The thicknesses of 2 mm circular QCM diaphragms are varied from 77 to 81 μm and the corresponding resonance frequencies are from 21.7 to 20.75 MHz. With decreasing quartz thickness, the dynamic range decreases while the resonance frequency and mass sensitivity simultaneously increases. Thus, MF-QCM can provide multi-sensitivity and multi-dynamic-range functionalities [14, 45], which is highly valuable for general applications whose sample concentration and detection range are unknown. For multisensitivity and multidynamic range purpose, all QCMs may be modified with only one kind of receptor and high

sensitivity and wide dynamic range of particular analyte can be realized in one experiment if MF-QCM is properly designed. The multisensitivity and multidynamic range QCM is useful for a wide variety of applications including chemical sensing, bio-sensing and monitoring of surface processes including electrochemical reactions. Moreover, QCMs in an array may be modified with different receptors for multicomponent analysis with mulit-sensitivity and/or multi-dynamic range capability.

The second kind of MF-QCM is an array of QCMs with the same quartz thickness but different electrode sizes as shown in Figure 2.20 (c). This scheme is advantageous in term of fabrication process, which is the same as standard QCM fabrication. The dependence of resonance frequency on electrode size can be accurately obtained from 3D finite element simulation [48]. In this simulation, the thickness of AT-cut quartz plate and gold electrode are 0.338 mm and 100 nm, respectively. Figure 2.20 (d) illustrates the simulated resonance frequency of TSM as function of the diameter of electrode on QCM surface. It is seen that the resonance frequency of TSM is decreased as electrode size increases. In addition, the resonance frequency becomes less dependent on diameter for very large diameter values and it will eventually reach the frequency value of one-dimensional theory given in eq. (2), in which the electrode width is assumed to be infinite. The simulated mass sensitivity as a function of the electrode width is shown in Figure 2.20 (e). It is seen that the mass sensitivity increases with increasing electrode width and it approaches the value given by Sauerbrey equation (eq (1)). Thus, the mass sensitivity reduces while resonance frequency increases as electrode width decreases. This is in contrast to thickness dependence, in which resonance frequency and mass sensitivity simultaneously increase with decreasing thickness. This is because more vibration energy is dispersed into the surrounding quartz plate region when the electrode width is reduced. Moreover, it can be seen that both resonance frequency and mass-sensitivity can be tuned over a relatively narrow range. Thus, this MF-QCM scheme has limited applicability.

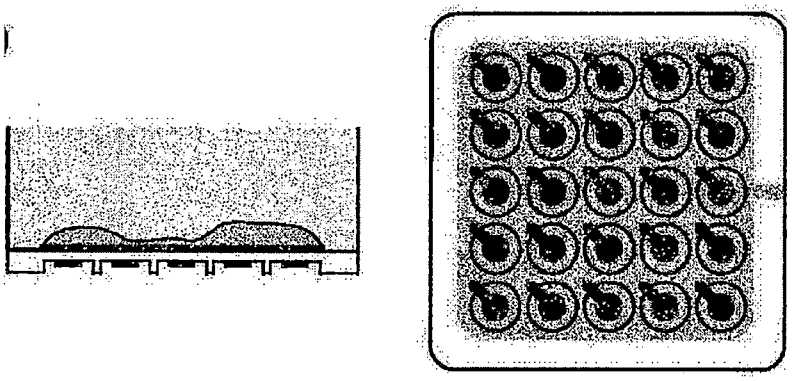

Figure 2.21. MQCM platform for 2D mass mapping.

2.2.3.4 Two-dimensional mass mapping

MQCM is potentially applicable to mapping of the two-dimensional (2D) distribution of mass changes on the solid surfaces [45]. The structure of MQCM platform for 2D mass mapping is illustrated in Figure 2.21. It is a high density QCM array, in which all QCMs have identical electrode and receptor. MQCM mass mapping scheme is advantageous over the other QCM based mass mapping scheme based on scanning-electrode quartz crystal analysis (SEQCA) technique [90, 91], which can only provide the qualitative mapping of mass distribution. In SEQCA, the quantitative mapping of mass distribution is not possible because mechanical oscillation propagates over the whole quartz plate, which is covered by large area gold electrode. In addition, MQCM mapping is faster but less expensive than SEQCA because there is no sequential mechanical scanning system. However, MQCM still needs to be further developed to attain 2D mass mapping with high lateral resolution. Presently, the size and inter-electrode spacing of most reported MQCM structure are in the order of several hundreds of micrometers. The lateral resolutions of these MQCMs are not yet satisfactory for general 2D mass mapping applications. It is thus important to further reduce the size and inter-electrode spacing while maintaining sufficiently low acoustic interference among QCMs. Further miniaturization of MQCM based on plano-inverted mesa MQCM is considered a promising route to achieve high density MQCM for 2D mass mapping platform

Chapter 3
INTRODUCTION TO BIOSENSORS

This chapter, deals with the general information of biosensors which concerned in the experiments of QCM based biosensor.

3.1 THE MEANING OF BIOSENSOR

The term "biosensor" is short for "biological sensor" It is a device that uses for biological detection by integrating biological agent detection system. The International Union of Pure and Applied Chemistry (IUPAC) definite the word "biosensor", is a self-contained integrated device, which is capable of providing specific quantitative or semi-quantitative analytical information using a biological recognition element (biochemical receptor), and a transducer in direct spatial contact (IUPAC 1996).

Biosensor detection system is consists of biological element, and a transducer, as shown in Figure 3.1. The biological element acts as a bioreceptor that providing bio-recognition to the analyte. Wide variety of biological element applied in biosensor development, such as, enzyme, antibody, antigen, nucleic acid, and microorganism. Recently, new synthetic chemical compounds (molecularly imprinted polymer, aptamer, etc.) also use as a recognition element material on this purpose. Another part of biosensor is

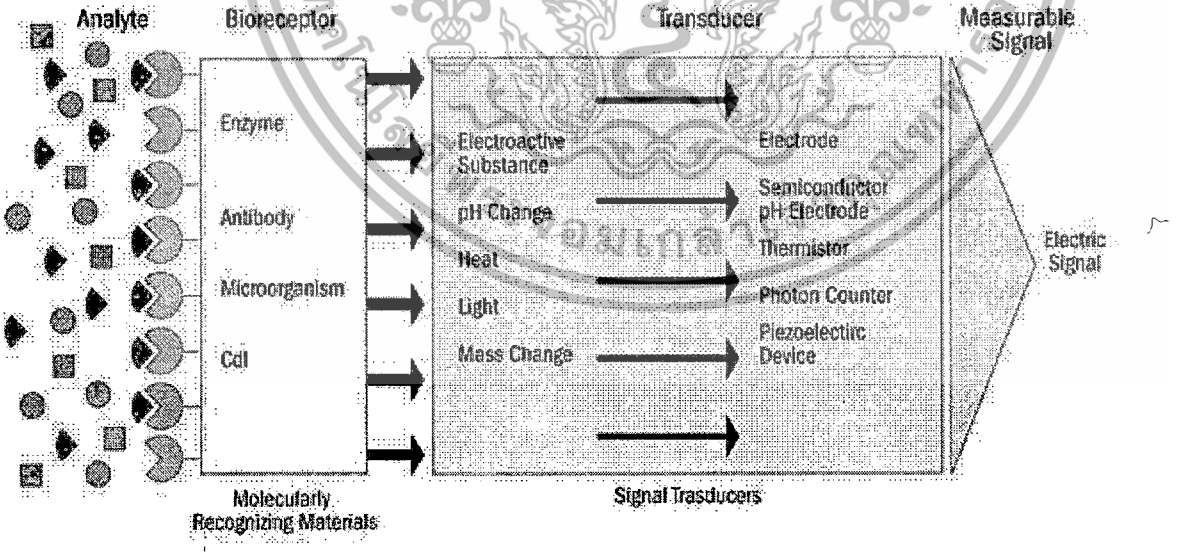

Figure 3.1 Principle of biosensors [92].

transducers or detector element, functioning to transduce the biorecognition reaction and convert into measurable signals. The combination of a biological element and a transducer, create an analytical device that allow to detection broad range of analytes in a complex sample matrices that easily to quantify, and user friendly.

Looking back to the past, the vest literature in the last 50 years related to biosensors. However, a studied of Prof. Leland C. Clark on the development of an oxygen probe by has considered as the Father of biosensors. His developed sensor device is called the "clark's oxygen electrode" which is using for oxygen sensing became the basis for biosensor technology. The idea of clarck's oxygen electrode illustrated by entrapping the glucose oxidase (enzyme) on dialysis membrane over on oxygen probe. The method of detection is based on the decrease in measured oxygen concentration which is proportional to the glucose concentration. His idea of the glucose sensor became the product commercialized in 1975 and become today's consumer healthcare diagnostics product expanded rapidly on the world market.

3.2 COMPONENTS OF BIOSENSOR

As described above, the biosensor consists of two main components; the biological elements, and the transducers. This section focuses on these two components which are interfacing into one unit by immobilization process.

The biological elements can be categorized into two groups, the biocatalytic elements and the affinity recognition element based on activity to recognize the analyte molecule with specificity. The biocatalytic element is the first generation of biological element used in biosensor technology. It contains of the molecule that providing catalytic activity such as enzymes, microbial cells and tissues. The affinity recognition elements are the next generation of biological element that utilize the affinity property of its molecule which specific capture to the analyte. This group includes antibodies, nucleic acids, and synthetic chemical compounds such as molecularly imprinted polymers, aptamer, peptide ligands or receptors. Biosensors also can be classified into various groups either by type of biological elements utilized or transducers employed.

3.3 CLASSIFICATION OF BIOSENSORS BASED ON TYPE OF BIOLOGICAL ELEMENTS

3.3.1 Enzyme-based biosensors

Integration of enzyme with transducer called enzyme-based biosensors; utilize the enzyme as biological element and interfacing to transducer. The function of enzyme in term of the recognition elements provides a wide variety of measurable reaction products arising from the catalytic process including protons, electron, light and heat. The advantages of using enzyme as the biological element are fast response and more specificity compared with microbial cells or tissues. However, the weak point of using enzyme is unstable and need cofactors for the detection of analyte. Example of the enzyme-based biosensors is glucose sensor which is a well-known device that utilize in clinical application to detection blood glucose in diabetes patient.

3.3.2 Cell-based biosensors

Cell-based biosensor is utilizes the whole cells of microorganism or tissue as a source of enzyme activity. Microbial cells are attached to transducer and generated signals include the assimilation of organic compounds, changes in respiration activity, the production of electrochemically active metabolites, bioelectric responses and metabolically-related pH or thermal responses which is unobtainable by other method. Higher eukaryotic, plant and animal cell lines are typically used as intact tissue slide. Since microbial cells and tissues continuously monitor and respond to their constantly changing extracellular, it was a reason that the intact microbial cells and tissues may eventually be proven to be the ultimate biological sensing elements for hybrid biosensor design.

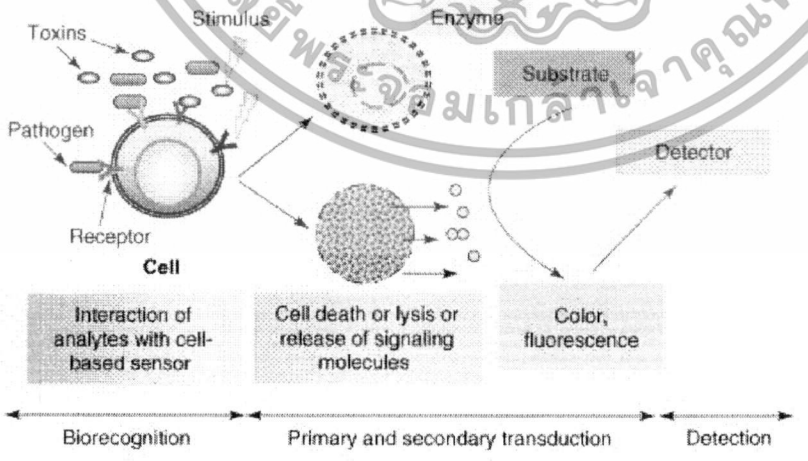

Figure 3.2 Schematic representations of cell-based biosensors [93].

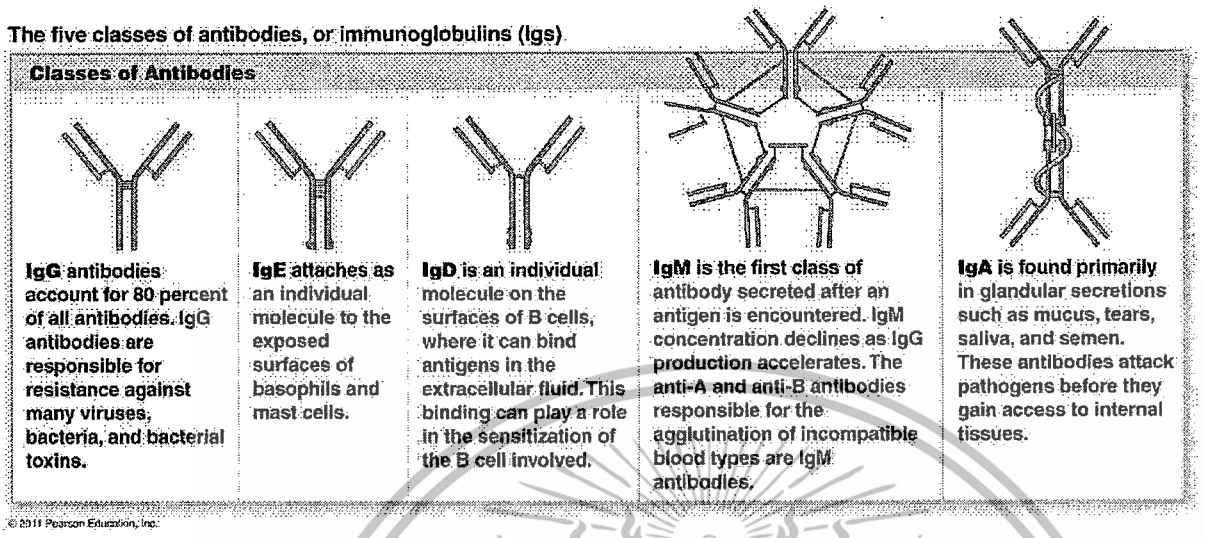

Figure 3.3 Schematic diagram of 5 types of antibodies [94].

3.3.3 Antibody-based biosensor

Antibody is known as immunoglobulins (Ig). It is a protein substance produced by immune system that normally used to identify substance called antigen, such as bacteria and viruses in body. The antibody has unique characterization that specifically recognizing structure of a target antigen. This biosensor detection system utilizes antibody to detect antigen. Antibodies will bind to specific antigens in a lock-and-key fashion, forming an antigen-antibody complex on transducer surface. The antibody-based biosensor also called as Immunosensor.

There are five classes of antibodies, immunoglobulin G (IgG), immunoglobulin E (IgE), immunoglobulin D (IgD), immunoglobulin M (IgM), immunoglobulins A (IgA), as shows in Figure 3.3. All of these antibodies, immunoglobulin G is an antibody mainly produced during the secondary immune response, and predominantely used in immunosensor applications. Basic structure of IgG is represent shown in Figure 3.4. The top end of the "Y" or Fab fragments contain the antigen-binding site, they retain specificity of the antibody.

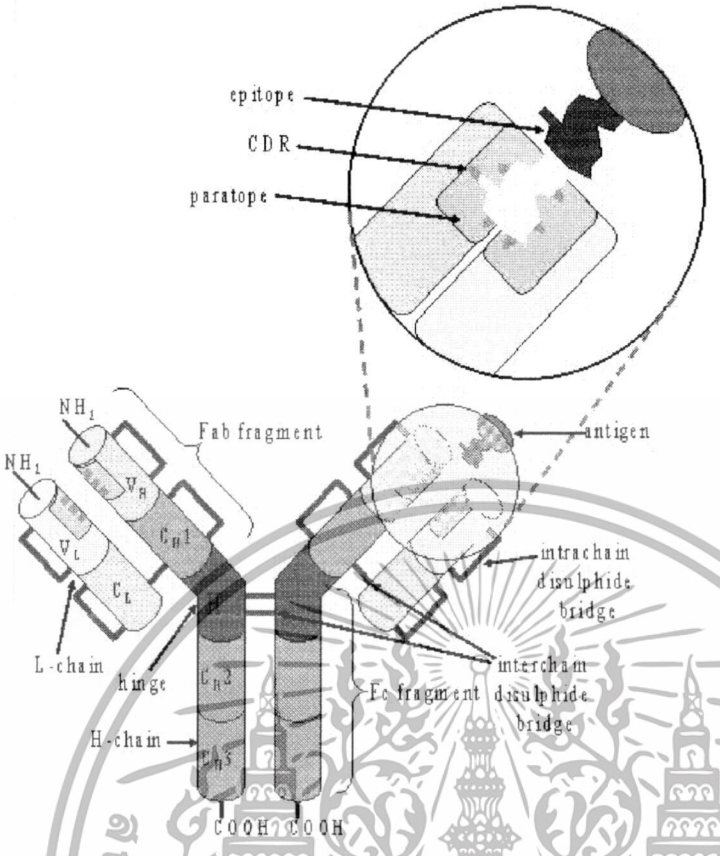

Figure 3.4 Schematic diagram of basic structure of Antibody (IgG).

The using of antibody as biological elements providing high specificity, versatile, and stably to target analysts (antigens). However, it is difficult to produce large quantities of antibodies to multi-target biosensor applications.

3.3.4 Nucleic acid-based Biosensors

Nucleic acid is an essential biological molecule which including DNA (deoxyribonucleic acid) and RNA (ribonucleic acid). Utilizing of nucleic acid in biosensor has been conducted by the complementary relationships between adenosine (A) and thiamine (T) and cytosine (C) and guanine (G) bases in DNA which is form the basis of specificity in nucleic acid-based biosensors. The detection of specific DNA fragments by hybridization with complimentary strands has gained considerable interest because of its important to the early diagnosis of diseases, such as cancer, hypercholesteremia. However, there is offers several drawbacks including the requiring of sample preparation, and the process of detection should be well-controlled of the contaminations.

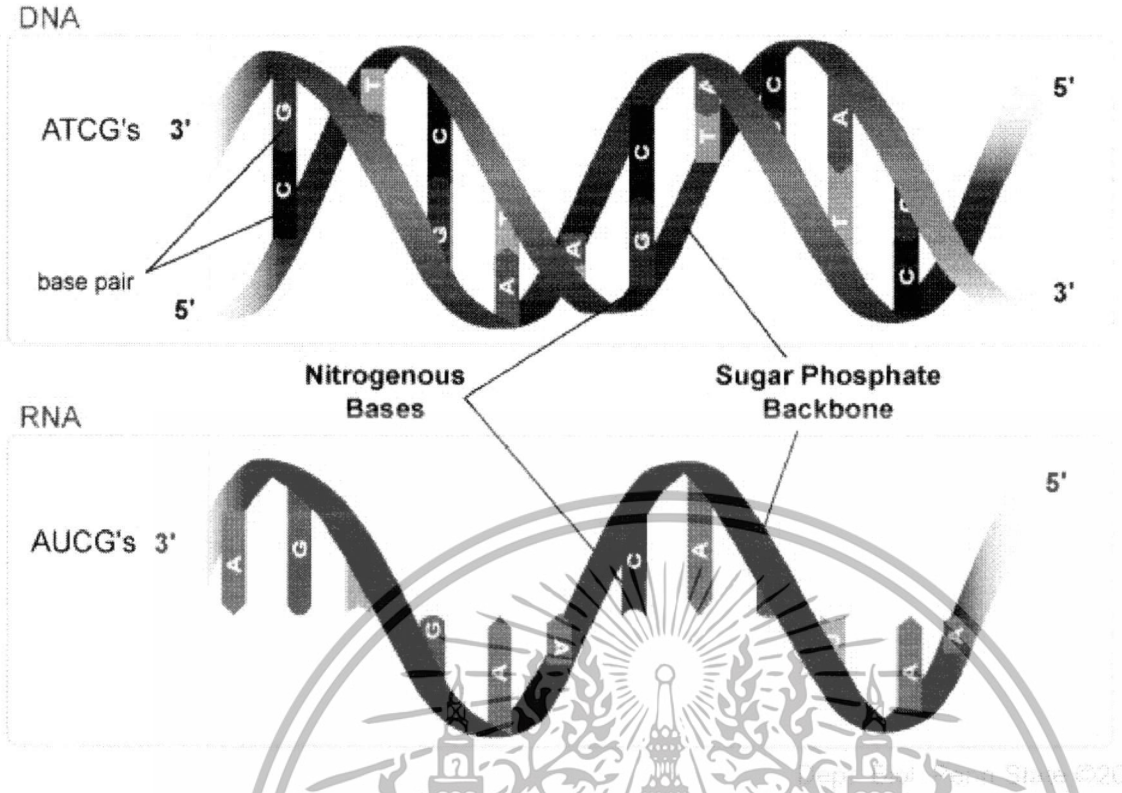

Figure 3.5 Schematic diagram of DNA and RNA [95].

Synthetic molecule-based biosensor

Recently, two new classes of semi-synthetic and fully synthetic binding molecules: high affinity RNA aptamer and molecularly imprinted polymers (MIPs) have been started. There are offer and alternative approach involving the use of artificial biomimetic recognition systems. The aptamer generated by random synthesis of RNA nucleotide. The MIPs can be synthesized by forming a polymeric network around the template and then created structure complementary of the analyte. However, both of these two kind of synthetic molecules are still exhibit drawbacks with regard to affinity, cross-reactivity and unspecific binding.

3.4 CLASSIFICATION OF BIOSENSORS BASED ON TYPE OF TRANSDUCERS

3.4.1 Electrochemical-based biosensors

The electrochemical-based biosensors have been described more than fifty years after Legend C. Clark introduced the principle of enzyme electrode. Currently, the enzyme is still the most common biological element of this type of biosensor. Several electrochemical

biosensor based on their operating principle, including potentiometric, amperometric, and impedimetric converting the chemical information. The sensor electrode usually contains two, three or more electrodes, simply called auxiliary electrode, reference electrode, and working electrode. The electrodes of an electrochemical sensor provide a surface at which an oxidation or a reduction reaction occurs to provide a mechanism whereby the ionic conduction of an electrolyte solution in contact with the electrodes is coupled with the electron conduction of each electrode to provide a complete circuit for a current. The applications of electrochemical sensors are frequently used in clinical diagnosis and environmental analysis.

3.4.2 Optical-based biosensors

The optical-based biosensors employed a number of techniques to detect the presence of the target analyte and are based on well-founded method including chemiluminescence, light absorbance, fluorescence, phosphorescence, light polarization, and rotation. Among optical methods, surface plasmon resonance (SPR) is currently the most used technique. The SPR-based sensor system was used based on the Kretschmann geometry of the attenuated total reflection (ATR) method and spectral investigation of SPR condition. Others optical-based techniques are fiber optics and evanescent wave.

Figure 3.6 shows that the light from the light source is focused through the prism on sensor surface, giving an incident light angles that monitored by a sensitive diode, and computer interpolation algorithms determine the angle of the SPR.

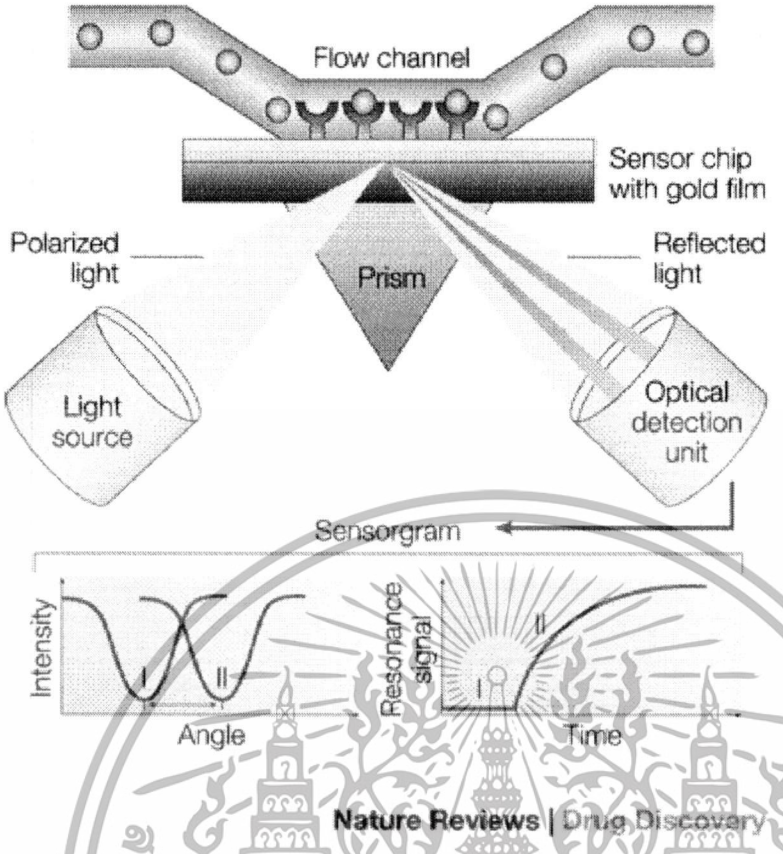

Figure 3.6 Principle of surface plasmon resonance (SPR) [96].

3.4.3 Piezoelectric-based biosensors

Piezoelectric-based biosensors are containing piezoelectric crystals of quartz materials. Detection of target analytes can be detected by detection of the small mass changes caused by biochemical binding to a piezoelectric crystal. Initially, a specific electrical signal can be applied to the crystal to cause them to oscillate at its resonance frequency. This frequency of oscillation depends on the electrical signal frequency and the mass of the crystal. As such the binding of the target of analyte will increase the mass of the crystal and subsequently change its resonance frequency, which can then measure electrically and used to determine the mass of the analyte of interest bound to the crystal. The QCM has been introduced by Sauerbrey in 1959 as a new method for mass sensing. Starting from the gas sensor, nowadays it is a transducer that widely used in sensor applications for detection of various chemical and biological species.

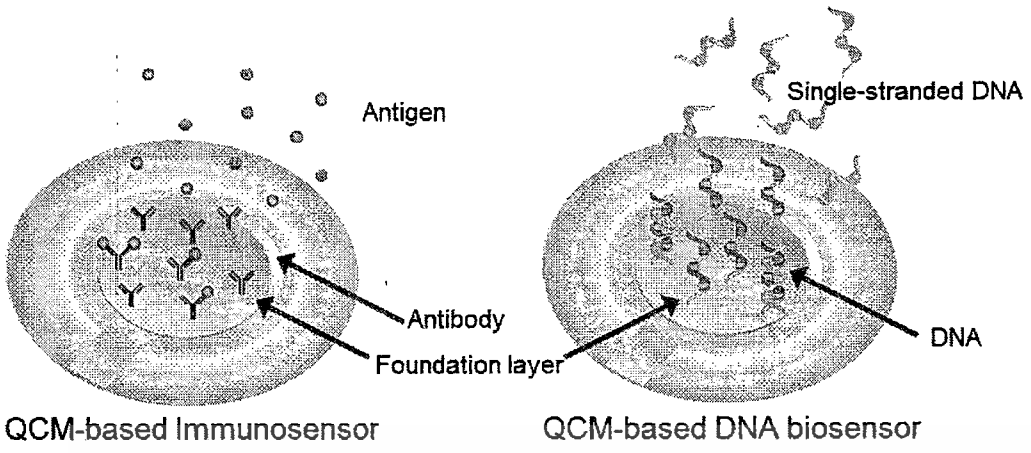

Figure 3.7 Illustration of using quartz crystal microbalance as the piezoelectric based biosensor.

3.5 IMMOBILIZATION OF BIOLOGICAL ELEMENT ONTO TRANSDUCER SURFACE

Immobilization is a technique used for the physical or chemical fixation of biological elements onto transducers which are solid matrix or retained by a membrane, in order to generate a sensing unit and stability. There are two main types of immobilization techniques are physical adsorption and chemical adsorption.

3.5.1 Physical adsorption

The physical adsorption is a simplest way to immobilize molecule of biological element onto the solid substrate of transducer surface. This technique is based on the physical adsorption of proteins on the water-insoluble substrate surface without any reagent treated, causes little or no conformation change of protein structure. The binding is mainly cooperated with the hydrogen bonds, multiple salt linkages, and van der Waal's forces that similarity to the situation found in biological system. A major advantage of physical adsorption as a general method of immobilizing proteins is that usually no reagents and only a minimum of activation steps are required. This method can be both simple and cheap. However, it has the disadvantage that the adsorbed molecules may leak from the substrate surface due to weak binding forces between protein and substrate. Another disadvantage is non-specific.

3.5.2 Chemical adsorption

The chemical adsorption or covalent binding technique provides high stability form of immobilization based on chemically modification between the reactive functional groups of surface substrates and biological elements. If the biomolecules are protein, there have varieties of functional groups for covalent binding such as lysine amino groups, cycteine thiol groups, tyrosine phenolic groups, arginine guanidine groups, histidine imidazole groups, cysteine disulfide groups, tryptophan indole groups, methionne thioester groups and serine and threonine hydroxyl groups. The reactive groups for covalent binding must be outside the active biological activity or binding site. The self-assembled monolayer (SAM) is one kind of chemical adsorption which consists of a single monolayer form of chemisorbed organic substances such as alkanethiols on gold surface caused monolayer, depicted as perfectly aligned closely packed alkane chains.

3.6 APPLICATION OF BIOSENSORS

Biosensor is applied in wide variety of fields. The attraction of biosensor is that it can detect minute quantities of substances by rapid and provide highly accurate with sufficiently sensitive and specificity, easy to use and suitable for non-specialist to deliver sophisticated analyzable in the fields or in home. Nowadays, exploration of new technologies such as micro/nano-electromechanical systems (MEMS/NEMS) technology, microfluidic technology, nanotechnology, plastic electronics technology, and microchip technology (small semiconductor-based crystal chips embedded with an IC capable of carrying out electronic functions) plays important role for development new generation of biosensor in miniaturization, which has resulted in smaller, more affordable, and more sensitive test monitors. A number of manufactures are trying to develop a single platform that can be used for multiple applications, produced in high throughput and easily manufactured with high rates. The following list describes some examples of the current applications:

Medical diagnosis or point-of-care

- Blood glucose sensor for monitoring the glucose concentration in diabetes patients.
- Blood gases and other vital sign sensing.
- Detection of bacterial and viral pathogens.

Agriculture and food industry

- Detection of fish and shellfish freshness.
- Fermentation control and analysis.
- Agriculture and food analysis.
- Detection of food pathogens in foods and drinks e.g.

Environment monitoring

- Microbial biosensor for detection of chemical contamination e.g. heavy metal contaminant in water.
- Biosensor for environmental pollution control e.g. detection of nitrate in air, water, soil, solid wastes and waste water indicate overuse and signs of pollution.

Military defense and bioterrorism

- Detection of bioterrorism agents e.g. anthrax (*Bacillus anthracis*), botulism (*Clostridium botulinum* toxin), etc.
- Detection of TNT explosive

3.7 INTRODUCTION TO QCM BASED BIOSENSOR

In this study focusing on development of QCM-based biosensor that utilized antibody as a bioreceptor and QCM as transducer for detection of analyte. The detection system was created by immobilized antibody on QCM transducer surface by chemical adsorption. In the presence of its antigen (analyte), the frequency shift of QCM is related to the concentration of analyte.

Chemical adsorption of antibody on to QCM surface by self-assembled monolayers (SAMs) described as simplicity and adaptability of and control over biomolecule surface orientation. Antibody immobilization in a manner which F_{ab} fragments pointing away from the surface, allowed for easy antigen-antibody binding. Protein A and protein G are used for this purpose as linker proteins. They are proteins specific to F_c portion of antibody molecules, and used to capture the antibody on sensor surfaces with properly orientations and maintaining antibody functionality. This chemical modification has been found to show

good reproducibility and coverage because the protein is covalently immobilized on the substrate.

Figure 3.8 shows the basic principle of using QCM as an immunosensor. At the state (a), one side of QCM gold electrode was prepared with SAM process and then assembled in to the sample flow system. After the buffer solution (generally used PBS as the buffer) was flowed pass through the surface, the resonance frequency will be recorded as the analysis data. In the state (b), some of the linker (in this case is Glutaraldehyde) was flowed to form the layer that have ability to bind with the antibody at Fc fragment. It should be noted that, after the layer was formed, the exceed molecules that not bind onto the electrode are removed with buffer flowed before the true frequency shift is expected. The removal of unbind molecules is a very importance step that must be done in every state before analyze the data to avoid of unwanted frequency shift signal. In the state (c), the antibody that specific to the target will be bind to the electrode. Then, the measured frequency after the exceed antibody removed will become the baseline to determine of the target analyte. At the state (d) and (e), the analyte will be flowed pass through the prepared electrode, the frequency will be shifted down as the function of bound molecules. The measured result will be used as the tool of target amount determination.

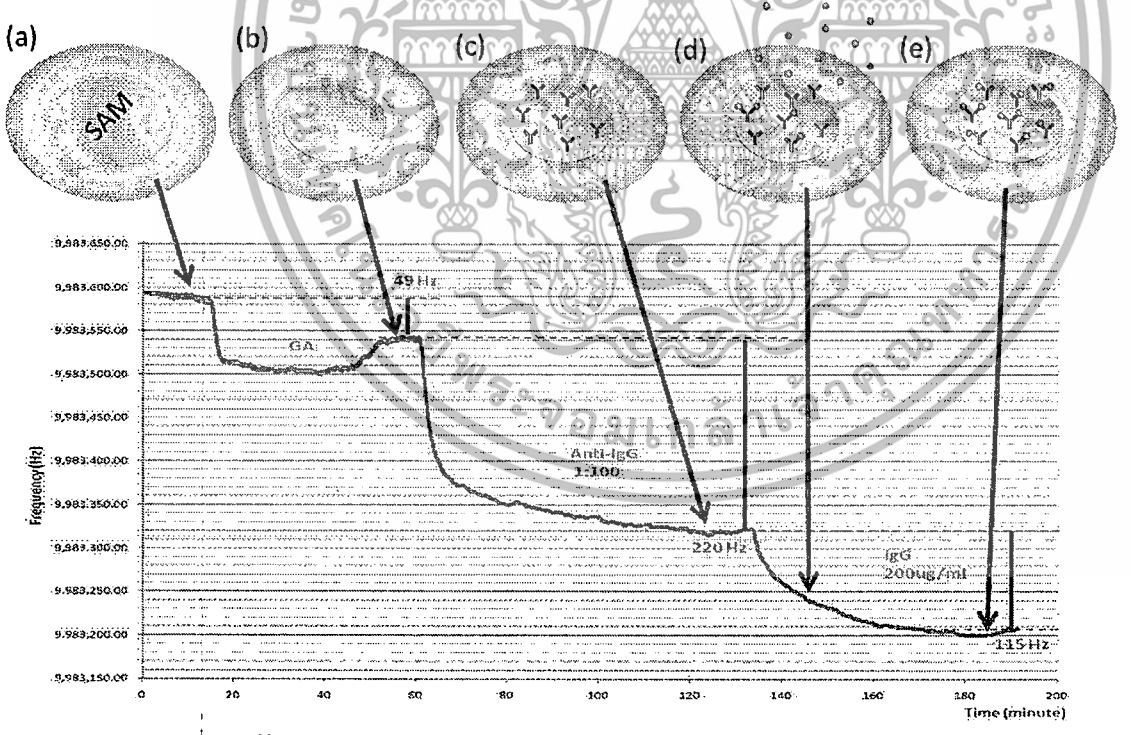

Figure 3.8 Illustration of QCM Immunosensor frequency response.

Chapter 4
EXPERIMENTS ON QCM BASED CHEMICAL AND BIOLOGICAL SENSOR

In this chapter, the experiments on QCM that was done before starting the MQCM study is presented. It is consisted of two main application based on chemical-sensing and bio-sensing respectively. For QCM in chemical-sensing application, was demonstrated through the use of QCM to determine the moisture content in gas-phase. And for QCM in bio-sensing application, was established through the real-time determination of Immunoglobulin-G in liquid-phase. In addition, the immobilization protocol that was used in this study will become the main protocol to immobilize the MQCM in next chapter as well.

4.1 EXPERIMENTS ON QCM BASED CHEMICAL SENSING IN GAS PHASE

QCM is one of the most favored device, be used as a gas sensor. The key advantages of QCM in gas sensing application are high-sensitivity and directly determine of gas concentration based on gas-molecular mass. The sensitivity of QCM gas sensor, based on two main factor which are the sensitivity of QCM and the adsorb/absorb ability of sensing layer coated on electrode to the target gas. The higher gas adsorb/absorb ability, the higher mass presented on electrode, effect to the higher frequency shift of QCM. In this section, a group of individual QCM are coated with varying the coating layer and be tested in the same condition, to prove the effect of sensing material quantity to the sensitivity.

In principle, QCM is very attractive for humidity sensing applications as it employs the most basic physical effect, which occurs when water molecule adsorption takes place on its electrodes. Many types of hygroscopic materials, such as SiOx thin-film, gelatin and various kind of polymers, were coated on the electrode as a sensing layer. Thus, the sensitivity of QCM humidity sensor considerably depends on water molecule adsorbility of material coated.

PEDOT/PSS, Poly (3, 4-ethylenedioxythiophene)/poly-styrene-sulfonic acid, is one of the most promising polymer composites in sensing application as they provide high physical and electrochemical stability compared to other polythiophenes. PEDOT itself can hardly be applied in inkjet printing method since it is insoluble in water. But, it can become printing solution by polymerization in a water soluble electrolyte such as PSS. PEDOT/PSS has received a great deal of attention for its unique properties including relatively high electrical conductivity/stability and simple solution processing. Furthermore, the pattern of sensing

layer can be precisely coated, since it can be apply in inkjet printing method. The advantage of this printing method makes it very attractive for QCM electrode coating. It provides us to control the sensing-layer pattern, area, also the thickness (number of layer) with very high precision. In addition, it is suitable for coating monolithic multichannel quartz crystal microbalance (MQCM) with difference sensing materials on neighboring electrodes.

The schematic of PEDOT/PSS printed QCM humidity sensor was shown in Figure 4.1. It consists of 12 MHz commercially available AT-cut quartz crystal resonator printed with PEDOT/PSS humidity sensing layer on its electrode. For the printing solution, print-ready PEDOT/PSS solution (clevios P jet N) was ordered from HC Starck, USA. The solution was printed by Fujifilm Dimatix materials inkjet printer on one side of QCMs electrode with varying number of layers from 1 to 20 layers (1, 3, 5, 10, 15 and 20 layers), as illustrated in Figure 4.2. The printing pattern area is 2.5 x 2.5 mm^2 square.

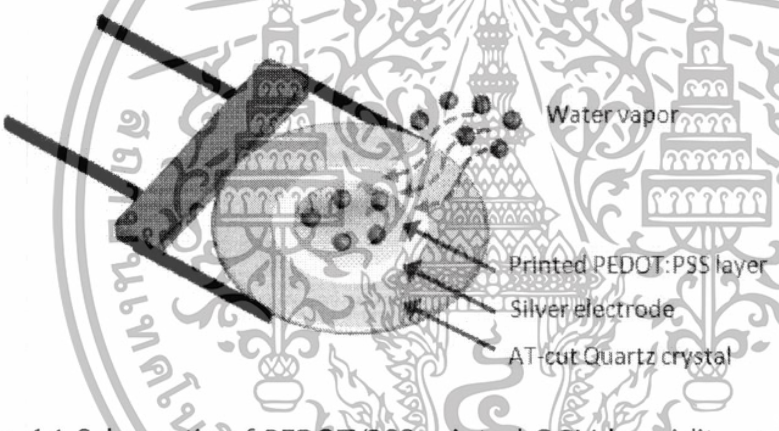

Figure 4.1 Schematic of PEDOT/PSS printed QCM humidity sensor.

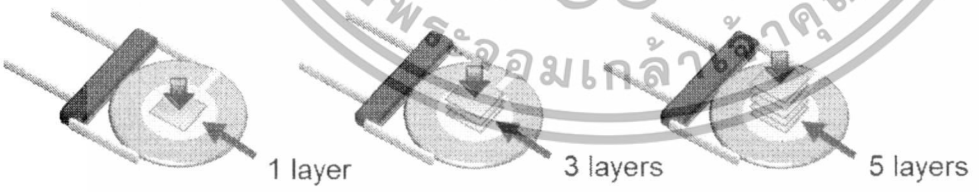

Figure 4.2 Schematic of multiple layer printed method.

The diagram of humidity sensing system is shown in Figure 4.3. The system can be divided into two parts, humidity control and data acquisition systems. The humidity control system is utilizing two mass-flow controllers with varying the ratio between dry and humid air. The air zero, pure and dry air, was flowed through two mass-flow controllers. The first one, mass-flow controllers A, was used to control to the flow rate of dry air, and the second one, mass-flow controllers B, was employed to control the flow rate of air bubbling in DI water for the purpose of producing high humidity air. Both output air were mixed and flowed through a sealed high-quality plastic chamber with low humidity absorption. The ratio between dry and humid air were controlled by computer via main controller of mass-flow controllers.

The oscillator circuit that used in this study is show in Figure 4.4 which is one of the standard logic gate oscillator. Not ordinary inverter gate is used, the Schmitt trigger logic gate is needed to enhance the oscillated frequency. The other parameters (C and R_2) was optimized through experiments.

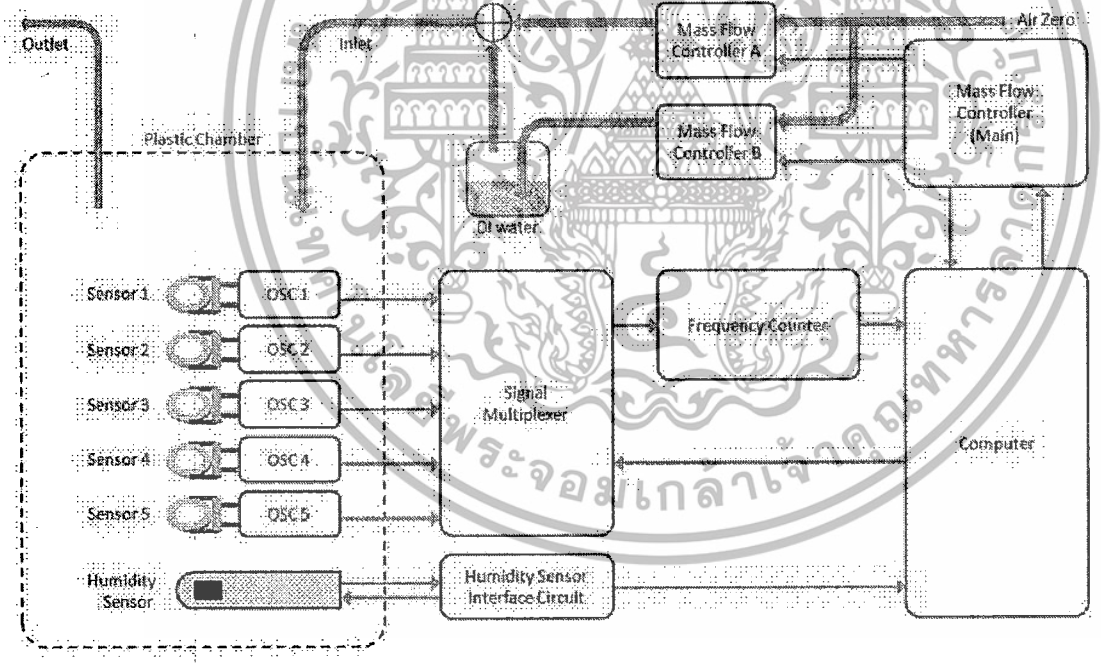

Figure 4.3 Diagram the experimental system.

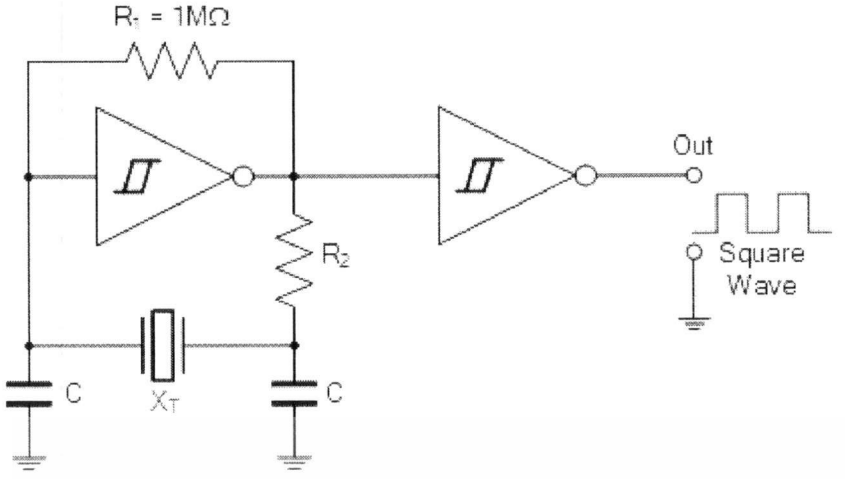

Figure 4.4 Schematic of the oscillator circuit used in this study.

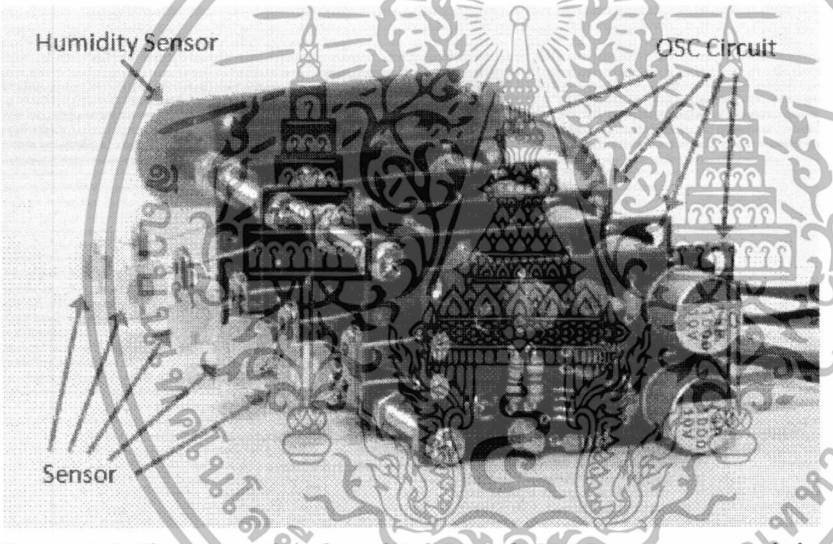

Figure 4.5 Photograph of multichannel QCMs sensor module.

For the data acquisition system, each quartz crystal resonator was connected to oscillator circuit, as shown in Figure 4.5. The output signals were multiplexed with signal multiplexer, controlled by computer. It should be noted that all of the circuit are custom made with the microcontroller based circuit. The multiplexed output signal was measured by a frequency counter and then the data was sequentially recorded in computer. The reference relative humidity and temperature was obtained from SHT15, a commercial humidity and temperature sensor. The measured relative humidity was also recorded at the same time as the measured frequency.

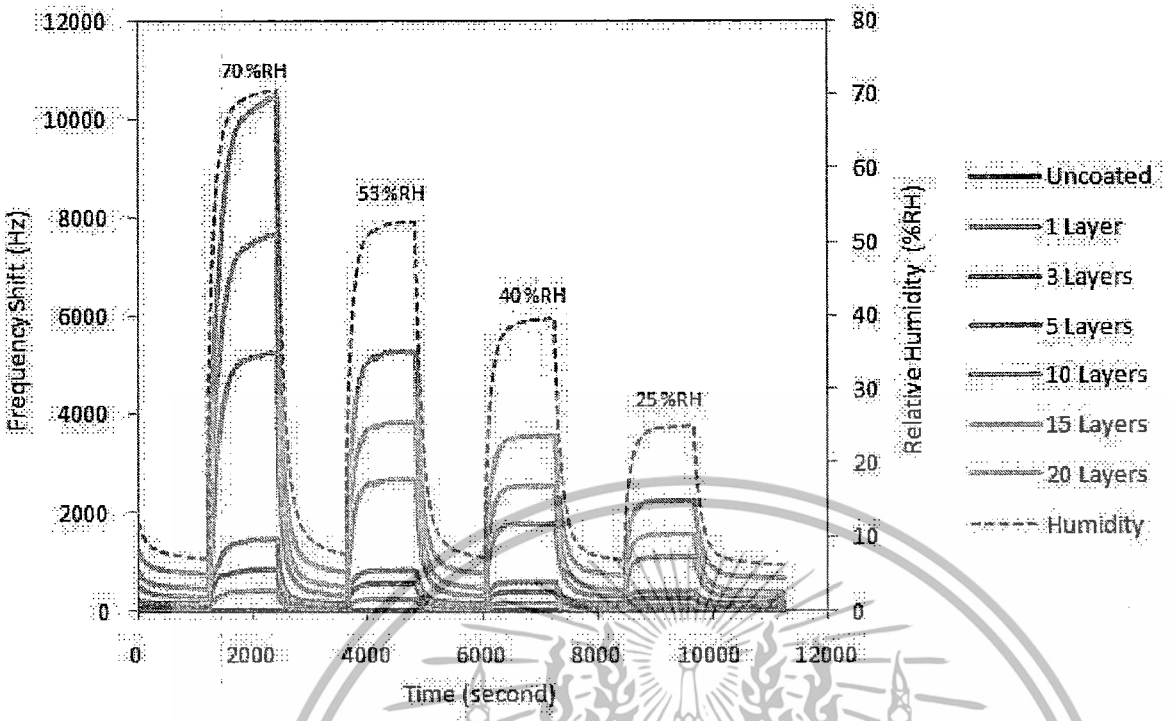

Figure 4.6 Typical dynamic response of PEDOT/PSS printed QCMs and corresponding dynamic relative humidity.

Typical dynamic response of the PEDOT/PSS printed QCMs with different numbers of printed layers (uncoated, 1, 3, 5, 10, 15 and 20 layers) and corresponding relative humidity measured by the commercial humidity sensor are shown in Figure 4.6. It can be seen that the printed QCMs have short response and recovery times comparable to the commercial humidity sensor. Also, the QCMs response was increased as a function of layer number. With 20 PEDOT/PSS printed layers, the frequency shift at 70%RH is higher than 10 KHz. In the other hand, uncoated QCM show negligible response to humidity.

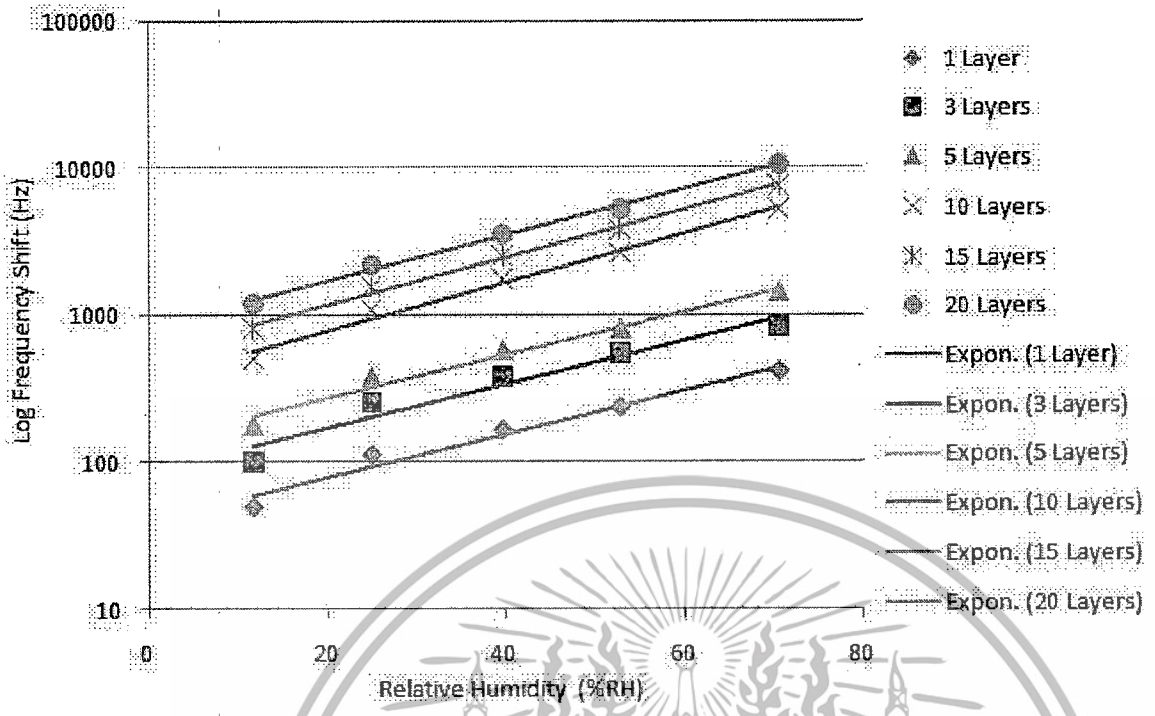

Figure 4.7 Log scale frequency shift as a function of relative humidity of PEDOT/PSS printed QCMs.

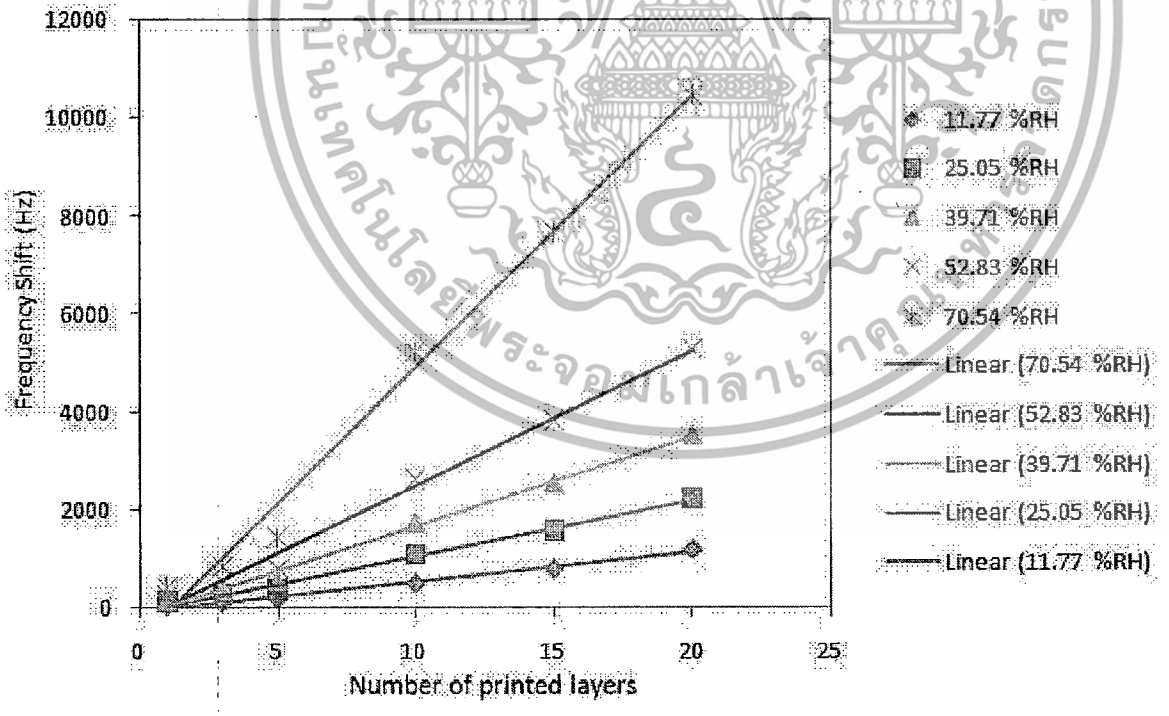

Figure 4.8 Frequency shift of PEDOT/PSS printed QCMs as a function of printed-layer number.

Figure 4.7 shows the log-scale frequency shift as a function of relative humidity of all QCMs. From the figure, it can be seen that the humidity response of QCM is significantly improved by PEDOT/PSS printing. The trend line is seen as a straight line when plotting in logarithm scale. Thus, the frequency shift response of QCMs is exponentially increased with relative humidity. The frequency shift as a function of PEDOT/PSS printed-layer number is shown in Figure 4.8. It is evident that the frequency shift at constant humidity is linearly increased with PEDOT/PSS printed-layer number. Thus, the humidity sensitivity is proportional to the deposited PEDOT/PSS amount on QCM sensor as expected. Therefore, inkjet printing method offers high precision of solution coating with accurately controlled area/volume and it is promising for coating sensing-material on QCM based sensor.

4.2 EXPERIMENTS ON QCM BASED BIOLOGICAL SENSOR

In the last chapter, the basic concept of bio-sensing using QCM was presented. Thus, in this section, those concept is demonstrated in real experimentation. Since, the bio-sample was naturally be in liquid buffer, the QCM based bio-sensor need flow-cell to capable of detect the sample in real-time. Figure 4.9 shows the flow-cell that was made for this study,

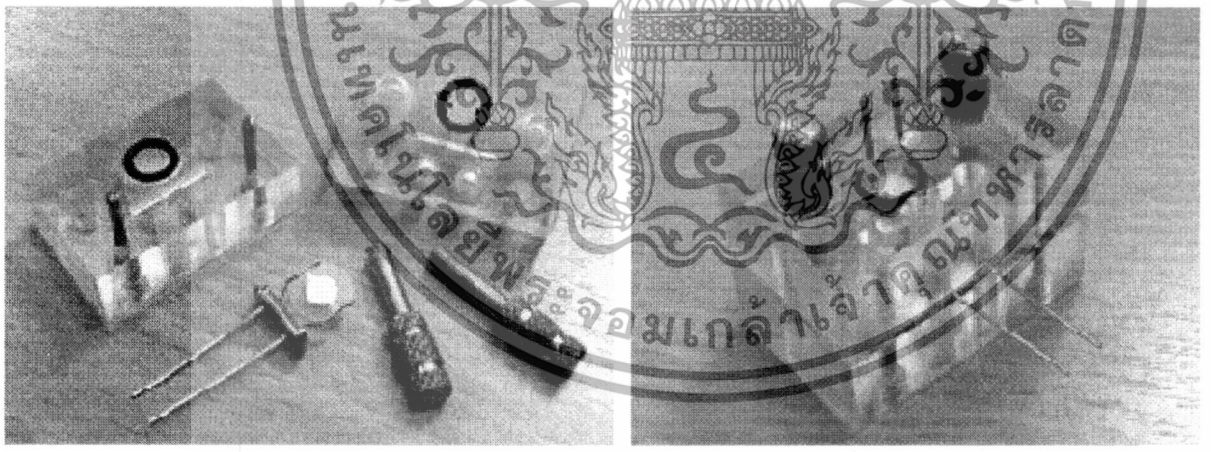

Figure 4.9 Lab-made QCM flow-cell.

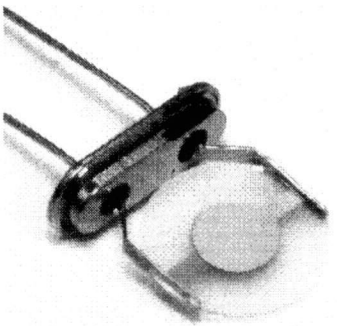

Figure 4.10 Gold electrode QCM in this study.

For the immobilization process, the most common method that use to bind biological element on to the electrode of QCM, based on chemical adsorption technique. Those are commonly known as self-assembly monolayer or SAM technique, and it's generally required gold electrode surface to form monolayer of chemisorbed organic substances such as alkanethiols. The 10 MHz gold electrode QCM in this study is illustrated in Fig 4.10, the quartz diameter is 9 mm and the electrode diameter size is 4 mm.

In the study, Cystamine, a bio-functional building block that had two functional end groups, including thiol (SH) and amine (NH_2), is used to form the SAM. The sulfur atoms of thiol group were bound to gold surface through weak acid-base interaction while the amine group would be left for subsequent reaction [97]. Firstly, the MQCM was cleaned with NaOH and HCl for 2 and 5 minutes respectively. Next, 5ul of 25mM Cystamine was drop on to the electrode to form the SAM layer for 24 hours. Then, the QCM was clean with de-ionized (DI) water and assembled in to the flow-cell.

The biological element used in this study, the anti-immunoglobulin G (anti-IgG) which is specifically bind with the analyte IgG. It was immobilized to the SAM layer through the linker. Glutaraldehyde (GA), the cross-linking reagent with two aldehyde functional groups, was used to anchor the amine functional group of the Cystamine-modified gold surface and antibody. The 20mM GA was feed in to the chamber of flow-cell with flow rate 10ul/min for 30 minutes while monitor the frequency shift simultaneously. 0.01M phosphate buffer saline (PBS, pH=7.4) was used as a reference buffer, it will be flowed through the chamber for 15 minute to remove of the exceed GA that not bond to the SAM layer. It should be noted that, current frequency response is considered as a baseline before immobilization of Anti-IgG. Next, anti-IgG was prepared by 1:100 dilution of 2.1 mg/ml anti-IgG source solutions and

then flowed through the flow-cell for 45 minutes, while the frequency was continuously monitored to realize the binding effect of anti-IgG. Then, the PBS was flowed in to the chamber for 15 minute to remove of exceed anti-IgG, the frequency at this point will be used as baseline frequency. Next, IgG which is the target molecule in this experiment was prepare in PBS and flowed into the chamber with varying concentration (50, 100, 200 ug/ml) for 45 minutes. Lastly, PBS was flowed for 15 minutes to remove unbind molecule out of the chamber, the last reading frequency will be compare the last baseline frequency and considered as the frequency to IgG binging response.

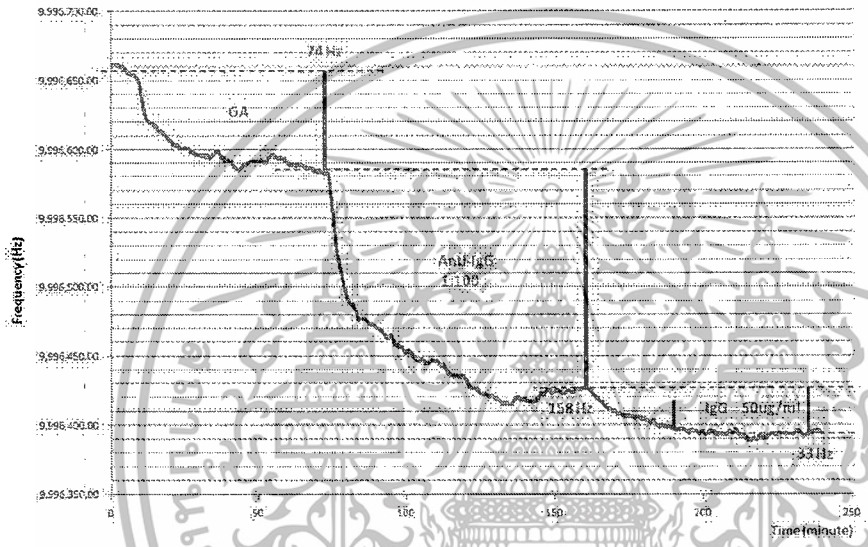

Figure 4.11 Frequency response of 50µg/ml IgG.

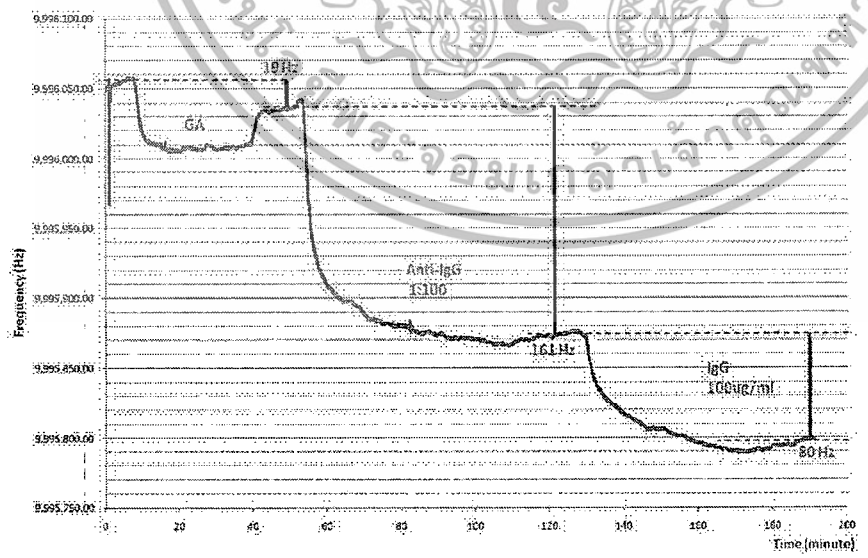

Figure 4.12 Frequency response of 100µg/ml IgG.

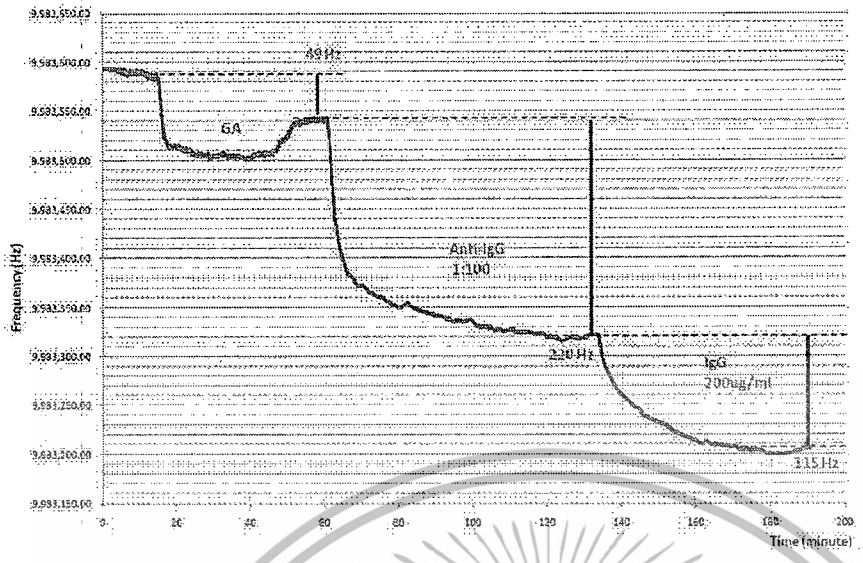

Figure 4.13 Frequency response of 200µg/ml IgG.

Real-time frequency response of QCM with IgG concentration 50, 100, 200 µg/ml was illustrated on Figure 4.11, 4.12, 4.13 respectively. The final frequency shift are 33Hz for 50 µg/ml IgG, 80Hz for 100 µg/ml IgG and 115Hz for 200 µg/ml IgG. It can be seen that, the higher concentration of IgG, the higher final frequency shift obtained. Even, this test is not concerned about non-specific binding effect, which can be blocked using the additional blocking material such as BSA (bovine serum albumin) molecules. But, the main objective of this experiment, to find the protocol of bio-sensing for our MQCM scheme, and the results confirmed the successive of anti-body binding with this protocol. Thus, this protocol will be applied to the MQCM bio-sensing in next chapter.

Chapter 5
EXPERIMENTS ON MQCM FOR MULTI-ANALYTE BIO-SENSING

In this chapter, all of the experiments about MQCM is presented. First, the fabrication of MQCM is revealed. Next, the problems of MQCM with non-interference blocking method are presented. And finally, the bio-sensing compatible interference-free MQCM is announced.

5.1 THE FABRICATION OF MQCM

As the principle of QCM, the fabrication of MQCM is fairly simple, it is the deposition of electrode on both side of AT-cut quartz-crystal substrate. However, it's require high-quality metal-thin-film depositing-machine to prevent of electrode damaged after use. In this study, all of the chromium/gold (Cr/Au) was deposit with multi-target sputtering system, which is the high-end multi material sputtering machine (this task was supported by MEMS-lab and OTL-lab at NECTEC). The Cr and Au sputtering condition are 100 W dc power at $3x10^{-3}$mbar for 2 and 10 minutes, respectively. The thickness obtained for Cr and Au layers were around 50 and 300 nm, respectively. In addition, the deposition need to be done on both side of quartz substrate to be come and "electrode-pair", ready to be used as a QCM. Since, this depositing condition have been used in every deposited electrode in this study. Hence, the term related to "electrode deposition" after this, can be explained by these Cr/Au depositing conditions.

A major different between QCM and MQCM is the number of electrode-pair deposited on a substrate. QCM had only one electrode-pair while the MQCM had multiple. So, the pattern of electrode depositing is everything to be design. In the sputtering process, we need the shadow-mask to create any patterned. There are few techniques capable of fabricating the mask, such as the patterned on photoresist coated on substrate, the use of metallic shadow mask etc. In this work, the shadow-mask was fabricated by nickel (Ni) electroplating on photoresist-patterned stainless-steel plate. The standard dry-film photolithography process was used to produce photoresist pattern of electrode designs on stainless steel plate, as shown in Figure 5.1. Uncovered area on stainless-steel plate was then coated by 40 μm thick Ni film by electroplating process. Ni electroplating was conducted in Nickel sulphate plating solution for 4 hours. Nickel shadow masks were

obtained by removing the photoresist by sodium hydroxide solution and detached the nickel film from stainless steel plate. Figure 5.2 shows typical fabricated Ni shadow masks.

Before QCM electrode deposition, blank quartz disc substrates were cleaned in piranya solution (1:4 mixture of 50% H_2O_2 and 97% H_2SO_4) at 120 °C for 10 minutes. The shadow mask was then aligned and attached on a blank quartz disc by a permanent magnet. The chromium (Cr)/ gold (Au) layers were deposited on one side of quartz substrates by sputtering through the top-side set of the shadow-masks. Then, the bottom-side shadow masks were aligned to the first pattern and deposit electrode through the shadow mask as well. Typical photographs of the fabricated QCM sensor array are shown in Figure 5.3. Even, there are various design of MQCM in this study, the fabrication process are the same.

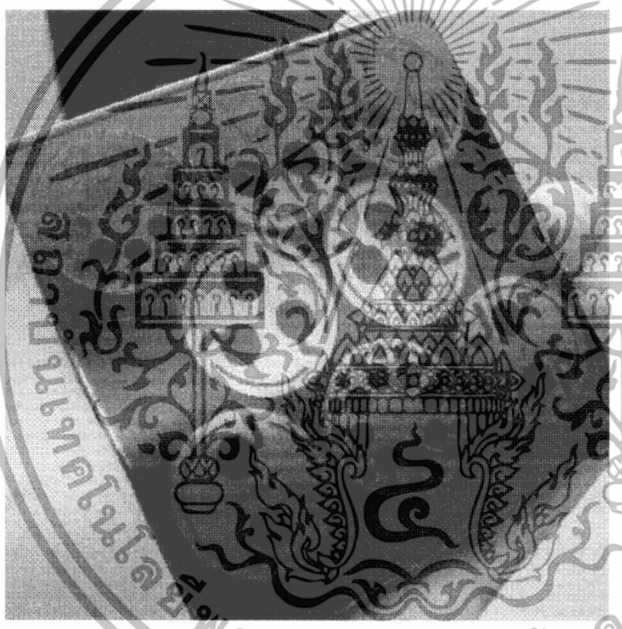

Figure 5.1 Photograph of photoresist-patterned stainless-steel plate.

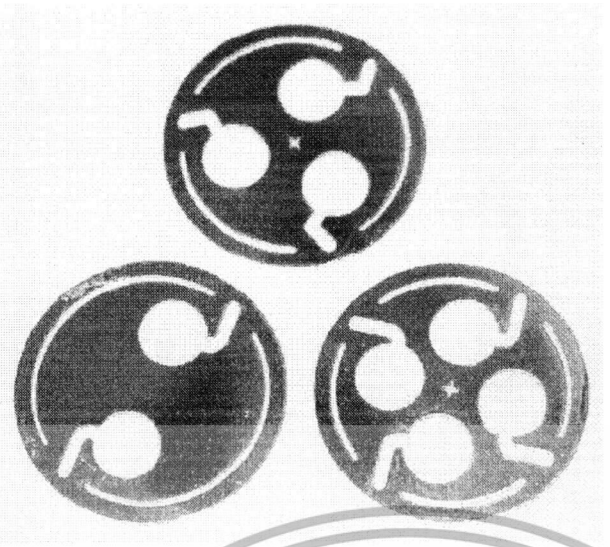

Figure 5.2 Photograph of fabricated micro shadows masks.

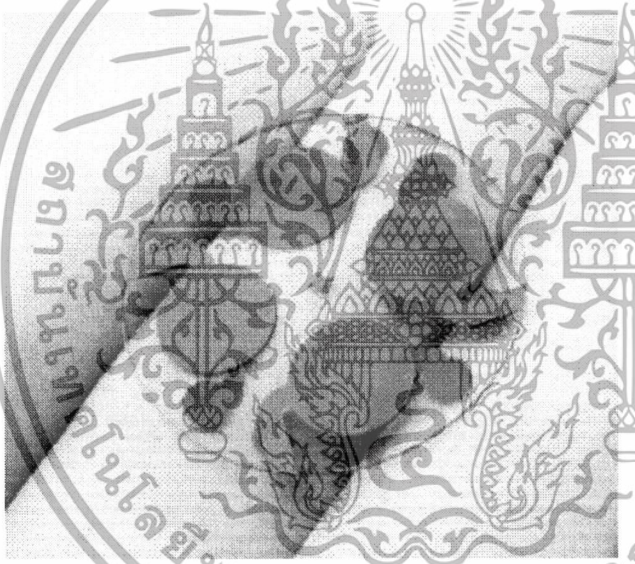

Figure 5.3 Photograph of fabricated QCM sensor array with 4 sensing electrode pairs.

5.2 EXPERIMENT ON MQCM BASED CHEMICAL GAS SENSING

In this experiment, the fabricated MQCM was demonstrated as volatile organic compound (VOC) detection. Poly-aniline (PANI), poly-ethyleneimine (PEI) and poly-vinyl-alcohol (PVA) gas sensitive polymers were deposited on different QCM electrodes by drop-coating method. The frequency shift characteristics of QCM sensors in the array are found to be distinct for methanol, ethanol, and acetone vapors and distinct patterns can probably be used to identification of different VOCs.

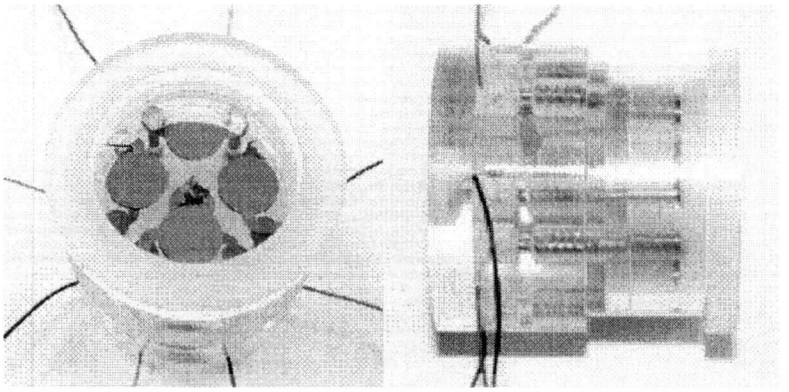

Figure 5.4 Photograph of MQCM in sensor holder.

The fabricated QCM array was attached to crystal holder for electrical connection as shown in Figure 5.4 and then placed in a 1.5 liter sealed glass chamber. Figure 5.5 shows the diagram of the gas sensing system for MQCM. Before VOC sensing, the chamber was filled with dry air. The MQCM was operated and resonance frequency data was sampled only one at a time by an electronic switching circuit to avoid frequency interference among QCM sensors on a quartz disc. The oscillation frequency was measured by a frequency counter circuit that continuously sent the data to the computer. Tested VOCs consist of methanol, ethanol, and acetone. For VOC sensing, 200 ul of VOC liquid source was introduced into the chamber while the frequency shift of MQCM were constantly monitor. The VOC liquid was uniformly evaporated and dispersed in the chamber by a low power electric fan. The final frequency shift was noted after VOC vapor reach its equilibrium and the frequency shift was stabilized.

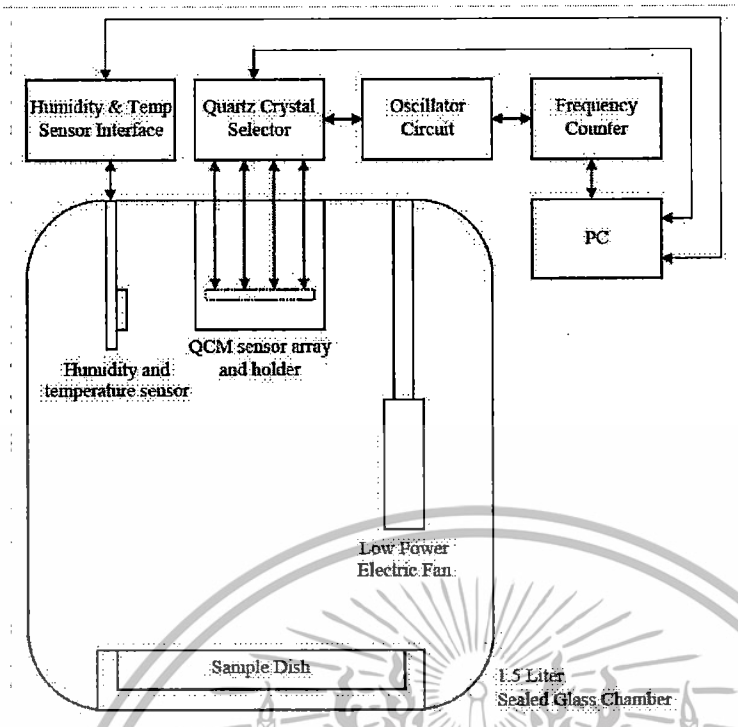

Figure 5.5 Diagram of the gas sensing system for QCM sensor array.

The VOC sensing results are shown in Figure 5.6-5.8. Figure 5.6 shows the sensing response to 200 ul of VOC samples of the MQCM. It can be seen that the sensing responses of PEI, PVA and PANI based QCM sensor array to different VOCs have considerably different levels of magnitude. In addition, the sensing patterns of various sensors' responses for different VOCs visually appear to be similar. In order to distinguish similar response patterns of different gases or odors, several pattern analysis algorithms such as principle component analysis (PCA), neural network, etc., have been proposed. These methods normally require complicated computational process. In this work, a simple sensing pattern analysis that uses only two calculation steps is proposed. Firstly, the raw sensing response (frequency shift) for all gases is normalized with respect to the sensor with highest sensitivity. It is evident that PEI coated sensor has the highest sensitivity to all VOCs while PANI coated sensor has the lowest response magnitude. As the result, PEI coated sensor was selected as the reference and its response is set to 100 % while the responses of other sensors are scaled proportionally with respect to PEI coated sensor's response. Figure 5.7 shows the calculated normalized result. It can be seen that the adjusted response magnitude for all VOCs are now in the same level. Secondly, the new response is now renormalized by using one of VOCs gases as a reference. In this case, methanol is selected as the reference so the methanol responses of all sensors are now changed to 100% and other VOCs' responses are scaled proportionally with respect to methanol response. The normalized response with

respect to methanol is illustrated in Figure 5.8. It can be seen that the final response patterns for different VOCs become considerably distinct and the final pattern can be used to distinguish methanol, ethanol and acetone from each other.

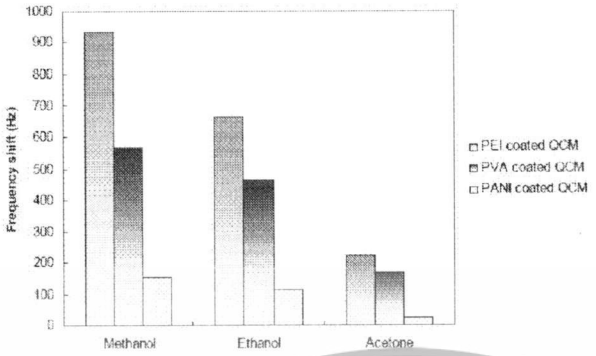

Figure 5.6 Sensing response to 200 ul of VOC samples of the MQCM gas sensor array.

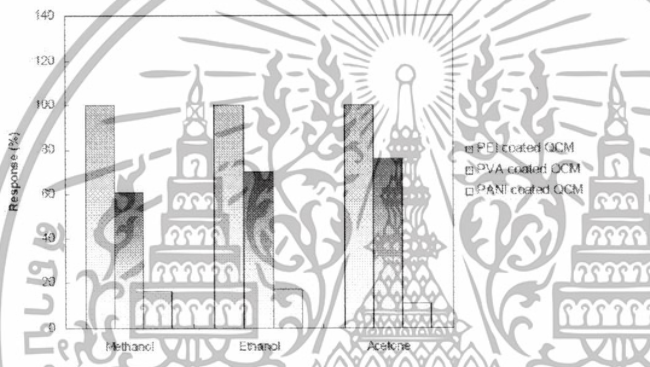

Figure 5.7 Sensing response to 200 ul of VOC samples, plotted using PEI coated QCM response as the reference value.

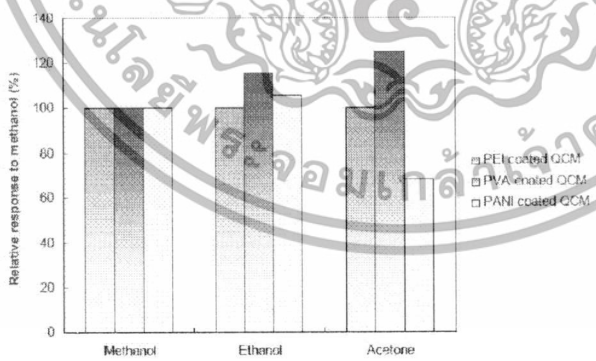

Figure 5.8 Sensing response to 200 ul of VOC samples, re-plotted using both PEI coated QCM response and methanol sensing response as co-references.

5.3 PROBLEMS OF MQCM IN LIQUID PHASE SENSING

In the last experiment, it can be seen that, there are not much problem for MQCM operating in gas-phase. As there are many report of gas-sensing MQCM reported up till now. However, it is not possible for bio-immunosensor to be real-time detected in gas-phase. So the MQCM in liquid-phase sensing still be challenged thus far. The first factor to be considered, it is require the attractive flow-cell chamber. Second, it is suffered from the flow typically. Lastly, it is distressed from sundry interferences.

5.3.1 The MQCM flow chamber

Unlike the individual QCM, MQCM required an area to be effectively used, since there are multiple electrode deposited full of its substrate. The lab-on-a-chip technology, the technology that can fabricate the flow channel precisely, was used to deal with the limitation in term of substrate area. The commonly fabrication method are mold-casting of Polydimethylsiloxane (PDMS) on the SU-8 photoresist mold. Figure 5.9 show the mold, used in this experiment. The fabrication process start with, silicon wafer were cleaned in piranha solution at 120 oc for 10 min, carefully rinsed several time in deionized water and dried with gentle stream of air. After that silicon wafer were dehydrated at 150-200 °C for 10 min. SU-8 photoresist was spin-coated on silicon wafer using a spin coater, then soft baked to remove all the solvent in the layer. The photore-sist coated wafers were exposed using UV expose machine then post-baked in order to selectively cross-link the exposed portions of the film. The sample was left in the desiccators to cool down slowly at room temperature for more than 13 hours. Finally sample was developed, cleaned with deionized water and isopropyl alcohol and gently dried with air.

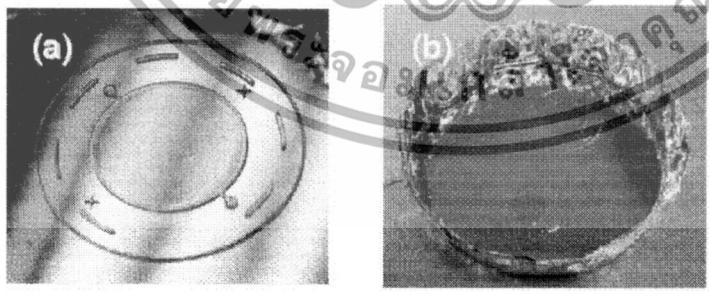

Figure 5.9 SU-8 mold on Si wafer and PDMS casting.

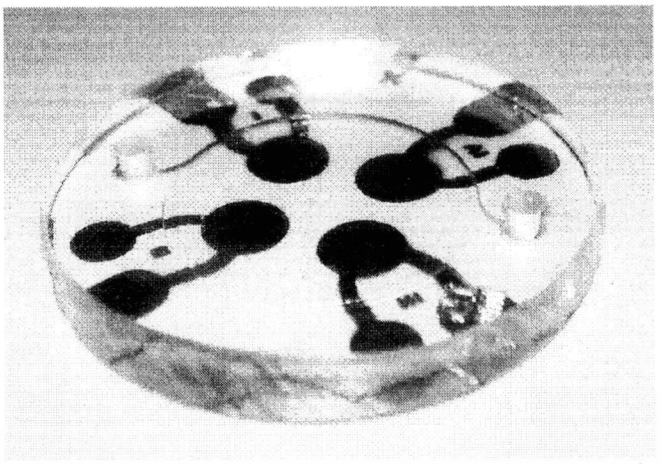

Fig 5.10 MQCM with PDMS micro chamber.

Sylgard 184 Silicone Elastomer kit (Dow Corning), consisting of PDMS was prepared by mixing the precursors sylgard with a curing agent at a ratio of 10:1 by volume. The prepolymer mixture was degassed at 20-50 mTorr in ambient temperature desiccator with a mechanical vacuum pump for 10 min to remove any air bubbles in the mixture. PDMS mixtures were gradually poured onto the SU8 master mold to the height over the depth of designed chamber. Next, PDMS slab was cured at 80 °c for 3 hour. Finally, it was peeled-off from the mold. Figure 5.10 shows the photograph of fabricated QCM sensor array with PDMS chamber.

5.3.2 The effect of flow-path

After finished of the PDMS micro chamber fabrication, the four QCMs on MQCM was tested in the same biosensing application but the frequency shift results are appeared randomly. The measured frequency shift are 52, 44, 163, and 73 that is disappointed, since it is not turn out as our expectation. One of the hypothesis to this problem is the shape of the sensing chamber

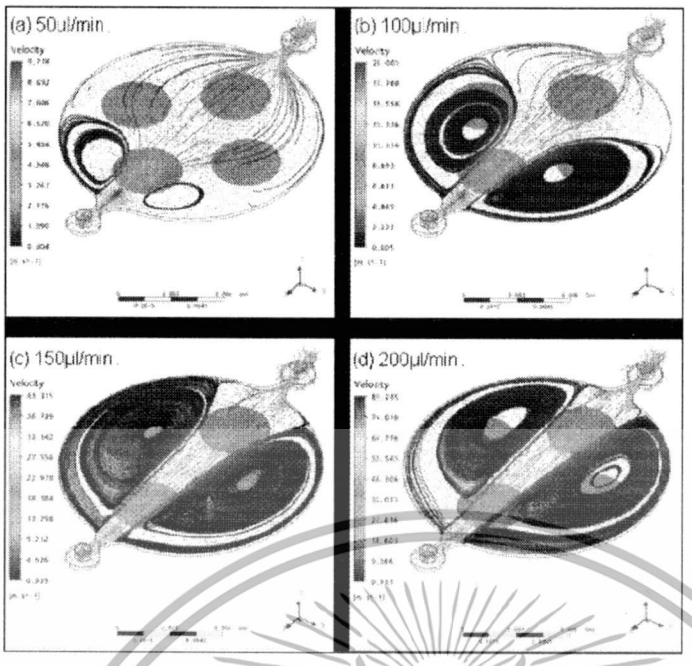

Figure 5.11 The geometries of turbulent flow effect inside circular chamber in 3D simulations and velocity variation over the sensor surface at different flow rate (a) 50ul/min, (b) 100ul/min (c) 150ul/min and (d) 200ul/min.

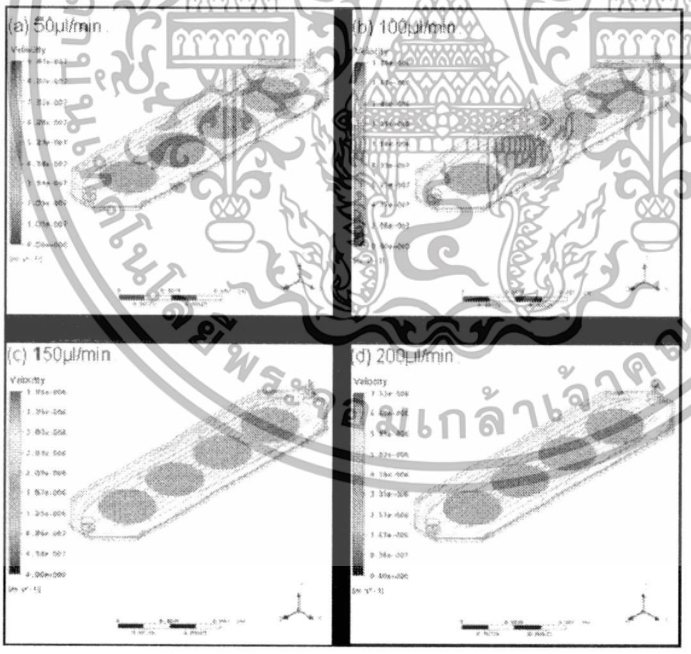

Figure 5.12 The rectangular geometry show linear of laminar flow across the sensing electrode at different flow rate
a) 50ul/min, (b) 100ul/min (c) 150ul/min and (d) 200ul/min.

The 3D-simulation of sample flow through each sensor surface was performed by ANSYS program. The fluid dynamic simulation was carried out by imposing a constant sample flow rate condition through the chamber. Figure 5.11 shows sample dispersion trajectories at various flow rates including 50ul/min, 100ul/min, 150ul/min, and 200ul/min, respectively. Simulation results show that the flow in this circular-shaped QCM chamber design is primarily turbulent. In addition, the degree of turbulence is increased with flow rate. The sample dispersion especially on both far sides of chamber where sensor electrodes are located is nonlinear. Thus, sensors at various locations see different sample dispersions causing their sensing behaviors to be significantly different. Therefore, the QCM chamber should be redesigned to obtain laminar flow through all sensor electrodes so that every sensor experiences the same sample dispersion under a constant flow condition.

The shape of QCM chamber is redesigned to be rectangular line. The computational simulation was performed again under the same boundary condition as that of circular QCM chamber. Figure 5.12 illustrates sample dispersion trajectories at various flow rates. The results clearly indicate a laminar flow over all sensing electrodes without non-uniform dispersion phenomena even at different flow rate. Thus, it can be the solution to the problem because flow in the new design is primarily laminar with uniform sample distribution.

5.3.3 The interference between channels in MQCM

Not only the effect of flowing path that interfere the frequency shift signal, the layout of the electrodes still be the most importance thing to be suspicious. As reviewed in Chapter 2, the interference between channels will become stronger if the adjacent channels become closer, and the effect is can easily be noticed from the instability of measured resonance frequency signal.

Figure 5.13 and 5.14 show 14 channels MQCM with a circular flow chamber. This work was planned to be operated with multiplexing method which the sensor will be selected and operated one channel per time, before switch to read the other channel. The main propose of using this multiplexing method is to avoid of the vibration from adjacent channel to interfere each other, by stop its working. However, even not applying any power, the mechanical stress of the adjacent channel can be strongly affected the frequency response, if the electrode was placed too close.

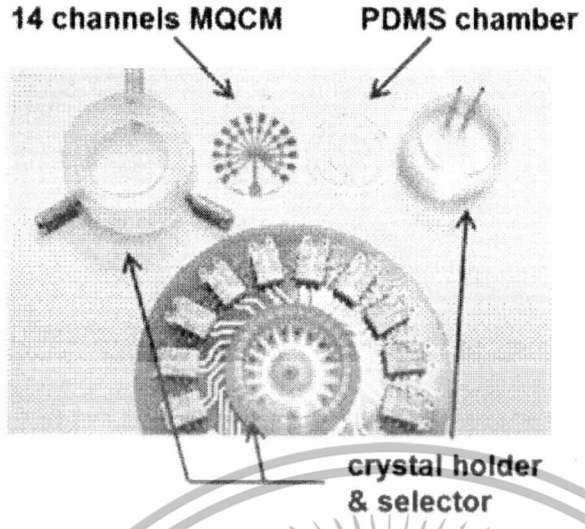

Figure 5.13 The parts of 14 channel MQCM.

(a) (b) (c)

Figure 5.14 Photograph of 14 channel MQCM,
(a) top-view, (b) side-view and (c) bottom-view.

Figure 5.15, shows the measure transmission magnitude of each channel that was measured by vector network analyzer. It can be seen that, each channel has more than one resonance frequency peak. When connected to an oscillator circuit, the resonance frequency cannot be maintained stable. As the result, the high-density planar-based MQCM cannot be successively operated without the concerning of frequency interference effect.

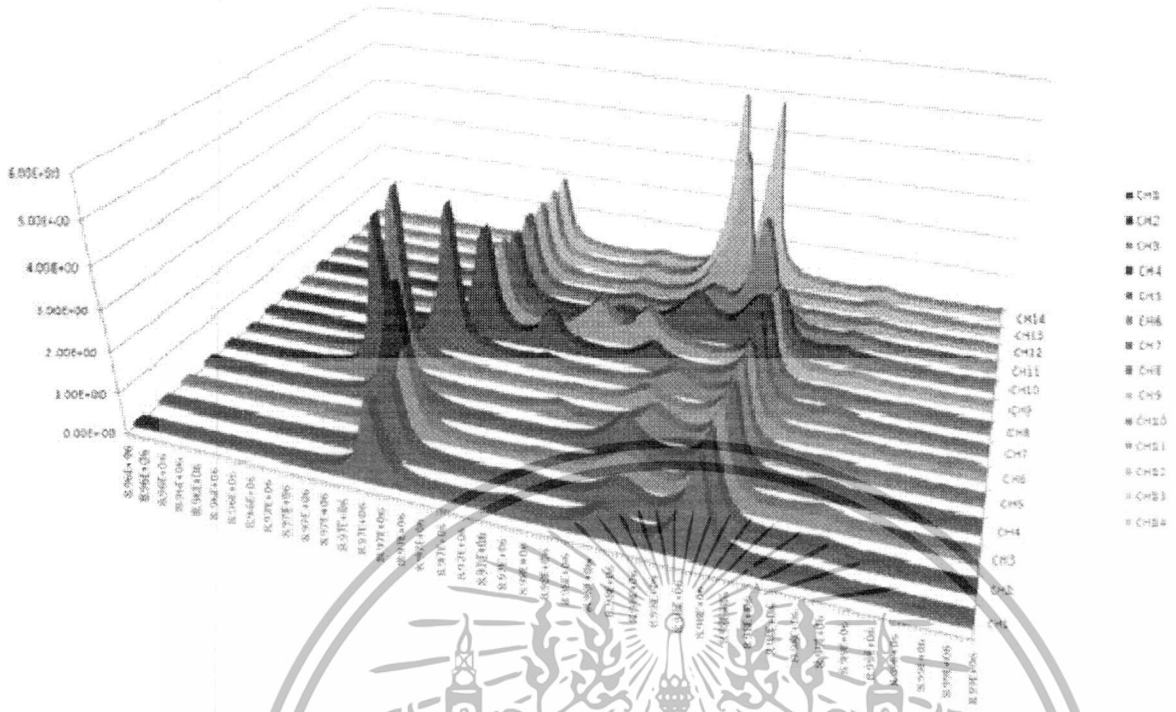

Figure 5.15 Frequency response of 14-ch MQCM measured by network analyzer.

5.4 THE NEW INTERFERENCE FREE MQCM

In this experiment, we proposed an inverted-mesa-like structure formed by interposing a polydimethyl-siloxane (PDMS) wall between adjacent QCM electrodes on a single quartz substrate to achieve the interference-free MQCM that is coupled with real-time flow system for multi-analyte bio-sensing applications. In addition, the electrical coupling between adjacent channels due to impedance of solution is suppressed by extending the flow path between them with a serial extended-design flow channel. Moreover, the serial extended-flow design can prevent turbulent flow of analyte within the system that may cause unpredictable sensing response. The MQCM is applied for real-time multi-analyte biosensing of immunoglobulin G (IgG) and human serum albumin (HSA).

5.4.1 Fabrication of MQCM and flow module

The structure of multi-analyte MQCM biosensor system is schematically illustrated in Fig 5.16. The system consisted of three main components including a single AT-cut quart crystal substrate with QCM electrodes, PDMS interposing slabs and the flow system made of acrylic. Firstly, three pairs of circular QCM electrodes with 4.5 mm in diameter were fabricated by dc sputtering of chromium/gold (Cr/Au) layers through a set of shadow masks on 15mm-diameter 8.2 MHz AT-cut quartz crystal substrates (AATA Japan Co., Ltd), using the condition presented in Chapter 5.1. The three QCM electrode pairs (with 4.5 diameter size) were located symmetrically and concentrically around the 15mm quartz disc.

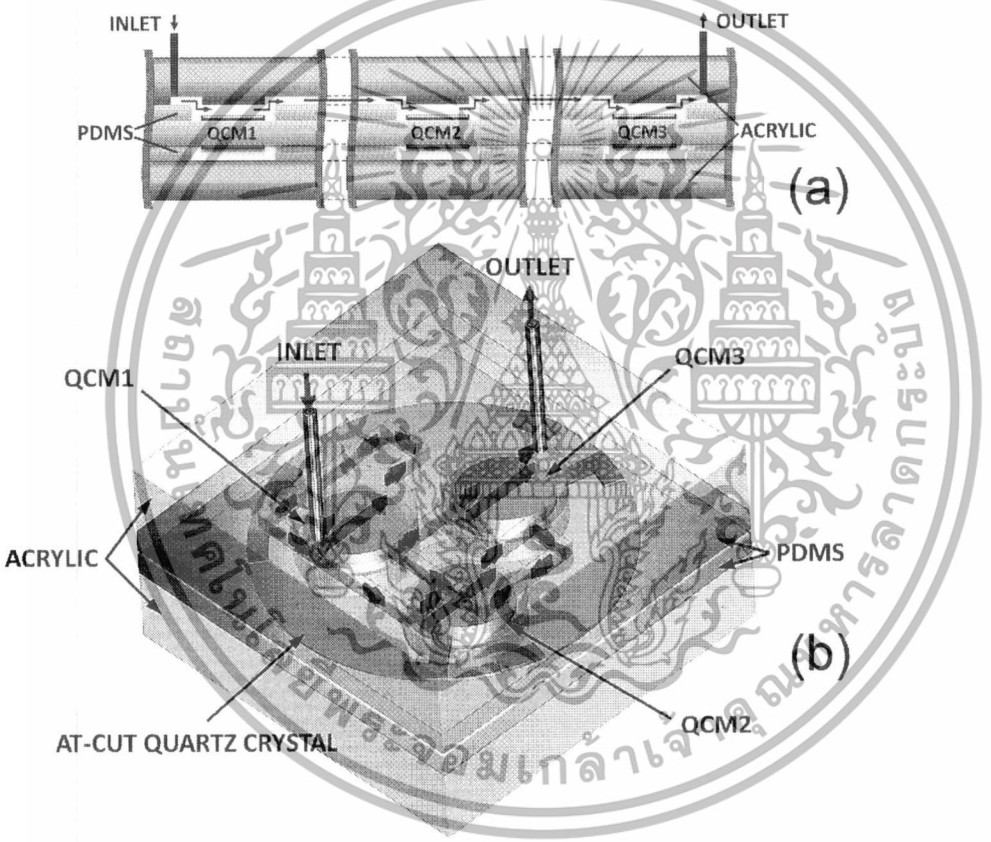

Figure 5.16 Structure of multi-analyte MQCM biosensors:
(a) the conceptual cross-sectional structure illustrating QCM electrodes embedded in inverted-mesa-like MQCM platform and
(b) 3D layout of the MQCM in serial flow cell module with extended-flow design.

Next, two PDMS interposing slabs (top and bottom) were fabricated by casting and cutting processes. PDMS prepolymer mixture was prepared by mixing PDMS precursor (Sylgard 184 Silicone Elastomer, Dow Corning) with curing agent at a volume ratio of 10:1 and then degassed at 20-50 mTorr in a vacuum desiccator for 10 minute to remove bubbles. Next, 6 ml of the mixture was casted on a 4-inch blank silicon wafer with aluminum walls on all edges and baked at 80C for 1 hour. The PDMS slab with 0.8 mm in thickness was cut into the designed shapes using a craft cutting machine. The shape of top slab was a 20 mm x 20 mm rectangular sheet with three 5 mm holes located concentrically with the three QCM electrodes while the bottom slab had the same shape but with additional small holes for the spring connectors to electrically connect with the electrodes on quartz substrate. In the last part, the acrylic flow system was manufactured by mechanical machining. The acrylic flow system consisted of top and bottom 5 mm-thick acrylic blocks. The top Acrylic block was milled to form the 1 mm-wide and 0.2 mm-deep flow channels connected between QCM chambers, which were placed on top of QCM electrodes. Next, holes for the inlet/outlet of flow channels and clamp screws were drilled. The bottom acrylic block only contained drilled holes used for mechanical clamping of the whole structure and passage of electrical connector from QCM electrodes. The photograph of the fabricated MQCM components is illustrated in the Figure 5.17.

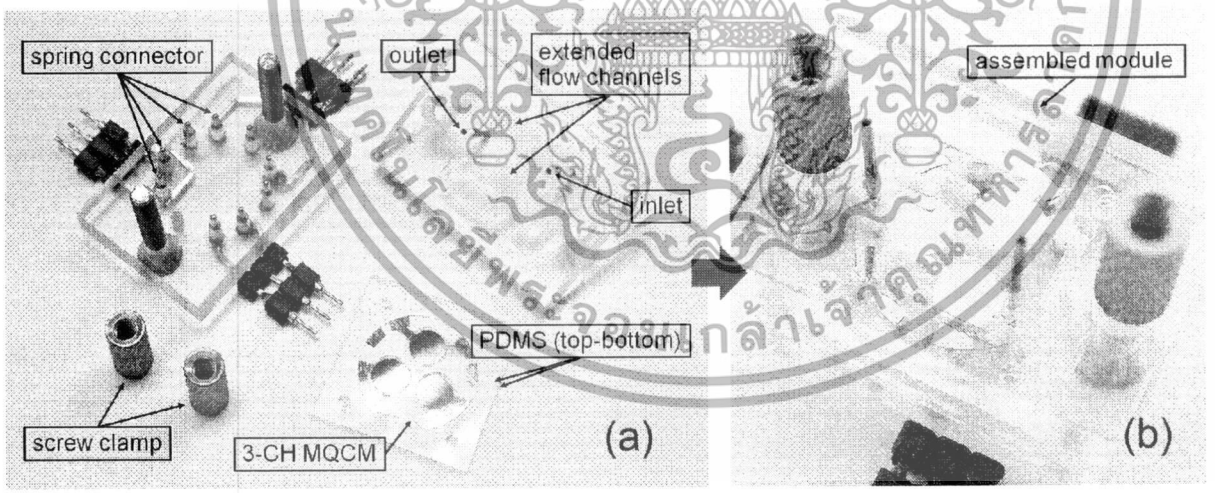

Figure 5.17 Photographs of the fabricated MQCM and serial flow cell: (a) components and (b) assembled module.

5.4.2 Immobilization of antibodies for IgG and HSA

The first and second QCM electrodes (assigned as channel 1 and channel 2) were immobilized with anti-immunoglobulin G (anti-IgG) and anti-human serum albumin (anti-HSA), respectively while the third electrode (designated as channel 3) had no immobilization and was used as the negative control as well as reference for temperature compensation as illustrated in Figure 5.18. Both antibodies were immobilized using the same protocol as shown in Scheme 2 (b). Firstly, the fabricated MQCM was cleaned in piranha solution (1:4 mixture of 30% H2O2 and 97% H2SO4) without external heating for 5 minutes to completely remove organic contamination. Next, PDMS slabs were aligned and attached on MQCM electrodes to confine reagent presented to each electrode. 20 µl of 25mM Cystamine (C7255, Sigma Aldrich) solution was then dropped on channel 1 and 2 of MQCM for 24 hours to form self-assembled monolayers (SAMs) on the gold electrodes followed by rinsing with de-ionized (DI) water. Cystamine was a bio-functional building block that had two functional end groups, including thiol (SH) and amine (NH2). The sulfur atoms of thiol group were bound to gold surface through weak acid-base interaction while the amine group would be left for subsequent reaction.

Next, 20 mM Glutaraldehyde (G-5882, Sigma Aldrich) was dropped on the two MQCM electrodes each with 20 µl and incubated for 1 hour before rinsing with 0.01M phosphate buffer saline (PBS, pH=7.4, P5368, Sigma Aldrich). Glutaraldehyde, the cross-linking reagent with two aldehyde functional groups, was used to anchor the amine functional group of the Cystamine-modified gold surface and antibody. Next, the anti-IgG and anti-HSA solutions were prepared by 1:100 dilution of 2.1 mg/ml anti-IgG (B8395, Sigma Aldrich) and 2.6 mg/ml anti-HSA (A3293, Sigma Aldrich) source solutions, respectively. 20 µl of anti-IgG and anti-HSA solutions were then dropped on MQCM channel 1 and 2, respectively. The antibodies were incubated at 4°C for 24 hours followed by rinsing with PBS buffer to remove any excess antibodies. In the last step, 20 µl of 1 mM Bovine serum albumin (BSA: A2153, Sigma Aldrich) solution was dropped on all channels of MQCM and incubated at 4°C for 2 hours. BSA was used to prevent signals from non-specific site binding in all QCM channels including channel 3, which has no immobilized antibody.

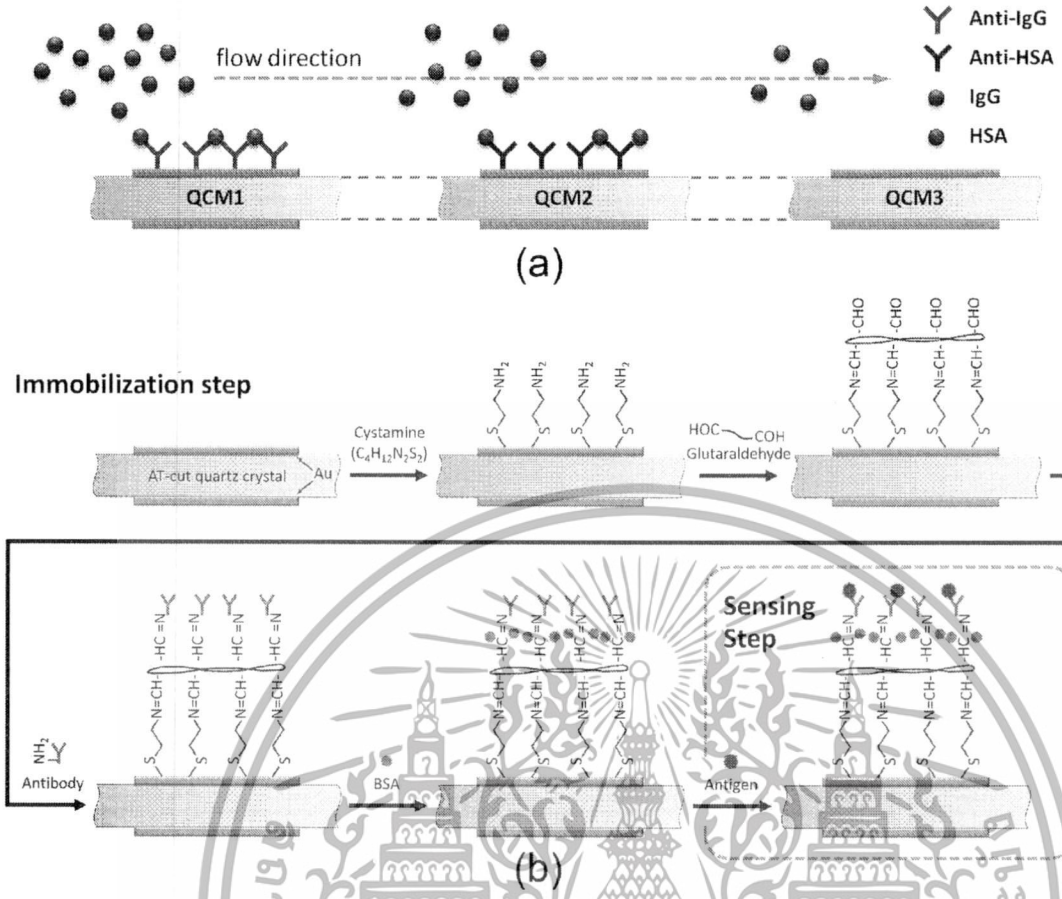

Figure 5.18 (a) MQCM representation for IgG and HSA detection and (b) the antibody immobilization protocol on MQCM electrodes.

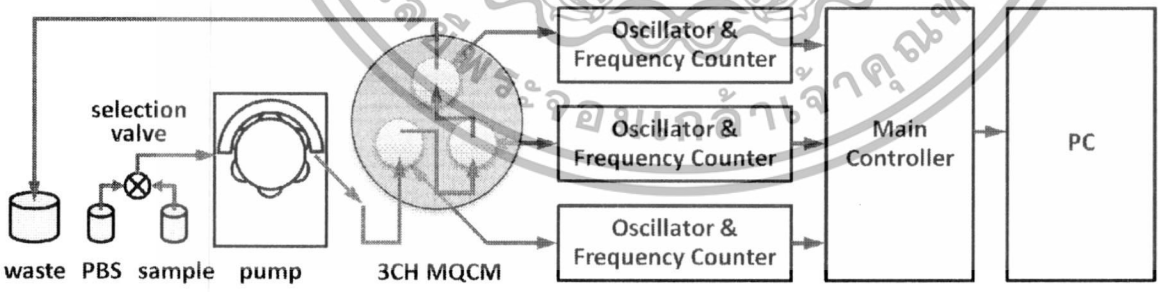

Figure 5.19 Diagram of the real-time flow-sensing experimental setup for multi-analyte MQCM biosensors.

5.4.3 Experimental Sensing system

To obtain the complete sensing module, the top acrylic block was aligned and attached with the modified MQCM via the top PDMS slab and then placed on the bottom acrylic block via guiding screws. The acrylic flow components were finally sealed with screw clamps. The photograph of assembled module is shown in Figure 5.17(b).The experimental setup for real-time bio-sensing of MQCM in serial flow module is shown in Figure 5.19. The red arrow dictates the electrical information transfer path while the blue arrow represents the solution flow path. Each MQCM channel was connected to individual oscillator and frequency counter circuit. The measured frequency data from all channels were sent to the main controller and to a personal computer via USB port for real-time recording and monitoring. For the solution flow path, the inlet and outlet of MQCM flow cell were connected to peristaltic pump (Ismatec® ISM831 REGLO Digital) and waste container via Tycon® polymer tube (ID = 0.38 mm). The solution was driven by the pump at a controlled flow rate (20 µl/min) through the first, second and last channels of MQCM along extended flow channels as indicated before exiting from the outlet to a waste container. Initially, PBS solution was flowed through MQCM and frequencies from all channels were constantly recorded. After stabilization of baseline signals, the solution containing IgG and/or HSA samples were introduced by switching the valves connected to the buffer and sample solutions while the frequency shift due to antigen/antibody binding were continuously recorded. The IgG and HSA sample solutions with various concentrations were prepared for injection by proper dilution of IgG and HSA stock solutions. For example, the IgG-HSA (200-200 µg/ml) solution was made by adding 20ul of IgG 10 mg/ml stock and 20ul of 10 mg/ml HSA stock into 960ul of PBS solution.

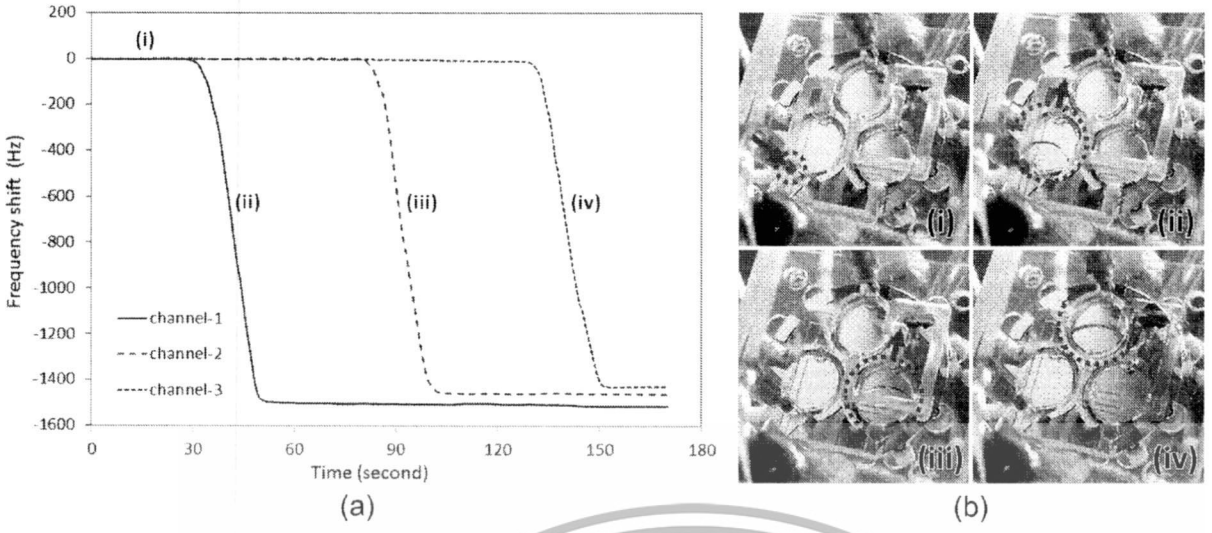

Figure 5.20 (a) Frequency shift response of the MQCM during initial stage of PBS flow through the flow cell module. (b) Photographs of the fabricated MQCM at various flow states when the PBS solution flows through (i) inlet, (ii) channel 1, (iii) channel 2 and (iv) channel 3, respectively.

5.4.4 Experimental results and discussion

Generally, liquid such as a buffer solution is a large load that strongly affects the oscillation frequency of QCM. It has been reported that a QCM will experience a frequency shift when liquid is applied on quartz substrate even at locations outside the sensing electrode due mechanical coupling between the load and bulk acoustic wave. Thus, interference behaviors of MQCM can be detected under liquid loading. The interference characteristics of MQCM have been evaluated from the effect of liquid loading occurred during the initial flow stage as shown in Figure 5.20. Figure 5.20 (a) shows the measured frequency shift of all QCM channels as PBS flows from the inlet to the outlet. It can be seen that the states of resonant frequency shifts of different QCM channels can be divided into four regions, which correspond to different states of liquid flow as photographically demonstrated in Figure 5.20 (b). In the first region (i), PBS is just fed into the inlet but has not reach the first QCM channel when there is no frequency shift in all channels. The second region (ii) begins when PBS passes through to first channel, causing a large frequency shift for QCM channel-1. The magnitude of frequency shift of QCM channel 1 rapidly increases and become steady after PBS completely fills its chamber. Interestingly, it can be seen that there is no resonant frequency shift for QCM channel 2 and 3 while QCM channel

1 undertakes such a large load. Similarly, only QCM channel 2 or 3 exhibits a change of resonant frequency as PBS goes through the corresponding QCM chamber (states (iii) and (iv)). The results demonstrate that liquid loading on one MQCM channel has no influence on resonant frequency of other channels. Since, liquid loading normally causes very large frequency shift and very strong interference between MQCM channels, it is expected that the MQCM should also exhibit no interference due to typical mass loading both in liquid and gas phases.

After the solution passed each QCM channel (when the frequency shift of the channel becomes steady), it can be observed that there is an approximately equal delay time of ~30 s before the next QCM channel begins to show a resonant frequency shift due to liquid loading. The delay time corresponds to the time that the solution takes to go through the extended flow channel between linked channels, which have been designed to have the same length for channels 1-2 and 2-3. At this point, it should be noted that the extended flow channel is specially designed to eliminate the inference due to electrical coupling between QCM channels. The electrical coupling has been observed when consecutive QCM chambers are connected with a direct flow channel. This electrical coupling is believed to be induced by the impedance of PBS solution that is electrically coupled among oscillator circuits. With the extended design, the coupling impedance is substantially increased such that the electrical interference becomes negligible as clearly seen from the experimental results.

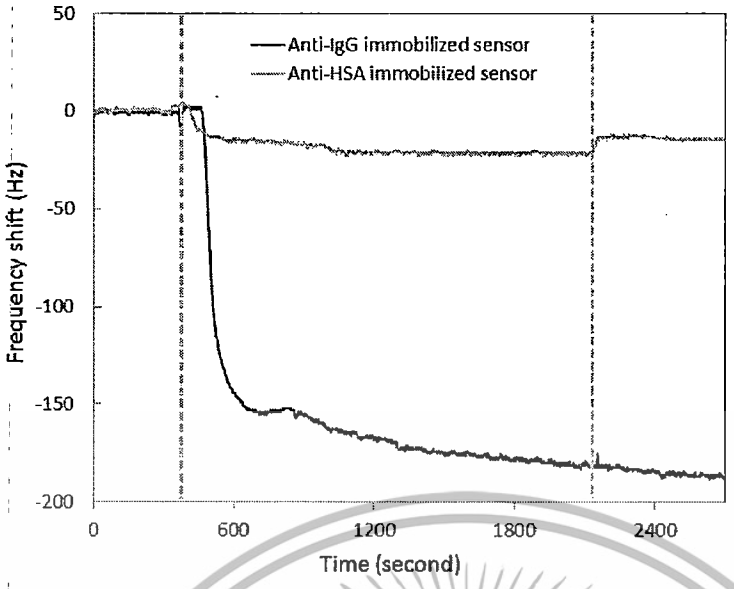

Figure 5.21 Frequency shift response of the Anti-IgG and Anti-HSA immobilized sensor: the response to IgG sample (200 µg/ml).

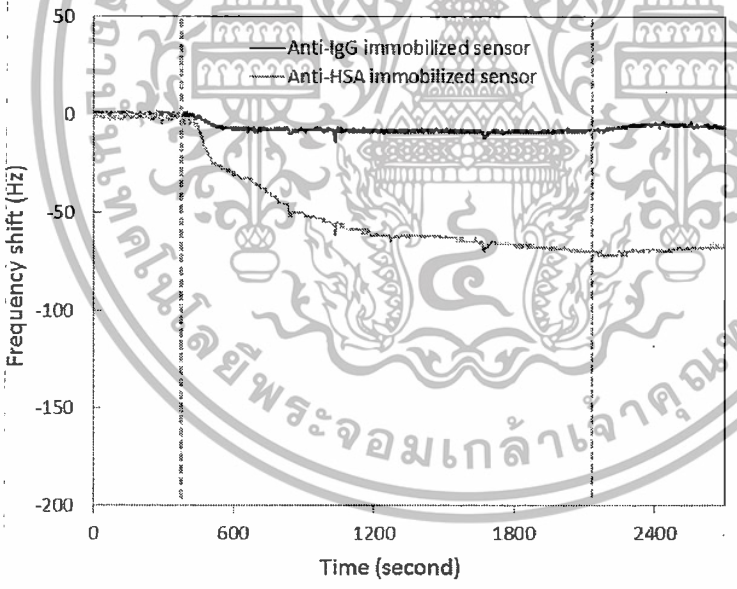

Figure 5.22 Frequency shift response of the Anti-IgG and Anti-HSA immobilized sensor: the response to HSA sample (200 µg/ml).

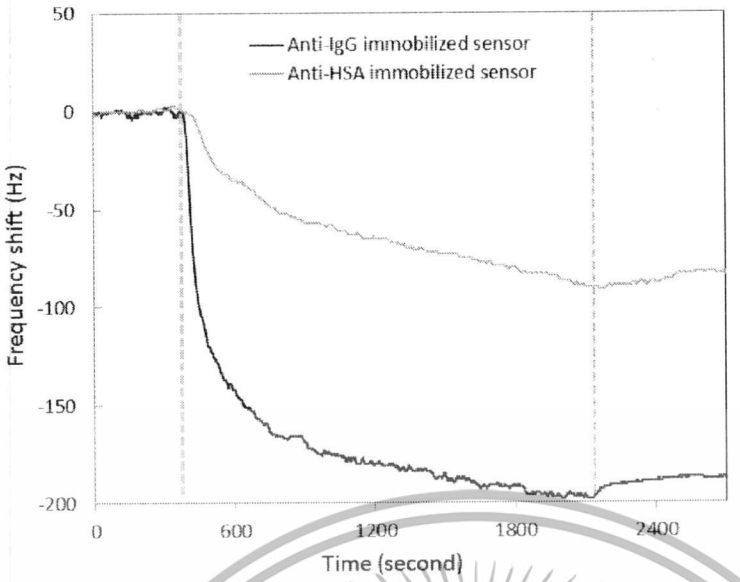

Figure 5.23 Frequency shift response of the Anti-IgG and Anti-HSA immobilized sensor: the response to IgG-HSA sample (200-200 µg/ml).

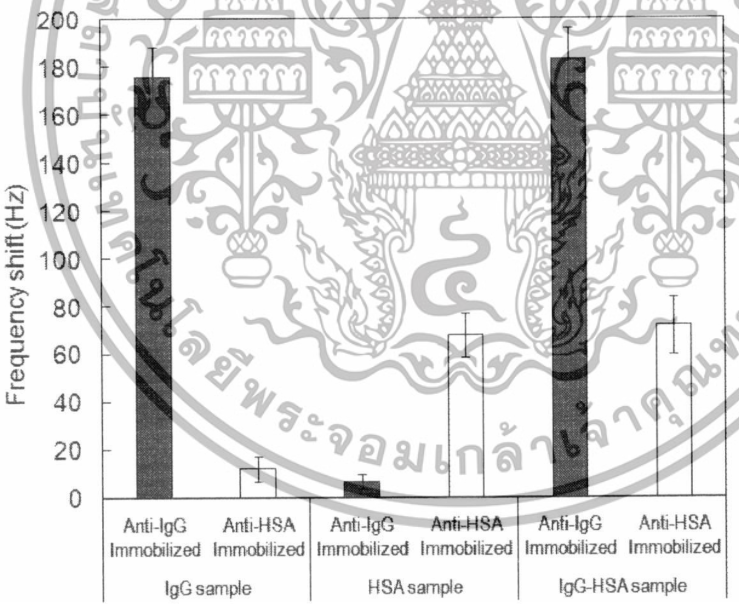

Figure 5.24 Frequency shift response of the Anti-IgG and Anti-HSA immobilized sensor: the net frequency shift of IgG and HSA sensors for single and double analyte samples.

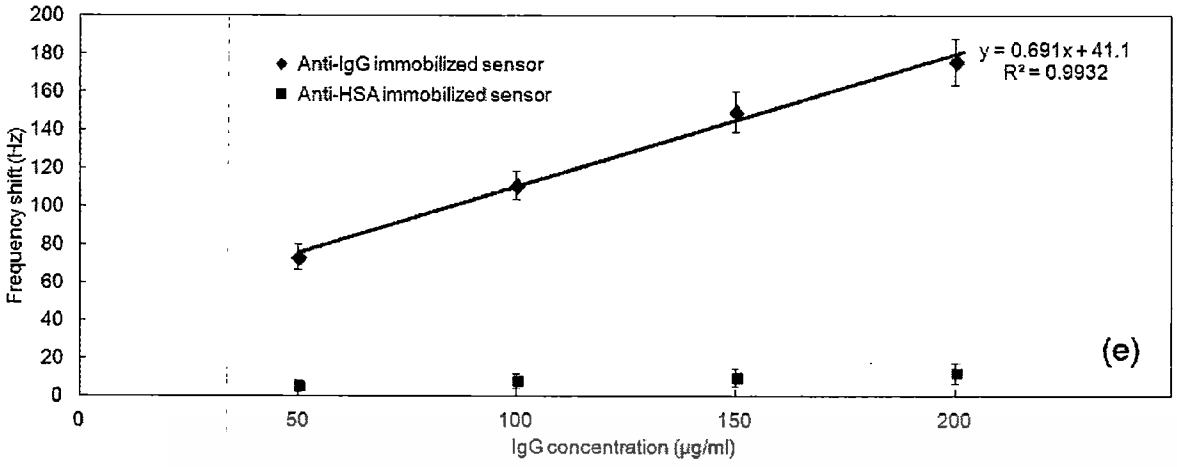

Figure 5.25 Frequency shift response of the Anti-IgG and Anti-HSA immobilized sensor: the resonant frequency shift of the sensors as a function of IgG concentration.

The immobilized MQCM device has been tested for real-time detection of single- and double-analyte samples. PBS buffer was flowed for 5 minutes to obtain stable baseline signal. The analyte sample was then fed for 30 minutes and PBS buffer was resumed for 10 minutes to remove unbound analytes. Figure 5.21, 5.22 and 5.23 shows the real-time frequency shift response of Anti-IgG and Anti-HSA immobilized biosensors upon introduction of IgG (200 µg/ml), HSA (200 µg/ml) and IgG-HSA (200-200 µg/ml) solutions, respectively. With single-analyte solutions (Figure 5.21 and 5.22), it can be seen the IgG and HSA QCM sensors only show frequency shift responses to their corresponding analyte while there are very small cross frequency shifts in another channel due possibly to remnant unspecific binding. In addition, the MQCM biosensors show relatively fast response with drastic frequency shift in the initial sensing period due to the abundance of unbound receptors on the electrodes. After that, the frequency shift becomes slowly and steadily increased with time because of lower probability of antibody-target binding. Moreover, the relative standard deviation (RSD) of environmental background noise and frequency shift of negative control (un-immobilized QCM) are found to be less than $\pm$1.3 and $\pm$3.2 Hz, respectively, confirming high stability of MQCM biosensors. When both analytes are present in the solution (Figure 5.23), IgG and HSA sensors give responses accordingly with similar frequency shift profiles to the cases of single analytes. Figure 5.24 compares the net frequency shift of IgG and HSA sensors for single and double analyte samples. It is seen that MQCM sensors give well-matched responses for single and double analytes of the same concentration. The

results clearly demonstrate that two analytes can be independently and reliably detected in real-time with multi-channel QCM sensors. In principle, the present system can practically work with three analytes without a negative control since three QCMs are proven to be interference free by the liquid-loading experiment. The multi-analyte detection performances can be attributed to effective suppression of acoustic and electrical coupling. The acoustic coupling between adjacent QCM channels is effectively blocked by inverted-mesa-like structure formed using doubled-sided PDMS wall on the quartz substrate. The application of PDMS to form the inverted-mesa-like structure allows the direct use of a simple planar quartz substrate for highly effective MQCM without the need of difficult quartz-substrate modification processes, making MQCM more practical for sensing applications. Moreover, the electrical coupling between adjacent electrodes is highly diminished by the extended-design flow channel. The flow path of sample solution between QCMs can significantly influence electrical signal of each QCMs via resistive/capacitive coupling due to ionic/dielectric conduction. In a typical MQCM system, all MQCM electrode are placed in a single chamber and QCMs are simultaneously resonated with different instantaneous potentials. There would be electrical conduction through the solution that couples potential from one electrode to another, leading to strong cross interference signals among various QCM electrodes. With the extended flow design system, such electrical conduction between electrodes is largely limited by a long and narrow channel between the electrodes, resulting in negligible coupling effect.

The sensing characteristics of MQCM sensors have been determined for analyte concentration in the range of 0-200 µg/ml. Figure 5.25 shows the typical resonant frequency shifts of Anti-IgG-immobilized and Anti-HSA-immobilized MQCM sensors as a function of IgG concentration. It can be seen that the frequency shift of Anti-IgG-immobilized sensor is approximately linear in the range of 50-200 µg/ml with a linear sensitivity of 0.69 Hz/(µg/ml) while the cross frequency shift of HSA-immobilized MQCM sensor has no correlation with IgG concentration. The error bars in Figure 5.24 and 5.25 represent RSD of measured frequency shifts from 8 detection experiments. The RSD is in the range of 6.5-9.6%, demonstrating good repeatability of MQCM sensors. The corresponding detection limit (3Signal/Noise) is estimated to be ~5 µg/ml, which still relatively poor compared with several reported IgG QCM biosensors whose detection limit is within the range of 0.005-0.5 µg/ml. The reported QCM biosensors employed various sensitivity-enhancement techniques including high operating resonance frequency (15-60 MHz), optimized protein-assisted antibody immobilization and nanoparticle-enhanced loading. These approaches can be well applied

to the developed MQCM platform. This preliminary MQCM biosensor work has mainly focused on the elimination of mechanical and electrical interference by low-cost inverted mesa-like PDMS-sandwich structure with extended flow design to achieve simultaneous interference-free detections of more than one analytes and demonstrated the results for the simplest case of dual-analyte biosensing with a negative control. This work was published in the journal "Biosensors and Bioelectronics" [98].

Even, concept of the platform has been proofed through the experiments, but there are still many point left for the additional study. Such as, the way to improve the sensing time (currently around 45 minute), the way of regenerating used-sensor to capable of reuse-ability, as well as the way to increase the channel number with high sensitivity and stability. We believed that, this simple methods that applied to solve the critical problem of the MQCM will shed light on the real-time effectively detection and quantification of multiple bio-analytes via MQCM in the near future.

Chapter 6
CONCLUSIONS

In conclusion, a new interference-free MQCM platform with integrated PDMS interposing wall and extended flow structure has been designed, fabricated and characterized for bio-sensing applications. The system consisted of three main components including a single AT-cut quart crystal substrate with QCM electrodes, PDMS interposing slabs and the acrylic flow system, which were fabricated by Cr/Au sputtering through electroplated shadow masks, casting/cutting and mechanical machining processes, respectively. The electrical-testing results during initial solution flow stage demonstrated that liquid loading on one MQCM channel had no influence on resonant frequency of other channels, indicating the achievement of interference-free MQCM. In addition, the electrical coupling due to the electrical impedance of solution is diminished by extending the flow path between them with an extended-design flow channel. MQCM has been applied for multi-analyte biosensing of IgG and HSA with individual immobilization of anti-IgG and anti-HSA on two adjacent QCM electrodes. The tested results with single- and double-analyte solutions under continuous flow of buffer clearly demonstrated that IgG and HSA QCM sensors only showed frequency shift responses to their corresponding analytes and there were very small cross frequency shifts. Moreover, MQCM sensors exhibit approximately linear frequency shift response with analyte concentration. The results indicate that multiple analytes can be simultaneously and quantitatively detected with negligible interference by the developed MQCM platform.

REFERENCES

[1] Cady, W. G., **Piezoelectricity, An introduction to the Theory and Applications of Electromechanical Phenomena in Crystals**. New York: Dover Publications, Inc., 1964.

[2] Boston Piezo-Optics Inc., "**Intro to Piezoelectric Transducer Crystals**," http://bostonpiezooptics.com/intro-to-transducer-crystals

[3] Hewlett Packard, "**Fundamentals of Quartz Oscillators**," Application note 200-2.

[4] Clarke, B., "**How are quartz crystals grown?.**"

[5] "**A single-crystal quartz bar artificially grown by the hydrothermal method.**," https://commons.wikimedia.org/wiki/File:Quartz_synthese.jpg

[6] Marx, K. A., "**Quartz crystal microbalance: A useful tool for studying thin polymer films and complex biomolecular systems at the solution - Surface interface**," *Biomacromolecules,* vol. 4, pp. 1099-1120, 2003.

[7] Wyszynski, B. and Nakamoto, T., "**Linking Biological and Artificial Olfaction: Biomimetic Quartz Crystal Microbalance Odor Sensors**," *IEEJ Transactions on Electrical and Electronic Engineering,* vol. 4, pp. 334-338, May 2009.

[8] Alder, J. F. and Mccallum, J. J., "**Piezoelectric crystals for mass and chemical measurements a review**," *Analyst,* vol. 108, pp. 1169-1189, 1983.

[9] Uludag, Y., Piletsky, S. A., Turner, A. P. F., and Cooper, M. A., "**Piezoelectric sensors based on molecular imprinted polymers for detection of low molecular mass analytes**," *FEBS J.,* vol. 274, pp. 5471-5480, Nov 2007.

[10] Su, X., Chew, F. T., and Li, S. F. Y., "**Design and application of piezoelectric quartz crystal-based immunoassay**," *Anal. Sci.,* vol. 16, pp. 107-114, 2000.

[11] Pavey, K. D., "**Quartz crystal analytical sensors: The future of label-free, real-time diagnostics?**," *Expert Review of Molecular Diagnostics,* vol. 2, pp. 173-186, 2002.

[12] Henderson, J., **Electronic Devices. Concepts and Applications**. NJ: Prentice Hall, 1991.

[13] QCM Research, "**Commercially Available QCM**," http://www.qcmresearch.com

[14] Rabe, J., Büttgenbach, S., Schröder, J., and Hauptmann, P., "**Monolithic miniaturized quartz microbalance array and its application to chemical sensor systems for liquids**," *IEEE Sens. J.,* vol. 3, pp. 361-368, 2003.

[15] Sauerbrey, G., "**The Use of Quartz Oscillators for Weighing Thin Layers and for Microweighing**," *Z. Physik,* vol. 155, pp. 206-222, April 1959.

[16] Keiji Kanazawa, K. and Gordon Ii, J. G., "**The oscillation frequency of a quartz resonator in contact with liquid**," *Anal. Chim. Acta,* vol. 175, pp. 99-105, 1985.

[17] Ward, M. D. and Delawski, E. J., "**Radial mass sensitivity of the quartz crystal microbalance in liquid media**," *Anal. Chem.,* vol. 63, pp. 886-890, 1991.

[18] Lin, Z., Yip, C. M., Scott Joseph, I., and Ward, M. D., "**Operation of an ultrasensitive 30-MHz quartz crystal microbalance in liquids**," *Anal. Chem.,* vol. 65, pp. 1546-1551, 1993.

[19] Rodahl, M. and Kasemo, B., "**Frequency and dissipation-factor responses to localized liquid deposits on a QCM electrode**," *Sens. Actuators, B,* vol. 37, pp. 111-116, 1996.

[20] Muramatsu, H., Tamiya, E., and Karube, I., "**Computation of equivalent circuit parameters of quartz crystals in contact with liquids and study of liquid properties**," *Anal. Chem.,* vol. 60, pp. 2142-2146, 1988.

[21] Rodahl, M., Höök, F., Fredriksson, C., Keller, C. A., Krozer, A., Brzezinski, P., *et al.*, "**Simultaneous frequency and dissipation factor QCM measurements of biomolecular adsorption and cell adhesion**," *Faraday Discuss.,* vol. 107, pp. 229-246, 1997.

[22] Penza, M., Cassano, G., Aversa, P., Antolini, F., Cusano, A., Cutolo, A., *et al.*, "**Alcohol detection using carbon nanotubes acoustic and optical sensors**," *Appl. Phys. Lett.,* vol. 85, pp. 2379-2381, 2004.

[23] Matsuguchi, M. and Uno, T., "**Molecular imprinting strategy for solvent molecules and its application for QCM-based VOC vapor sensing**," *Sens. Actuators, B,* vol. 113, pp. 94-99, 2006.

[24] Brousseau Iii, L. C. and Mallouk, T. E., "**Molecular Design of Intercalation-Based Sensors. 1. Ammonia Sensing with Quartz Crystal Microbalances Modified by Copper Biphenylbis(phosphonate) Thin Films**," *Anal. Chem.,* vol. 69, pp. 679-687, 1997.

[25] Ding, B., Kim, J., Miyazaki, Y., and Shiratori, S., "**Electrospun nanofibrous membranes coated quartz crystal microbalance as gas sensor for NH₃ detection**," *Sens. Actuators, B,* vol. 101, pp. 373-380, 2004.

[26] Wang, X., Zhang, J., and Zhu, Z., "**Ammonia sensing characteristics of ZnO nanowires studied by quartz crystal microbalance**," *Appl. Surf. Sci.,* vol. 252, pp. 2404-2411, 2006.

[27] Ward, M. D., **Physical Electrochemistry: Principles, Methods & Applications**. New York: Rubenstein, I., Ed.; Marcel Dekker, 1995.

[28] Asakura, N., Kamachi, T., and Okura, I., "**Motion of redox molecules in solution monitored by the highly-sensitive EQCM technique**," *Res. Chem. Intermed.*, vol. 32, pp. 341-355, 2006.

[29] Lukaszewski, M. and Czerwhiski, A., "**Comparative EQCM study on electrooxidation of carbon oxides adsorption products on noble metals and their alloys. Polycrystalline Pd-based systems**," *J. Electroanal. Chem.*, vol. 606, pp. 117-133, Aug 2007.

[30] O'sullivan, C. K. and Guilbault, G. G., "**Commercial quartz crystal microbalances - Theory and applications**," *Biosens. Bioelectron.*, vol. 14, pp. 663-670, 1999.

[31] Janshoff, A., Galla, H. J., and Steinem, C., "**Piezoelectric mass-sensing devices as biosensors - An alternative to optical biosensors?**," *Angew. Chem., Int. Ed.*, vol. 39, pp. 4004-4032, 2000.

[32] Wegener, J., Janshoff, A., and Steinem, L., "**The quartz crystal microbalance as a novel means to study cell-substrate interactions in situ**," *Cell Biochem. Biophys.*, vol. 34, pp. 121-151, 2001.

[33] Čavić, B. A., Hayward, G. L., and Thompson, M., "**Acoustic waves and the study of biochemical macromolecules and cells at the sensor-liquid interface**," *Analyst*, vol. 124, pp. 1405-1420, 1999.

[34] Ricci, F., Volpe, G., Micheli, L., and Palleschi, G., "**A review on novel developments and applications of immunosensors in food analysis**," *Anal. Chim. Acta*, vol. 605, pp. 111-129, Dec 2007.

[35] Skottrup, P. D., Nicolaisen, M., and Justesen, A. F., "**Towards on-site pathogen detection using antibody-based sensors**," *Biosens. Bioelectron.*, vol. 24, pp. 339-348, Nov 2008.

[36] Hirst, E. R., Yuan, Y. J., Xu, W. L., and Bronlund, J. E., "**Bond-rupture immunosensors - A review**," *Biosens. Bioelectron.*, vol. 23, pp. 1759-1768, Jul 2008.

[37] Hug, T. S., "**Biophysical methods for monitoring cell-substrate interactions in drug discovery**," *Assay Drug Dev. Technol.*, vol. 1, pp. 479-488, 2003.

[38] Bottom, V. E., **Introduction to Quartz Crystal Unit Design**. New York: Van Nostrand Reinhold, 1982.

[39] Bruckenstein, S., Fensore, A., Li, Z., and Hillman, A. R., "**Dual quartz crystal microbalance compensation using a submerged reference crystal. Effect of surface roughness and liquid properties**," *J. Electroanal. Chem.*, vol. 370, pp. 189-195, 1994.

[40] Bruckenstein, S., Michalskl, M., Fensore, A., Zhufen, L. I., and Hillman, A. R., "**Dual quartz crystal microbalance oscillator circuit. Minimizing effects due to liquid viscosity, density, and temperature,**" *Anal. Chem.,* vol. 66, pp. 1847-1852, 1994.

[41] Dunham, G. C., Benson, N. H., Petelenz, D., and Janata, J., "**Dual quartz crystal microbalance,**" *Anal. Chem.,* vol. 67, pp. 267-272, 1995.

[42] Uno, T., "**Temperature compensation of thickness shear mode resonators formed on artificial twinned quartz plates,**" presented at the Frequency Control Symposium, 1996. 50th., Proceedings of the 1996 IEEE International., 1996.

[43] Berg, S. and Johannsmann, D., "**Laterally coupled quartz resonators,**" *Anal. Chem.,* vol. 73, pp. 1140-1145, 2001.

[44] Shen, F., Lee, K. H., O'shea, S. J., Lu, P., and Ng, T. Y., "**Frequency interference between two quartz crystal microbalances,**" *IEEE Sens. J.,* vol. 3, pp. 274-281, Jun 2003.

[45] Tatsuma, T., Watanabe, Y., Oyama, N., Kitakizaki, K., and Haba, M., "**Multichannel quartz crystal microbalance,**" *Anal. Chem.,* vol. 71, pp. 3632-3636, 1999.

[46] Tuantranont, A., Wisitsora-At, A., Sritongkham, P., and Jaruwongrungsee, K., "**A review of monolithic multichannel quartz crystal microbalance: A review,**" *Analytica Chimica Acta,* vol. 687, pp. 114-128, 2011.

[47] Hung, V. N., Abe, T., Minh, P. N., and Esashi, M., "**Miniaturized, highly sensitive single-chip multichannel quartz-crystal microbalance,**" *Appl. Phys. Lett.,* vol. 81, pp. 5069-5071, 2002.

[48] Lu, F., Lee, H. P., Lu, P., and Lim, S. P., "**Finite element analysis of interference for the laterally coupled quartz crystal microbalances,**" *Sens. Actuators, A,* vol. 119, pp. 90-99, 2005.

[49] Martin, S. J., Granstaff, V. E., and Frye, G. C., "**Characterization of a quartz crystal microbalance with simultaneous mass and liquid loading,**" *Anal. Chem.,* vol. 63, pp. 2272-2281, 1991.

[50] Cernosek, R. W., Martin, S. J., Hillman, A. R., and Bandey, H. L., "**Comparison of lumped-element and transmission-line models for thickness-shear-mode quartz resonator sensors,**" *IEEE T. Ultrason. Ferr.,* vol. 45, pp. 1399-1407, 1998.

[51] Tiersten, H. F., **Linear Piezoelectric Plate Vibrations**. New York: Plenum, 1969.

[52] Shen, F. and Lu, P., "**Influence of interchannel spacing on the dynamical properties of multichannel quartz crystal microbalance,**" *IEEE T. Ultrason. Ferr.,* vol. 51, pp. 249-253, Feb 2004.

[53] Mindlin, R. D. and Lee, P. C. Y., "**Thickness-shear and flexural vibrations of partially plated, crystal plates**," *Int. J. Solids Struct.*, vol. 2, pp. 125-139, 1966.

[54] Yong, Y.-K., Stewart, J. T., Detaint, J., Zarka, A., Capelle, B., and Zheng, Y., "**Thickness-shear mode shapes and mass-frequency influence surface of a circular and electroded AT-cut quartz resonator**," *IEEE T. Ultrason. Ferr.*, vol. 39, pp. 609-617, 1992.

[55] Li, L., Abe, T., and Esashi, M., "**Microfabricated spherical bi-convex quartz crystal microbalance array**," presented at the Proceedings of the IEEE International Conference on Micro Electro Mechanical Systems (MEMS), 2005.

[56] Ishizaki, A., Sekimoto, H., Tajima, D., and Watanabe, Y., "**Analysis of spurious vibrations in mesa-shaped AT-cut quartz plates**," presented at the Proceedings of the IEEE Ultrasonics Symposium, 1995.

[57] Goka, S., Sekimoto, H., and Watanabe, Y., "**Experimental study of vibrations of mesa-shaped AT-cut quartz plates**," presented at the Proceedings of the Annual IEEE International Frequency Control Symposium, 1999.

[58] Hirama, K., Aoyama, Y., and Naito, M., "**AT-cut quartz resonators with inverted-mesa electrodes**," *Jpn. J. Appl. Phys., Part 1*, vol. 36, pp. 6432-6436, 1997.

[59] Lakin, K. M., Kline, G. R., and Mccarron, K. T., "**Self limiting etching of piezoelectric crystals**," presented at the Proceedings of the Annual IEEE International Frequency Control Symposium, 1995.

[60] Sekimoto, H., Goka, S., and Watanabe, Y., "**Analysis of 3-D vibrations of rectangular AT-cut quartz plates with a bi-mesa structure**," *IEEE T. Ultrason. Ferr.*, vol. 48, pp. 1302-1307, 2001.

[61] Kreutz, C., Lörgen, J., Graewe, B., Bargon, J., Yoshida, M., Fresco, Z. M., *et al.*, "**High frequency quartz micro balances: A promising path to enhanced sensitivity of gravimetric sensors**," *Sensors*, vol. 6, pp. 335-340, 2006.

[62] Goka, S., Sekimoto, H., and Watanabe, Y., "**Decoupling effect of stepped mesa structures on spurious vibrations of AT-cut quartz plates**," presented at the Proceedings of the Annual IEEE International Frequency Control Symposium, 2000.

[63] Iwata, H., "**Measured resonance characteristics of a 2-GHz-fundamental quartz resonator**," *IEEE T. Ultrason. Ferr.*, vol. 51, pp. 1026-1029, 2004.

[64] Iwata, H., "**Multistage chemical etching for high-precision frequency adjustment in ultrahigh-frequency fundamental quartz resonators**," *IEEE T. Ultrason. Ferr.*, vol. 52, pp. 1435-1442, 2005.

[65] Shen, F., O'shea, S. J., Lee, K. H., Lu, P., and Ng, T. Y., "**Frequency interference between two mesa-shaped quartz crystal microbalances,**" *IEEE T. Ultrason. Ferr.,* vol. 50, pp. 668-675, Jun 2003.

[66] Shen, F., Lu, P., O'shea, S. J., and Lee, K. H., "**Frequency coupling and energy trapping in mesa-shaped multichannel quartz crystal microbalances,**" *Sens. Actuators, A,* vol. 111, pp. 180-187, Mar 2004.

[67] Goka, S., Tamura, K., Sekimoto, H., Watanabe, Y., and Sato, T., "**Decoupling effect of multi-stepped bi-mesa AT-cut quartz resonators,**" presented at the Proceedings of the Annual IEEE International Frequency Control Symposium, 2003.

[68] Nagaura, Y., Kinoshita, K., and Yokomizo, S., "**High-frequency, plano-convex quartz oscillators made by a dual-face lapping machine,**" in *Frequency Control Symposium and Exhibition, 2000. Proceedings of the 2000 IEEE/EIA International*, 2000, pp. 255-259.

[69] Li, L., Abe, T., and Esashi, M., "**Fabrication of miniaturized bi-convex quartz crystal microbalance using reactive ion etching and melting photoresist,**" *Sens. Actuators, A,* vol. 114, pp. 496-500, 2004.

[70] Nagaura, Z., Nagaura, K., Imani, K., and Nagaura, Y., "**Changing process of two convex-lens shape resonators on one quartz blank,**" in *Frequency Control Symposium and Exposition, 2005. Proceedings of the 2005 IEEE International*, 2005, pp. 588-593.

[71] Noge, S., Kamiyama, E., Ueoka, Y., and Uno, T., "**Monolithic integration of AT-cut resonators using artificial twin quartz plate,**" presented at the Ultrasonics Symposium, 1997. Proceedings., 1997 IEEE, 1997.

[72] Noge, S., Kurita, M., and Uno, T., "**Simulation of sensitivity in an optical-access type piezoelectric sensor array,**" presented at the Ultrasonics Symposium, 1999. Proceedings. 1999 IEEE, 1999.

[73] Noge, S. and Uno, T., "**Multi-frequency resonator array using laser beam twinning technique,**" in *Frequency and Time Forum, 1999 and the IEEE International Frequency Control Symposium, 1999., Proceedings of the 1999 Joint Meeting of the European*, 1999, pp. 477-480 vol.1.

[74] Mannelli, I., Minunni, M., Tombelli, S., and Mascini, M., "**Quartz crystal microbalance (QCM) affinity biosensor for genetically modified organisms (GMOs) detection,**" *Biosens. Bioelectron.,* vol. 18, pp. 129-140, 2003.

[75] Höök, F., Rodahl, M., Kasemo, B., and Brzezinski, P., "**Structural changes in hemoglobin during adsorption to solid surfaces: Effects of pH, ionic strength, and ligand binding,**" *Proc. Natl. Acad. Sci. U. S. A.,* vol. 95, pp. 12271-12276, 1998.

[76] Etorki, A. M., Robert Hillman, A., Ryder, K. S., and Glidle, A., "**Quartz crystal microbalance determination of trace metal ions in solution,**" *J. Electroanal. Chem.,* vol. 599, pp. 275-287, 2007.

[77] Mildner-Szkudlarz, S. and Jeleń, H. H., "**The potential of different techniques for volatile compounds analysis coupled with PCA for the detection of the adulteration of olive oil with hazelnut oil,**" *Food Chem.,* vol. 110, pp. 751-761, 2008.

[78] Martinez, A. M. and Kak, A. C., "**PCA versus LDA,**" *IEEE T. Pattern. Anal.,* vol. 23, pp. 228-233, 2001.

[79] Pavlou, A., Turner, A. P. F., and Magan, N., "**Recognition of anaerobic bacterial isolates in vitro using electronic nose technology,**" *Letters in Applied Microbiology,* vol. 35, pp. 366-369, 2002.

[80] Boilot, P., Hines, E. L., Gongora, M. A., and Folland, R. S., "**Electronic noses inter-comparison, data fusion and sensor selection in discrimination of standard fruit solutions,**" *Sens. Actuators, B,* vol. 88, pp. 80-88, 2003.

[81] Branca, A., Simonian, P., Ferrante, M., Novas, E., and Negri, R. M., "**Electronic nose based discrimination of a perfumery compound in a fragrance,**" *Sens. Actuators, B,* vol. 92, pp. 222-227, 2003.

[82] Dutta, R., Morgan, D., Baker, N., Gardner, J. W., and Hines, E. L., "**Identification of Staphylococcus aureus infections in hospital environment: Electronic nose based approach,**" *Sens. Actuators, B,* vol. 109, pp. 355-362, 2005.

[83] Peris, M. and Escuder-Gilabert, L., "**A 21st century technique for food control: Electronic noses,**" *Anal. Chim. Acta,* vol. 638, pp. 1-15, 2009.

[84] Chen, L. F., Liao, H. Y. M., Ko, M. T., Lin, J. C., and Yu, G. J., "**New LDA-based face recognition system which can solve the small sample size problem,**" *Pattern Recognition,* vol. 33, pp. 1713-1726, 2000.

[85] Hastie, T. and Tibshirani, R., "**Discriminant adaptive nearest neighbor classification,**" *IEEE T. Pattern. Anal.,* vol. 18, pp. 607-616, 1996.

[86] Li, C., Heinemann, P., and Sherry, R., "**Neural network and Bayesian network fusion models to fuse electronic nose and surface acoustic wave sensor data for apple defect detection,**" *Sens. Actuators, B,* vol. 125, pp. 301-310, 2007.

[87] Jaruwongrungsee, K., Maturos, T., Sritongkum, P., Sangworasil, M., Wisitsora-At, A., and Tuantranont, A., "**Analysis of quartz crystal microbalance sensor array with circular flow chamber,**" *International Journal of Applied Biomedical Engineering,* vol. 2, pp. 50-54, 2009.

[88] Jaruwongrungsee, K., Maturos, T., Sritongkum, P., Wisitsora-At, A., Pintavirooj, C., Sangworasil, M., *et al.*, "**Design and simulation of flow cell chamber for quartz crystal microbalance sensor array**," presented at the ECTI-CON 2010 - The 2010 ECTI International Conference on Electrical Engineering/Electronics, Computer, Telecommunications and Information Technology, 2010.

[89] Abe, T. and Esashi, M., "**One-chip multichannel quartz crystal microbalance (QCM) fabricated by Deep RIE**," *Sens. Actuators, A,* vol. 82, pp. 139-143, 2000.

[90] Oyama, N., Tatsuma, T., Yamaguchi, S., and Tsukahara, M., "**Scanning Electrode Quartz Crystal Analysis**," *Anal. Chem.,* vol. 69, pp. 1023-1029, 1997.

[91] Hess, C., Borgwarth, K., and Heinze, J., "**Integration of an electrochemical quartz crystal microbalance into a scanning electrochemical microscope for mechanistic studies of surface patterning reactions**," *Electrochim. Acta,* vol. 45, pp. 3725-3736, 2000.

[92] "**Principle of biosensors**," http://www.dddmag.com/images/0409/HTS1_lrg.jpg

[93] TRENDS in Biotechnology, "**cell-based biosensors**,"

[94] Pearson Education, Inc., "**The Immune System**," http://www.highlands.edu/academics/divisions/scipe/biology/faculty/harnden/2122/notes/immune.htm

[95] The Pennsylvania State University, "**The Origins and Diversity of Life**," https://wikispaces.psu.edu/display/BIOL110F2013/The+Origins+and+Diversity+of+Life

[96] Cooper, M. A., "**Optical biosensors in drug discovery**," *Nature Reviews Drug Discovery,* pp. 515–528, 2002.

[97] Starodub, N. F. and Ogorodnijchuk, J. O., "**Immune Biosensor Based on the ISFETs for Express Determination of Salmonella typhimurium**," *Electroanalysis,* vol. 24(3), pp. 600-606, 2012.

[98] Jaruwongrungsee, K., Waiwijit, U., Wisitsoraat, A., Sangworasil, M., Pintavirooj, C., and Tuantranont, A., "**Real-time multianalyte biosensors based on interference-free multichannel monolithic quartz crystal microbalance**," *Biosensors and Bioelectronics,* vol. 67, pp. 576-581, 2015.

ประวัติผู้เขียน

ชื่อ-นามสกุล นาย คทา จารุวงศ์รังสี (KATA JARUWONGRUNGSEE)
วัน เดือน ปีเกิด 6 มกราคม 2525 (กรุงเทพมหานคร)

ประวัติการศึกษา

2546 วิศวกรรมศาสตรบัณฑิต (วศ.บ.) สาขาวิชาอิเล็กทรอนิกส์ สถาบันเทคโนโลยีพระจอมเกล้าเจ้าคุณทหารลาดกระบัง
2547 นิเทศศาสตรบัณฑิต (นศ.บ.) สาขาวิชาวิทยุโทรทัศน์ มหาวิทยาลัยสุโขทัยธรรมาธิราช
2548 วิศวกรรมศาสตรมหาบัณฑิต (วศ.ม.) สาขาวิชาอิเล็กทรอนิกส์ สถาบันเทคโนโลยีพระจอมเกล้าเจ้าคุณทหารลาดกระบัง

ประสบการณ์การทำงาน

พ.ศ.2549-2556 ตำแหน่งผู้ช่วยวิจัย ห้องปฏิบัติการวิจัยนาโนอิเล็กทรอนิกส์และเครื่องกลจุลภาค ศูนย์เทคโนโลยีอิเล็กทรอนิกส์และคอมพิวเตอร์แห่งชาติ

พ.ศ.2557-ปัจจุบัน ตำแหน่งนักวิจัย ห้องปฏิบัติการวิจัยนาโนอิเล็กทรอนิกส์และเครื่องกลจุลภาค ศูนย์เทคโนโลยีอิเล็กทรอนิกส์และคอมพิวเตอร์แห่งชาติ

รางวัล

พ.ศ.2554-2555 รางวัลผลงานประดิษฐ์คิดค้นระดับดี (ผู้ร่วมวิจัย) จากสภาวิจัยแห่งชาติ สาขาด้านเกษตรศาสตร์ และอุตสาหกรรมการเกษตร ในผลงาน “เครื่องวัดความขุ่นสำหรับตรวจเชื้อไวรัสในกุ้ง”

พ.ศ.2558-2559 รางวัลผลงานประดิษฐ์คิดค้นระดับดี (ผู้ร่วมวิจัย) จากสภาวิจัยแห่งชาติ สาขาเทคโนโลยีสารสนเทศและนิเทศศาสตร์ ในผลงาน “เครือข่ายเซนเซอร์ไร้สายเพื่อการเฝ้าระวังน้ำป่าไหลหลากและดินถล่มสำหรับหมู่บ้านเสี่ยงภัยพื้นที่ลุ่มน้ำ”